Simulating the Predevelopment Hydrologic Condition of the San Joaquin Valley, California

by

Benjamin Luke Bolger

A thesis

presented to the University of Waterloo

in fulfillment of the

thesis requirement for the degree of

Master of Science

in

Earth Sciences

Waterloo, Ontario, Canada, 2009

AUTHOR'S DECLARATION

I hereby declare that I am the sole author of this thesis. This is a true copy of the thesis, including any required final revisions, as accepted by my examiners.

I understand that my thesis may be made electronically available to the public.

Abstract

The San Joaquin Valley is part of the Great Central Valley of California, a major agricultural centre and food supplier for the United States. This area has significant water management concerns given the very high water demand for an increasing state population and for intense irrigation in a hot, temperate to semi-arid climate where the overall rate of evapotranspiration (ET) is high, and the overall rate of precipitation is low. Irrigation heavily relies upon groundwater and surface water extractions. Through the historical and current concerns of regional water resources reliability, land surface subsidence, water quality issues, and the health of ecosystems, a need for regional-scale water resource management and planning has developed.

The physically-based surface-subsurface HydroGeoSphere (HGS) model is used to examine the regional-scale hydrologic budget of a large portion of the San Joaquin Valley. The objective of this investigation is to develop a steady-state groundwater-surface water model of the San Joaquin Valley representative of predevelopment hydrologic conditions. The groundwater-surface water system has undergone drastic changes since the employment of groundwater and surface water extractions for irrigation and mining, and is still responding to past and present stresses. The only certain stable initial condition must therefore be that of the natural system. The model input parameters were constrained by all relevant available hydrologic data. The model was not calibrated to subsurface hydraulic heads or river flows. However, the model does provide a fair match between simulated and actual estimated water table elevations. Historic river flow estimates were not used to calibrate the model, because data consistent with that collected by Hall (1886) and representative of the natural system were not available. For this investigation, water enters through precipitation and the inflow of major rivers only. The subsurface domain is bounded by no-flow boundaries, and groundwater is therefore only able to exit the subsurface through discharge to surface water features or through ET. Surface water is only able to exit the model through discharge via the San Joaquin River and through ET. Average river inflows circa 1878 to 1884 documented by Hall (1886) were applied where the rivers enter into the valley. The spatially variable average rate of precipitation (years 1971 to 2000) from a PRISM dataset was applied to the top of the model.

The spatially variable long term average potential ET rates from the California Department of Water Resources (DWR) et al. (1999) were applied to the top of the model. Averaged overland flow parameters and vegetation factors needed to calculate actual ET were specified at the top of the model based on literature values and the 1874 spatial distribution of natural vegetation provided by California State University at Chico et al. (2003). Hydrogeological data including hydraulic conductivities, porosities, specific storage, and unsaturated zone properties are based on literature values from other relevant studies.

The resulting steady state model is therefore characterized by historical long term average data assumed to be representative (as close as possible) of the flow system circa 1848. Results indicate that the natural hydrologic setting of the San Joaquin Valley is a complex one. Complex hydrologic processes, including significant groundwater-surface water interaction along the major rivers and within wetland areas formed by flooded surface water, as well as ET and impacted root zone processes were identified in the model domain. Identification and simulation of the complex recharge and discharge relationships in the model domain sheds insight into the hydrologic nature of some historic natural wetlands. Evapotranspiration is a very significant sink of both surface water and groundwater (44.8 % of the water balance input), and has a major impact on hydrologic processes in the root zone. The presence and path of the major rivers in the domain are well defined in the model output and agree well with their actual locations. The model simulates gaining and losing reaches of the major rivers, replicating the historic recharge-discharge relationship documented by others. The general location, formation, and hydrologic processes of some significant wetlands simulated by the model have a fair agreement with historical records. As mentioned above, there is also a fair match between simulated and actual estimated water table elevations. Successful simulation of the complex hydrologic processes and features that characterize the predevelopment hydrologic conditions of the San Joaquin Valley and that resolve the water balance of the natural system underscores the importance and necessity of using an integrated model. This steady state model should serve as a reasonable initial condition for future transient runs that bring the model up to current hydrologic conditions capable of estimating present and future water budgets.

Acknowledgements

Firstly, I would like to thank my supervisor Dr. Andre Unger for giving me the opportunity to work with him, and for undertaking this research endeavour with me, his guidance and motivation is much appreciated. I am also very thankful for the constant guidance and technical support of Rob McLaren and Dr. Young-Jin Park, who provided a wealth of knowledge, skill, advice, and answers to many questions.

Funding for this work was provided by the Natural Sciences and Research Council of Canada Industrial Postgraduate Scholarship (NSERC IPS), industrial partner HydroGeoLogic Inc., and grants held by Dr. Andre Unger. I thank NSERC for funding this project, Dr. Peter Huyakorn and HydroGeoLogic for co-sponsoring with NSERC, and Dr. Andre Unger for additional financial support.

I am grateful for all technical information and the work experience received while collaborating with HydroGeoLogic Inc.

I also extend thanks to Dr. George Matanga, Lorri Peltz-Lewis, Lisa Rainger, and Alba Scott from the US Bureau of Reclamation (BOR) for providing me with data and their assistance in finding literature and technical information.

I acknowledge and thank Al Steele from the California Department of Water Resources (DWR) for providing additional subsidence data, technical information, and answering many questions.

I thank Jeff Randall for his mentorship, technical support, and guidance.

I thank my family and friends for their prayers, support, reassurance, and encouragement throughout my schooling and life.

Table of Contents

List of Tables

List of Figures

Chapter 1 Introduction

The San Joaquin Valley (SJV) in Central California has been subject to evolving hydrologic and hydrogeologic conditions and features since the development of irrigated agriculture began in the 1800's and since the Gold Rush of 1849. Presently the SJV is highly developed, with the majority of the land being used for agriculture. Agriculturally, the SJV can be thought of as the 'the nation's salad bowl' (CERES, 2007), supplying a significant proportion of all food consumed in the United States. Irrigation water demands for the SJV are met primarily by groundwater pumping, and the diversion and importation of surface water from rivers. The proportion of water supply derived from either groundwater or surface water has varied throughout time and has been dependant on different factors such as climate conditions, new technology, land development, population growth, water policy and law, water transport methods, and government initiatives/projects. The agriculture industry and highly populated cities and communities have and will continue to make reliability of the groundwater and surface water resources of the SJV a major issue at a regional scale. In addition to regional water resources reliability severe enough to cause historical droughts and land surface subsidence, water quality, and ecosystem health are significant issues that emphasize the need for a high level of regional-scale water resource management and planning. The need for a physically-based model is justified in this study and others like it by the recognized importance of integrating the regional-scale hydrologic budget into the water resource plans (Li et al., 2008, Sudicky et al., 2008, and Jones et al., 2008). The onset of climate change as well as uncertain population growth dynamics also underscores the value of predicting the future supply of water resources.

1.1 Objective and Scope of Investigation

The objective of this work is to (1) develop a regional-scale integrated surface-subsurface finite element model of a large portion of the San Joaquin Valley at a predevelopment hydrologic condition (circa 1848) and (2) characterize and simulate the predevelopment hydrologic system, including river flows, recharge and discharge of both groundwater and surface water, precipitation, ET, and the nature of wetlands. The year of simulation, 1848, is given as a time

before water development for mining became prevalent (Gold Rush of 1849) and as a time in which irrigation may have began in the Central Valley (between 1790 and the late 1960's) (Williamson, 1989, after Hall, 1889). The groundwater flow system has undergone considerable change since the development of irrigated agriculture. The present-day flow system is in a transient state and is responding to stresses imposed on it in both the past and the present (Belitz and Heimes, 1990). Due to the dynamic and ever changing nature of the groundwater and surface water systems of the valley and the changing stresses on the systems, it is necessary to simulate the hydrologic conditions of the natural system before large-scale mining and irrigation, and before major surface water and groundwater extractions were employed to meet the rapidly increasing water needs. Significant land surface subsidence has occurred, changing the surface topography and subsurface setting in the San Joaquin Valley, mainly due massive groundwater pumping for irrigation. The surface water system of the valley has changed drastically as well, and is presently responding to natural and anthropogenic alterations. Thus, arriving at a predevelopment hydrologic condition is the only certain stable initial condition. The model will therefore be a steady-state groundwater-surface water model of the San Joaquin Valley at a predevelopment hydrologic condition.

According to Li et al. (2008), physically-based surface-subsurface hydrologic models that meet the Freeze and Harlan (1969) blueprint, and that are capable of addressing regional-scale groundwater and surface water management issues include InHM (VanderKwaak, 1999), MODHMS (HydroGeoLogic, 2000 and Panday and Huyakorn, 2004), and HydroGeoSphere (Therrien et al., 2007). To meet the objectives of this investigation, the model HydroGeoSphere (Therrien et al., 2007) was applied to the San Joaquin Valley study area. HydroGeoSphere is a comprehensive, fully-integrated, physically-based and distributed numerical model that accounts for 3-dimensional variably-saturated subsurface flow and 2-dimensional overland/stream flow.

The model input parameters were constrained by all relevant available hydrologic data. The model was not calibrated to subsurface hydraulic heads or river flows. However, the model does provide a fair match between simulated and actual estimated water table elevations. Historic river flow estimates were not used to calibrate the model, because data consistent with

that collected by Hall (1886) and representative of the natural system were not available. For this investigation, water enters through precipitation and the inflow of major rivers only. The subsurface domain is bounded by no-flow boundaries, and groundwater is therefore only able to exit the subsurface through discharge to surface water features or through ET. Surface water is only able to exit the model through discharge via the San Joaquin River and through ET. Average river inflows circa 1878 to 1884 documented by Hall (1886) were applied where the rivers enter into the valley. The spatially variable average rate of precipitation (years 1971 to 2000) from a PRISM dataset was applied to the top of the model. The spatially variable long term average potential ET rates from the California Department of Water Resources (DWR) et al. (1999) were applied to the top of the model. Averaged overland flow parameters and vegetation factors needed to calculate actual ET were specified at the top of the model based on literature values and the 1874 spatial distribution of natural vegetation provided by California State University at Chico et al. (2003). Hydrogeological data including hydraulic conductivities, porosities, specific storage, and unsaturated zone properties are based on literature values from other relevant studies.

1.2 Previous Studies

Previous surface-subsurface hydrologic modelling studies concerning the San Joaquin Valley or the entire Central Valley have been reviewed from literature. While many of these studies are useful, and have even provided conceptual and physical data used for this investigation, this investigation is unique in that it is the only investigation of the San Joaquin Valley that simulates the true predevelopment conditions using a physically-based surface-subsurface hydrologic model that meets the Freeze and Harlan (1969) blueprint. Previous hydrologic modelling studies that concern this study area, but either do not incorporate a true predevelopment condition, do not model as large an area, or do not use a physically-based surface-subsurface hydrologic model that meets the Freeze and Harlan (1969) blueprint include Williamson et al. (1989), Belitz and Phillips (1995), Phillips et al. (2007), Phillips and Belitz (1991), Brush et al. (2004), Burow et al. (2004), Lee et al. (2007), Weissmann et al. (1999), Burow et al. (1999), Quinn et al. (2004), Quinn et al. (2001), and Brekke et al. (2004).

Chapter 2 Conceptual Model

The conceptual model for this investigation describes both the hydrological and geological factors that influence groundwater and surface water flow within the system at a pre-development condition. Available geological and hydrological data that is relevant to this pre-development condition and the general flow system of the San Joaquin Valley have been reviewed as part of the conceptual model. The governing processes and equations for modelling the hydrologic cycle using HydroGeoSphere are described in detail in Panday and Huyakorn (2004) and Therrien et al. (2007). Appendix I of this study provides a condensed summary of these processes and equations, focusing only on those physical processes that are most critical in characterizing the hydrologic system of the San Joaquin Valley at its predevelopment condition. Appendix I is largely a reproduction of the appendix from Li et al. (2008). An estimate of the total hydrologic budget of the San Joaquin Valley is made invoking the following main components of the hydrologic cycle:

$$P \cdot A = (Q_{S2} - Q_{S1}) + (Q_{G2} - Q_{G1}) + (ET_S + ET_G) \cdot A + (Q_s^w + Q_G^w) + (\Delta S_S + \Delta S_G)\Delta t \quad (1)$$

where P is the net precipitation [L/T] (actual precipitation - interception), A is the area of the watershed [L^2], Q_{S1} and Q_{S2} are the surface water inflow and outflow [L^3/T], Q_{G1} and Q_{G2} are the groundwater inflow and outflow [L^3/T], ET_S is the evapotranspiration from the surface flow system, ET_G is the evapotranspiration from the subsurface flow system, Q_s^w is the surface water withdrawal [L^3/T], Q_G^w is subsurface water withdrawal [L^3/T], ΔS_S is the change in surface water storage [L^3] over time step Δt [T], and ΔS_G is the change in subsurface water storage [L^3] over time step Δt [T]. Wherefore the objective is to arrive at the predevelopment condition, surface water and subsurface water withdrawals are both assumed to be negligible. At steady-state, the changes in surface water and subsurface water storage are also negligible.

2.1 Study Area Location

The San Joaquin Valley is more than 400 km long, 40 to 90 km wide, and makes up the southern two-thirds of the Central Valley of California, the other third in the north being the Sacramento Valley (Phillips et al., 2007). These two valleys are appropriately named after the major rivers that they are drained by. The SJV is bounded by the delta of the Sacramento and

San Joaquin Rivers on the north, the Tehachapi Mountains on the south, the Coast Ranges on the west, and the Sierra Nevada on the east. The study area location and model boundary are shown in Figure 1. A conceptual diagram of San Joaquin Valley and subsurface is provided in Figure 2. The model extents were chosen to match the same areal extent of the Middle San Joaquin - Lower Chowchilla sub-watershed and the Middle San Joaquin - Lower Merced - Lower Stanislaus sub-watershed (hydraulic unit codes 18040001 and 18040002 respectively), as well as a portion of the Tulare - Buena Vista Lakes sub-watershed (hydrologic unit code 18030012) (Seaber et al., 1987). The model boundary and the boundaries of the surface water sub-watersheds within are shown in Figure 3 using spatial data from Steeves and Nebert (1994). The model boundary, like the sub-watersheds boundaries, corresponds with surface water flow divides and topographic features such as mountain ranges. The southern bounds of the model were extended south to parts of the Kings River as well as southern parts of the Westside groundwater sub-basin boundary (sub-basin number 5-22.09). The model boundary and the groundwater sub-basins boundaries within are shown in Figure 4 using spatial data from California Department of Water Resources (2000). The modelled study area is about 17,232 km^2. The model fully encompasses the first two sub-watersheds mentioned above (18040001 and 18040002). These two sub-watersheds are only part of the broader San Joaquin River Basin (SJRB, Subregion 1804) which contains parts of the eastern and western mountains bounding the SJV. The Tulare - Buena Vista Lakes sub-watershed partially contained by the model is part of the broader Tulare - Buena Vista Lakes Basin (TBVLB, Subregion 1803) which, like the SJRB, contains parts of the Sierra Nevada and the Coast Ranges.

Therefore, the model completely contains two sub-watersheds of the San Joaquin River Basin, and a northern portion of a sub-watershed of the Tulare Buena-Vista Lakes Basin, with the model boundaries conforming to surface water and groundwater flow divides. The model fully contains the San Joaquin hydrographic subregion and partially contains the Tulare hydrographic subregion of the Central Valley (Bertoldi et al., 1991). Surface water watershed and sub-watershed boundaries are discussed in more detail in section 2.5.1.

2.2 Climate

The climate of the San Joaquin Valley varies spatially and is described as both Mediterranean and Steppe; both temperate/mesothermal and semi-arid (Planert and Williams, 1995; Williamson et al., 1989; and Phillips et al., 2007). It is characterized by hot, dry summers and mild, wet winters, which allows for a year-round growing season (Planert and Williams, 1995).

Three weather stations located in the model domain were selected to help characterize the climate. Long term averages for temperature and precipitation from these stations for the period 1971 to 2000 were selected and appear to be consistent and reasonable. A long term average over the 1971 to 2000 period is assumed to be representative of the SJV predevelopment hydrologic condition circa 1848. The locations of the selected weather stations are shown in Figure 5.

Average temperatures observed at these three weather stations are generally characteristic of the model domain and are summarized in Table 1. During the summer (using June, July, August) average temperatures in the model domain are in the range of 22.9 to 27.4°C, while during the winter (using December, January, and February) the average ranges from 7.3 to 11.2°C. The warmest time of the year appears to be July with a monthly average temperature range of 25.2 to 27.4°C. December is the coldest time with a monthly average temperature range of 7.3 to 7.9°C.

Roughly 85 percent of annual precipitation occurs during the winter and early spring season (November to April). The summer months (June, July, and August), are the driest time of year. The majority of precipitation occurring in the study area (valley floor) evapotranspirates before it can infiltrate downward and recharge the subsurface (Planert and Williams, 1995). The SJV and the eastern slopes of the Coast Ranges are in a rain shadow wherefore cloud moisture moving east from the Pacific Ocean is collected by the Coast Ranges (Gronberg et al., 1998; and Flay, 2002). Average precipitation estimates at the three stations are quite variable over the year and are summarized in Table 2. According to these weather station estimates, the long term average precipitation ranges from 0.51 to 0.96 mm/d. The spatial distribution of total annual average precipitation in the model domain is shown in Figure 5. This estimate

represents the total cumulative precipitation for one year; an average over the period from 1971-2000 using a PRISM (Parameter-elevation Regressions on Independent Slopes Model) data set (PRISM Group, 2008) converted to a daily rate. From Figure 5, one may observe that the least amount of precipitation falls in the northern portion of Tulare Basin, roughly 0.43 to 0.66 mm/d on an average annual basis. The highest amount of precipitation falls in the northern portion of the SJV (north-eastern part of model domain), roughly 1.41 to 2.28 mm/d on an average annual basis. The PRISM estimates are of the same order of magnitude as the weather station estimates but with a broader range. The PRISM data is much more continuous, complete, and convenient to use compared to the weather station data. The PRISM data is also generally consistent with the weather station point estimates, averaged over the same time period. A comparison of historical station records of precipitation documented by Hall (1886) with point extractions at the same locations from the PRISM data set is provided in Table 3. The locations of the historical stations sampled from the Hall (1886) data set are shown in Figure 5. The data set is the oldest precipitation data readily available. From Table 3, one can see that the PRISM data values are the same order of magnitude as the Hall (1886) values. The difference between these two data set samples varies from 0.01 to 0.27 mm/d; in most cases the difference implies that the PRISM data is representative of slightly wetter conditions than that of the Hall (1886) data. A mean annual precipitation map using data averaged from 1911 to 1960 shows that precipitation within the model domain varies from 0.35 mm/d to 1.39 mm/d (Gronberg et al., 1998, after Rantz, 1969). If one takes the average of the midpoints of the two precipitation categories/zones of the 1911 to 1960 data set that cover the model domain roughly equal proportion, one obtains a spatially averaged precipitation estimate for the entire model domain of 0.78 mm/d. The PRISM estimates were used as model input. Therefore, precipitation varies spatially over the model domain from a minimum of 0.43 mm/d to a maximum of 2.28 mm/d on an average annual basis. The spatially averaged rate of precipitation (averaged over the entire domain using PRISM data) is 0.79 mm/d and discussed in section 4.1. The PRISM estimates appear strikingly similar to the 1911 to 1960 data set. Considering the annual precipitation is shown to vary significantly (Williamson et al., 1989; and Gronberg et al., 1998), the absence of historic precipitation data circa 1848, and the continuity, completeness, consistency, years sampled, and the utility of the PRISM data, it is

assumed to be the most reliable data set which is both representative of the SJV and similar to a long term predevelopment hydrologic condition.

Evapotranspiration is a significant component of the total water budget for the entire area. The potential ET is an estimate of how much water can be potentially lost due to evaporation and plant transpiration. Potential ET takes into account climatic factors such as solar radiation, temperature, humidity, and wind. Actual ET is a function of both the potential ET (climatic factors), as well as land cover / vegetation type, and soil properties. Potential ET zones and the corresponding long term average potential ET rates occurring in the model domain are presented in Figure 6 using spatial data from Jones et al. (1999). The potential ET values are provided by the California Department of Water Resources (DWR) et al. (1999) as part of the California Irrigation Management Information System (CIMIS). Potential ET as provided by the DWR is calculated using a modified version of the Penman-Monteith equation (Pruitt and Doorenbos, 1977) and a wind function developed at the University of California at Davis (California Department of Water Resources, 2009). HydroGeoSphere uses ET parameters based on plant type (LAI, rooting depth) and ET parameters based on soil type (ET limiting moisture contents) in conjunction with potential ET values in order to estimate actual ET. As estimated by CIMIS, the potential ET rates within the model domain range from 3.42 to 4.35 mm/d on an average annual basis, and is similar to the potential ET (3.41 mm/d) reported by Bertoldi et al. (1991) for the centre of the Central Valley. As one might surmise, potential ET is lowest during the winter and highest during the summer. For the zones that occur within the model domain, the potential ET rate increases with increasing zone number. Vegetation types and the corresponding ET parameters are discussed in more detail in section 2.5.3. The theory behind the calculation of ET is discussed in Appendix I.

On an annual basis, the potential evapotranspiration (ET) exceeds the total precipitation for any given year, causing an annual moisture deficit throughout the valley. Precipitation in the Sierra Nevada east of the model domain is a great deal higher and can exceed 5.57 mm/d (80 in/yr) (Planert and Williams, 1995). The western slopes of the Sierra Nevada receive high levels of precipitation as they force warm cloud moisture from the Pacific Ocean upwards which cools and condenses (Gronberg et al., 1998).

2.3 Topography

The present day topography for the modelled area is shown in digital elevation model (DEM) form in Figure 7 using spatial data from the U.S. Geological Survey (USGS, 1999). The ground surface elevations for this model are from a USGS National Elevation Dataset (NED) having 30 m resolution, and subsequently adjusted by available subsidence data to represent pre-development topography (see section 3.2). The relief of the Central Valley is relatively flat and of low altitude. Within the model area, the valley floor slopes towards the San Joaquin River from the Sierra Nevada foothills and the Coast Ranges. The land surface elevations of the model vary from about 2.5 to 677 m, a range of 674 m. According to Phillips et al. (2007), land surface elevation gradients in part of the SJV range from less than 1m/km near the river (topographic lows) to more than 5 m/km near the foothills and adjacent to streams and rivers. Slope calculations showed that elevation gradients within the model domain range from 0 to 144.4 % (~0 to 144,356 m/km). Land surface elevation gradients generated for the present day topography within in the model area are shown in Figure 8.

2.4 Geology

The San Joaquin Valley is a northwest trending asymmetrical structural trough that is filled with both continental and marine sediments (Williamson et al., 1989). Structurally, it can also be called a down-warping geosyncline, or a large scale syncline fold (Sneed, 2001). The marine sediments in the valley were mainly deposited by periods of submersion by the Pacific Ocean, and the continental deposits were deposited by the erosion and transport of surrounding mountain rock by fluvial processes (Planert and Williams, 1995). A conceptual geologic cross-section of the modelled area is shown in Figure 2.

2.4.1 Bedrock Geology

The occurrence of the underlying bedrock surface throughout the model domain is illustrated in Figure 9. Along the eastern part of the valley, the sediments are underlain by pre-Tertiary crystalline and metamorphic rocks of the Sierra Nevada (Davis et al., 1959; Olmsted and Davis, 1961). The sediments along the western portion of the eastern margin are thought to be underlain by a pre-tertiary mafic and ultramafic complex (Cady, 1975). The Sierra Nevada is

said to be comprised of mainly granite and associated plutonic rocks, but also some metasedimentary and metavolcanic rocks (Bertoldi et al., 1991). Only minor quantities of water occur within the small scale discontinuities (fractures, joints, cracks) of these rocks (Williamson et al., 1989).

The sediments on the western side of the valley are underlain by the folded and faulted, semi consolidated to consolidated clastic sediments of the Coast Ranges. These deformed sedimentary rocks consist of pre-Tertiary and Tertiary consolidated sediments of marine origin. Marine rocks of the Coast Ranges and other areas of outcrop in the Central Valley are said to be comprised of mainly conglomerate, siltstone, sandstone, mudstone, and shale (Page, 1986). This sedimentary basement extends eastwards and thins out towards the Sierra Nevada (Williamson et al., 1989).

2.4.2 Overburden Geology

The geology of the overburden is characterized by unconsolidated and partially consolidated lenses of sands and gravels interbedded with lenses of finer silts and clays. The upper part of the overburden deposits are described as continental in origin, post-Eocene to Holocene epoch in geologic age, and containing mostly fluvial deposits, some volcanic material, and some lacustrine deposits (Williamson et al., 1989). The most significant feature within the continental deposits is the Corcoran Clay, an extensive and well documented Pleistocene age lacustrine deposit and member of the Tulare Formation. The presence of the Corcoran Clay has important implications on the subsurface flow system, and is therefore discussed in more detail in sections 2.6.1 and 2.6.2. The continental deposits are said to overly shallow marine deposits of variable level of consolidation from the Late Cretaceous and Tertiary Periods of geologic time (Sneed, 2001). The underlying marine deposits are later referred to as part of the lower overburden which also contains continental deposits. Subsurface materials, their contacts, and their distribution across the SJV are widely variable and not necessarily known, continuous or present locally in the general simplified description given here. The contact between the continental and marine deposits is not always certain or well defined because they interfinger in some areas (Bertoldi et al., 1991). In the western part of the SJV, poorly

consolidated flood plain, deltaic, alluvial-fan, and lacustrine deposits are said to be found in the lower zone of the overburden (Belitz and Heimes, 1990).

According to Phillips et al. (2007), the parent rocks for the overburden sediments consist of pre-Tertiary granitic rocks (eroded from the Sierra Nevada), marine and metavolcanic rocks (eroded from foothill belt of Sierra Nevada), as well as consolidated marine and continental sediments (eroded from sedimentary rocks of the Coast Ranges). On the west side of the valley, alluvium from the Coast Ranges interfingers eastward with sediment eroded from the Sierra Nevada (Belitz and Heimes, 1990).

As alluded to, the depositional environment for the overburden deposits is primarily fluvial (transport by rivers and streams) as well as lacustrine (transport by lakes and shallow seas or ocean inundation). At surface, the SJV can be divided into one of three physiographic regions: the western alluvial fans, the eastern alluvial fans, and basin deposits (Phillips et al., 2007). The average thickness of sediments and subsequently, of aquifer material in the Central Valley is roughly 730 m (~2,400 ft). In the southern part of the model domain (northern portion of the Tulare Basin), sediment thicknesses reach over 2,134 m (~7,000 ft) (Bertoldi et al., 1991). Sediment thicknesses of 900 to 1,200 m (~3,000 to 4,000 ft) occupy about half of the SJV's areal extent (Williamson et al., 1989).

The distribution and classification of surficial materials are available in the State Soil Geographic (STATSGO) Database created by the National Soil Survey Center, a part of the U.S. Department of Agriculture (USDA). The surficial soils were not differentiated in this model due to their complex and fine arrangement and variable thicknesses.

2.5 Hydrology

2.5.1 Watershed Boundaries

To recap, the model extents were chosen such that the model includes two sub-watersheds of the San Joaquin River Basin, and a northern portion of a sub-watershed of the Tulare Buena-Vista Lakes Basin, with the model boundaries conforming to surface water and groundwater divides. Surface water flow divides and topographic features are used to define watershed

boundaries. Hydrologic unit maps developed by the USGS for river basin units present approved hydrologic boundaries and the corresponding numerical codes (Seaber et al., 1987). The numerical codes for the map units are designed such that they separate the United States into 21 major water-resources regions, 222 subregions, 352 accounting units, and 2,149 cataloging units. These are the four levels of classification that comprise the hydrologic units from the largest elements (regions) to the smallest elements (cataloging units) in the hierarchy. Each sub-watershed is assigned a unique hydrologic unit code (HUC), as well as a boundary and name based on the principal hydrologic feature(s) within the unit (Seaber et al., 1987).

As stated earlier, the model contains only part of Subregion 1804, the broader San Joaquin River Basin (SJRB). As one might presume, the model is located within Region 18, the California water-resource region. Subregion 1804 is further subdivided into 14 sub-watersheds. As mentioned earlier, the model domain fully encompasses 2 of these 14 sub-watersheds, the Middle San Joaquin - Lower Chowchilla sub-watershed and the Middle San Joaquin - Lower Merced - Lower Stanislaus sub-watershed (hydrologic unit codes 18040001 and 18040002 respectively). Together these two sub-watersheds completely contain the portion of the San Joaquin River occurring in the model domain.

Similarly, the model also contains only part of Subregion 1803, the broader Tulare Buena-Vista Lakes Basin (TBVLB), which is also part of Region 18. Subregion 1803 is subdivided into 12 sub-watersheds. The model domain partially contains 1 of these 12 sub-watersheds, namely a northern portion of the Tulare Buena-Vista Lakes sub-watershed (hydrologic unit code 18030012). The sub-watersheds contained in the model domain are shown in Figure 3.

2.5.2 Major Surface Water Features

Within the model domain, surface water running off from the surrounding mountains (mostly from the Sierra Nevada on the east) drains into the valley, eventually joining the San Joaquin River which flows to the Sacramento-San Joaquin Delta, then through Suisun Bay and San Francisco Bay and out to the Pacific Ocean. Most of the mountain runoff and stream flow comes from the Sierra Nevada, wherefore runoff from the Coast Ranges mainly drains westward to the Pacific Ocean (Planert and Williams, 1995). The Coast Ranges are also of

lower altitude, receive lower amounts of rainfall, and drain less area compared to the Sierra Nevada, and thus are less capable of sustaining stream flow (Williamson et al., 1989).

The major rivers that flow into and through the model domain start from the Sierra Nevada in the east, their source mainly being mountain rainfall and snowmelt. The major surface water features in the model, as well as the Kings River (forms part of the model boundary) are shown in Figure 1 using spatial data from U.S. Bureau of Reclamation (2004). As mentioned previously, the San Joaquin River is the major river draining the SJV, with 5 major tributaries joining it within the model domain. A summary of mean annual inflow rates (long term average) converted to average daily estimates for the six major rivers (flowing into and through the model domain) and the total river inflow rate over the period from 1878 to 1884 are summarized from Hall (1886) in Table 4. The SJR has the highest mean inflow rate of all the rivers in the domain, 7,531,777 m^3/d, while the Chowchilla River has the lowest, 373,423 m^3/d and the Fresno River has the second lowest, 407,727 m^3/d. The total inflow rate for the major rivers in the domain is 23,695,008 m^3/d.

Presently, river flows in the SJV are highly regulated by means such as reservoir dams and are diverted and transported by systems of canals and other water management or conveyance structures. Surface water diversions on at least some of the rivers would have been present by or before the time flow measurements were recorded (1878), yet the river flow estimates selected for this model were measured at locations upstream of diversions where possible and/or using scaling methods that attempt to estimate the full flow of the given river in its natural setting (Hall, 1886). The estimates of river flow or discharge documented by Hall (1886) were made using the method of scale of discharge with water stages (based on water levels), and the method of drainage areas in different combinations depending on the quality and period of data recorded for each river. Therefore, in this predevelopment model, there are no surface water diversions, no losses dues to diversion structures, and no rerouting or redistributing of surface water outside of the river channels. The locations of the historical river flow observations made by Hall (1886) are illustrated in Figure 1 and Figure 5. Stream flow data for these locations or similar locations, as well as locations within the model domain are available for later dates (McGlashin and Dean, 1912). Longer term average estimates of

stream flows are also available, a mean from 1889-1929 (California Division of Water Resources, 1930, p.67) and means over various periods (Mendenhall et al., 1916, after McGlashin and Dean, 1912). The stream flow data tabulated by California Division of Water Resources (1930) is the same order of magnitude as the Hall (1886) data, but lower in magnitude. The stream flow data summarized by Mendenhall et al. (1916) after McGlashin and Dean (1912) varies where flows for some rivers are higher and others lower than that estimated by Hall (1886). This difference in flow magnitude between data sets may be due to different measurement dates and time, different measurement methods, influence of surface water and/or groundwater extractions, and different measurement locations. It is possible that the more recent data sets do not consistently attempt to estimate the full flow of the rivers in an unaltered state and are lower in magnitude due to water diversions or extractions. The data documented by Hall (1886) are assumed to be the data most representative of predevelopment conditions in the SJV, and thus the more recent data were not used in the model.

Irrigation, which presently is heavily relied upon for agriculture in the valley, has not been included as a model input, attempting to arrive at a predevelopment condition. Irrigation is an example of a post-development stress that has altered the flow system by adding or increasing the amount of recharge to the shallow subsurface, as well as increasing the amount of runoff to rivers and other surface waters.

According to Belitz and Heimes (1990), during pre-development conditions, a significant amount of recharge in the western part of the Fresno County was due to infiltration of water from intermittent streams and potentially from even smaller ephemeral streams. The intermittent streams that would have contributed to this recharge in this section of the SJV include Little Panoche, Panoche, Cantua, and Los Gatos Creeks. Intermittent streams would only flow during the winter rainy season and the smaller ephemeral (short lived) streams flow only after storm events (Bull, 1964a). The intermittent and ephemeral stream courses do not reach the San Joaquin River or Fresno Slough in the trough (central/axial low elevation area) of the valley. The intermittent and ephemeral streams lose their flow and dry up due to evaporation and infiltration before reaching the valley floor. Davis and Poland (1957) estimated that the four intermittent creeks listed above typically have a combined total flow of

about 61.7 cubic hectometres (61,700,000 m^3 or 50,000 acre-feet) per year of which 60 to 80 percent infiltrates and recharges the groundwater. This yearly combined total flow is equivalent to an average daily rate of 169,041 m^3. Parts of the intermittent stream courses listed above and other minor streams are within the bounds of this study. The minor streams within the model domain are not documented as well as the major rivers that flow from the Sierra Nevada. The historical discharge (mean from 1889-1929) of Panoche, Cantua, and Los Gatos Creeks, as well as several other minor streams that may or may not be in the model domain are available in literature (California Division of Water Resources, 1930, p.67). The minor stream locations, flow paths, measurement locations, potential extractions and alterations, and predevelopment character are not certain. It is thereby not certain if the available flow measurements for the minor streams are representative of what would enter the model domain at predevelopment conditions. While these intermittent streams may be significant for a study of a much smaller or local area, they are relatively insignificant in a study of the entire San Joaquin Valley (17,232 km^2). The total inflow of the four intermittent creeks listed above is less than 1 % of the total mean inflow of the major rivers that enter the SJV from the Sierra Nevada. From the perspective of water supply for the SJV, Mendenhall et al. (1916) indicates that the west-side streams are negligible. These four intermittent creeks and other minor streams were therefore not included in the model.

According to Gronberg et al. (1998), recharge in the SJV was primarily via streams entering from the Sierra Nevada. Precipitation and snowmelt are considered to be minimal or secondary sources of groundwater recharge. Recharge from streams took place mainly in the upper reaches of the rivers close to where they enter the valley. Belitz and Heimes (1990) indicate that water exiting the unaltered system (water budget loss) was primarily via evapotranspiration (ET) and the flow of rivers along the trough of the valley. Outflow to the Sacramento-San Joaquin Delta is the only mode of natural discharge of surface or ground water from the system (Gronberg et al., 1998, after Bertoldi et al., 1991).

Within the model domain, the San Joaquin River formed natural levees north of where it meets with the Merced River. At high flows, the SJR would flood the land surface south of the Merced River, causing large freshwater marshes to form in the trough of the valley (Gronberg

et al., 1998; Katibah, 1984; Warner and Hendrix, 1985). There was believed to be additional wetland areas formed by San Joaquin River overflow in an area near Stockton (Gronberg et al., 1998; San Joaquin Valley Drainage Program, 1990). In the unaltered natural setting, the model domain would have been bounded by the Kings River (still present), and a large, shallow, and temporary inland lake – Tulare Lake (presently dried up). While Tulare Lake existed, it received water from the Kings, Kaweah, and Tule Rivers within the Tulare Basin (Gronberg et al., 1998). These major surface water features are outside of the model domain and were not simulated, wherefore they serve as part of the outer model boundary. It is possible for runoff to leave the system by flowing over the southern model boundary.

Although the majority of naturally occurring wetlands have been drained for agriculture, they have always been an important surface water feature of the SJV and are considered to be a major water issue presently. Wetlands are made up of unique ecosystems, and inhabited by diverse plants and wildlife (Gronberg et al., 1998). Wetlands are also reported to be significant reservoirs for the natural storage of carbon, pertinent to climate change. Some important functions that underline the value of wetlands in the SJV include: water quality protection and improvement, flood control and groundwater recharge, erosion control, fish and wildlife, biological diversity, and recreation (CWIS, 1998). Some natural wetlands have been conserved or protected, while controlled seasonal wetlands have been created to replace the wet-dry cycle historically observed in natural wetlands. If seasonal wetland drainage is not carefully managed, it can negatively impact downstream water quality.

2.5.3 Land Cover

As stated previously, extensive agriculture and highly populated urban centres currently characterize the SJV; however, it is the predevelopment characterization of the area that is the focus of this investigation. Prior to the proliferation of agriculture, water resource development, and settlement of the central valley, the primary land cover was natural vegetation. Pre-development natural vegetation types circa 1874 were researched and mapped by the California State University at Chico et al. (2003) as part of the Central Valley Historical Mapping Project. The distribution of natural vegetation across the model domain around the time of 1874 is provided in Figure 10. The vegetation types that occurred within the model

domain during predevelopment conditions in descending order of land area covered in the domain include Grassland, Other Floodplain Habitat, Wetland, Riparian, Alkali Desert Scrub, Aquatic, Valley/Foothill Hardwood, and Chaparral. The total model area covered by each vegetation type is summarized in Table 5. Wetlands covered roughly 4.3 % (749 km^2) of the model area in 1874. Together, the Grassland, Other Floodplain Habitat, and Wetland vegetation types make up just over 95 % of the model area. The first five vegetation types listed are considered to have predevelopment occurrences in the model area large enough to be distinguished. The remaining three types occurred in insignificant geometries and quantities.

Land cover is a factor that is able to influence the surface water and groundwater flow systems through processes such as overland flow, infiltration, unsaturated groundwater flow, and evaporation and plant transpiration combined as evapotranspiration (ET). ET is part of the total water budget, and represents a water loss or sink. The amount of water lost through ET is dependent on climatic conditions, land use, the distribution and type of vegetation, and soil moisture. The amount of ET also influences the amount of water available for runoff, infiltration and recharge, and interflow. The dominant species for the main predevelopment vegetation types are listed in Table 6 (Nelson et al, 2003). The five major vegetation types and the corresponding mean leaf area index (LAI) and rooting depth available in literature are provided in Table 7. Table 7 also contains the corresponding root zone density function, maximum evaporation depth, and evaporative depth function for each vegetation type. One will observe in Table 7 that the evaporative depth is assumed to be equal to rooting depth, and that EDF is assumed to be equal to the RDF. For vegetation types with rooting depths of 5 m, the RDF is assumed to be cubic. For vegetation types with rooting depths less than 5 m, the RDF is assumed to be linear. A summary of the evaporation limiting saturations, the transpiration limiting saturations, the canopy storage parameter, and dimensionless fitting parameters used in this investigation and similar investigations is provided in Table 7. As one may observe, the oxic limit and anoxic limit of water saturation are both set to one, implying that full transpiration can occur in the root zone even when fully saturated. It is assumed that transpiration in fully saturated conditions is possible in wetland and related environments

occurring in the Central Valley. Overland flow parameters such as friction factors (Manning's n) and storage depths for the major land cover types are shown in Table 8.

2.6 Hydrogeology

2.6.1 Hydrostratigraphic Units

The ground water aquifer within the model domain from which groundwater extraction has been made since the mid 1800's, rests above the bedrock basement and is present throughout the entire extent of the model. Groundwater basin boundaries within this extensive aquifer have been delineated by the California DWR based on geological, hydrological, and hydrogeological features and conditions that affect groundwater flow such as the location of impermeable bedrock, constrictions in permeable material, low permeability materials (rocks or sediments), geologic structures (such as faults and arches), significant surface water features (stream, lake, ocean), groundwater divides, and adjudicated basin boundaries (California Department of Water Resources, 2009; California Department of Water Resources, 2003; Page, 1986). The groundwater sub-basin boundaries within the model domain are shown in Figure 4. As mentioned previously, part of the Westside (5-22.09) groundwater sub-basin boundary is used to form part of the model boundary. The groundwater sub-basin name is listed for each groundwater sub-basin number in Table 9.

This aquifer is composed of the upper and lower overburden materials discussed previously. Recapping, the upper overburden (upper aquifer zone) materials are mainly lenses of sand and gravels interbedded with significant amounts of finer grained silts and clays. Lenses and beds of fine grained silt and clay deposits are distributed throughout the aquifer, and comprise more than half of the aquifer materials observed by wells and boreholes (Williamson et al., 1989). The lower overburden (lower aquifer zone) materials are mainly unconsolidated to consolidated continental and marine deposits. The most extensive and hydraulically significant clay feature in the SJV is referred to as the Corcoran Clay, a Pleistocene age lacustrine deposit and Member of the Tulare Formation. The Corcoran Clay is also correlated with and subsequently referred to as the E-Clay, as well as other given names based on where it is found and its properties (Phillips et al., 2007). The interpreted areal extent of the Corcoran Clay

within the model domain shown is shown in Figure 11. The clay material beds have a much lower vertical permeability and hydraulic conductivity; and collectively act as confining aquitards within the larger aquifer, resulting in varying groundwater heads with depth. Formerly, researchers thought that the San Joaquin Valley contained an upper unconfined to semi-confined aquifer separated from a lower aquifer confined by the Corcoran Clay. Recent studies indicate that the Central Valley actually contains a single heterogeneous aquifer system that contains water under unconfined, or water-table, conditions in the upper zone; these unconfined conditions grade into more confined conditions with depth (Planert and Williams, 1995). The confining conditions are not due to one distinct confining unit; rather they are the culmination of numerous overlapping lens-shaped clay beds. Although the Corcoran Clay constitutes only a small percentage of the total thickness of clay layers in the aquifer system (Planert and Williams, 1995), it is most extensive and continuous single confining bed in the region. Spatial data concerning the extent, thickness, and depth to the top surface of the Corcoran Clay were provided by the US Bureau of Reclamation (BOR) based on maps by Page (1986).

For this investigation, the aquifer is considered to be one unit as described above, having an upper zone (unconfined zone) and a lower zone (semi-confined to confined) with differing hydraulic parameters. The Corcoran Clay has also been incorporated into the model as a separate unit with distinct hydraulic parameters. Some investigations have chosen to average the hydraulic properties of the clay lenses with the other materials (such as appropriate mean hydraulic conductivities), and therefore do not model the Corcoran Clay as a separate unit (Williamson et al., 1989). Other simulations and numerous studies of the SJV have delineated the Corcoran Clay as a distinct unit, representing it as a separate layer with distinct properties (Phillips et al., 2007) or as the model bottom boundary (Phillips and Belitz, 1991). In most studies where the Corcoran Clay is present within the model domain, the importance of accounting for this feature is recognized and the hydraulic properties are adjusted accordingly, even if a separate model layer is not created for this purpose. It follows that it is acceptable and appropriate to represent the Corcoran Clay as a distinct model layer. Therefore, the model contains two distinct units, the Corcoran Clay aquitard unit and the main aquifer unit which

subdivided into two zones vertically. The entire three-dimensional model with the major hydrostratagraphic units is shown in Figure 12. The hydrostratagraphic units are more clearly visible in a close up of the model at the outlet in Figure 13.

As stated previously, the fractures, joints, and cracks in the crystalline bedrock generally contain minor amounts of water due to low porosity and permeability, and are not known to provide favourable hydraulic conditions for groundwater flow through the material. The bedrock materials are generally assumed to be impermeable, and flow across the overburden-bedrock interface is assumed to be insignificant. Above the groundwater flow inhibiting crystalline rock, minimal groundwater flows through the consolidated marine sediments. Groundwater within these deposits is typically saltwater or brine; however, some freshwater is withdrawn in several locations across the Central Valley (Planert and Williams, 1995).

According to Sneed (2001), three distinct groundwater bodies can be found in parts of the western, central, and south eastern parts of the valley. In downward succession, these groundwater bodies include (1) a zone of unconfined and semi-confined fresh water in alluvial deposits overlying the Corcoran Clay unit, (2) an extensive reservoir of fresh water in alluvial and lacustrine deposits confined beneath the Corcoran Clay, and (3) a zone of saline water contained in marine sediments that underlies the fresh water body throughout the area. Ground water occurs as one fresh water body of considerable depth particularly in the areas characterized by both the presence of major streams and the absence of the Corcoran Clay in the eastern part of the valley (Lofgren, 1976). Most of the fresh groundwater in the Central Valley is contained in the post-Eocene continental deposits (Page, 1986; Bertoldi et al., 1991). Differences in water density and salinity are not accounted for in this modelling investigation. For the purposes of this model, freshwater and constant water density is assumed throughout the domain.

2.6.2 Hydraulic Properties of Subsurface Materials

Vertically, the model is discretized to conform to the primary hydrostratigraphic features of the model: surficial sediments in the unsaturated zone, upper unconsolidated aquifer zone, Corcoran Clay semi-confining unit, and lower unconsolidated aquifer zone. The model

discretization and layers are discussed in detail in section 3.1. The surficial sediments as well as the upper and lower unconsolidated zones are assumed to be part of one main aquifer unit, yet are distinguished based on their different material properties such as hydraulic conductivities, location, and level of confinement. Hydraulic properties identified in literature and those assigned for the hydrostratigraphic units described above are shown in Table 10.

The surficial layers (root zone layers) are assigned the same hydraulic properties as the upper aquifer zone. As mentioned in section 2.4.2, the spatial distribution of soil type at ground surface is not incorporated into the model wherefore the occurrence of these soils with depth in the unsaturated zone and the associated variable hydraulic relationships are not certain. Instead, the unsaturated zone parameters (α, β, and S_{W_r} of equation 5) are assumed to be constant across the model domain and similar to that of a sandy aquifer wherefore the overburden contains sand lenses. The unsaturated zone parameters used in this investigation are shown in Table 10, and are characteristic of Borden Sand aquifer material (Abdul, 1985). The upper aquifer zone has a higher horizontal hydraulic conductivity than the lower aquifer zone in parts of the eastern side of the valley (eastern alluvial fan); this difference in hydraulic conductivity between the upper and lower zone is assumed for the entire model domain. Hydraulic properties from separate zones within the alluvial deposits, including deposits above the Corcoran Clay, on the east side of the SJR were averaged to represent the properties of the entire upper aquifer zone. Hydraulic properties from separate zones within the alluvial deposits, including deposits below the Corcoran Clay, on the east side of the SJR were averaged to represent the properties of the entire lower aquifer zone. The aquifer materials are assumed to possess anisotropic hydraulic conductivities based on estimates from previous studies with the vertical hydraulic conductivity being three orders of magnitude smaller than the horizontal hydraulic conductivity. Based on the estimates of previous studies (Phillips et al., 2007), the anisotropy in hydraulic conductivity (horizontal:vertical) appears to be 376:1 and 318:1 in the upper aquifer zone and lower aquifer zone respectively. The hydraulic conductivities used in this study for the upper and lower aquifer zones are based on estimates from a previous study that used the distribution of sediment texture and the hydraulic conductivities of the lithologic end members (Phillips et al., 2007, Figure 19, page 28). The

horizontal hydraulic conductivity is estimated to be 33.90 m/d for the upper aquifer zone and 26.43 m/d for the lower aquifer zone by the method described above. Based on a similar sediment texture method, a previous modelling study of the entire Central Valley estimated the average horizontal hydraulic conductivity of the entire permeable subsurface to be similar to the values used in this study, about 10.16 m/d (Bertoldi et al., 1991; and Williamson et al., 1989). The estimates used in this study are also of similar magnitude as those computed using slug tests (single-well hydraulic tests) in this area, having a mean of 85 m/d (Phillips et al., 2007). The porosity and specific storage, 35 % and 3.05 x 10^{-6} m^{-1} respectively, are assumed to be the same for the upper and lower aquifer zones. The porosity value is based on an assumption made by Ireland et al. (1984). The specific storage value is based on a selection made by Ireland et al. (1984) from a range of probable values reported by Riley and McClelland (1972) from aquifer pumping tests.

As one may notice in Table 10, the hydraulic conductivity values estimated for the Corcoran Clay vary widely, the range being three orders of magnitude. The lower estimates are most likely more representative of the clay in its undisturbed setting, prior to being punctured by numerous boreholes and wells. The higher estimates may be due enhanced intraborehole flow through the clay made possible by numerous wells screened above and below the flow impeding clay unit (Phillips et al., 2007; Williamson et al., 1989; Belitz and Phillips, 1995). In order to simulate the predevelopment hydrogeologic conditions, a hydraulic conductivity estimate of lower magnitude (1.9 x 10^{-6} m/d) was chosen for the Corcoran Clay. This value is an average of values determined from laboratory consolidation tests performed on the Corcoran Clay intervals of boreholes within the model domain (summarized by Sneed 2001, Table 3, after Johnson et al., 1968, Table 9). Previous studies have assumed reasonably that the Corcoran Clay unit is isotropic, and so also here the unit is assigned equal vertical and horizontal hydraulic conductivities. Based on the same laboratory consolidation tests used to determine the hydraulic conductivity, the Corcoran Clay was assigned a specific storage of 6.5 x 10^{-4} m^{-1}. The Corcoran Clay was assigned a porosity of 52 % based on values determined by the volumetric flask method in laboratory tests performed on material samples (summarized by Page, 1998, Table 6, after Johnson et al., 1968, Table 5).

Although the upper and lower aquifer zones were assigned generalized constant values over the entire model, materials and subsequent aquifer properties are widely variable over the domain and with depth. Previous studies reveal that the aquifer materials and properties differ on the east side compared to the west side of the valley. This east to west contrast is due to the difference in geology of the source or parent rocks as well as the depositional environments on either side of the valley (characteristics such as transport energy and velocity, distance of travel, and topography). Even within either eastern or western region of the valley the materials are quite variable. Within the Coast Ranges alluvium in the western region of the valley, deposits are coarser (mostly sand and gravel) in the upper parts of the alluvial fans (fan heads) grading outward and downward into finer texture sediments (mostly silt and clay) in the lower and distal parts of the fans (Belitz and Heimes, 1990). Streams channels intersecting the alluvial fans bring with them their own depositional environment and can have differing sediment textures and hydraulic properties than the surrounding materials.

In consistency with characterizing the predevelopment hydrologic system, groundwater pumpage was not incorporated into the model nor is it described here. As mentioned previously, groundwater development has significantly altered the flow system and will continue to be a key issue in the SJV; however this is not part of the natural setting of the flow system.

2.7 Land Surface Subsidence

The San Joaquin Valley is a text book example of widespread land surface subsidence of high magnitudes. The largest volume of anthropogenic triggered land subsidence worldwide is in the Central Valley (Bertoldi et al., 1991). By 1972, the maximum amount of observed subsidence within the SJV since the mid-1920's had reached 8.84 m (~29 ft) (Poland et al., 1975). This maximum reached 9.05 m (~29.7 ft) in 1981 (Ireland, 1986). Subsidence between 1972 and 2004 was measured to be as high as 2.44 m at a point along Highway 198 in the SJV (Steele, 2008). Problems caused by land subsidence include damage to roads, highways and surface water structures (differential settlement, cracks in canals, etcetera), farming problems (damage to irrigation and drainage systems), changing slopes of water channels, changing slopes and courses of natural streams causing unexpected flooding, inordinately high pumping

lifts, changing benchmark elevations (require resurveying for construction and topographic maps), costly pre-compaction of areas susceptible to hydrocompaction before building canals, and numerous well casings failures (Bertoldi et al., 1991; Ireland, 1986 and Poland et al., 1975). According to Williamson et al. (1989), the major causes of land subsidence in the Central Valley in order of significance include:

1. Compaction of the aquifer system caused by lowering of the hydraulic head in the aquifer system (head declines due to heavy ground-water pumpage);

2. Oxidation and compaction of peat soils following land drainage in the Delta region;

3. Hydrocompaction - compaction of moisture-deficient deposits following the application of water at land surface to previously dry sediments;

4. Compaction of deposits below the aquifer system caused by fluid extraction from oil and gas fields; and

5. Deep seated tectonic settling.

Agriculture in the Central Valley began as early as the 1700's through the use of surface water. Man-induced subsidence in the Central Valley began by the middle to late 1800's when the peat soils of the Delta region were drained for cultivation (Williamson et al., 1989). Groundwater development began around 1880, to supplement the surface water supply which had greatly decreased in the SJV due to a drought (Manning, 1967). By 1910, almost the entire SJV surface water supply had been diverted, which created a greater need for groundwater development (Williamson et al., 1989). Irrigation with groundwater in the SJV increased rapidly in the 1920's, and even more so after World War II (Davis and Poland, 1957). The timing for increased use of groundwater coincides with the beginning of aquifer compaction and subsidence in the SJV (1920's). Groundwater pumpage continued to increase through the 1960's and consequently so did subsidence (Bertoldi et al., 1991). Around 1970 subsidence had slowed, attributed to the sharp decline in groundwater pumpage after surface water importation from the Sacramento Valley to the western San Joaquin Valley via the California Aqueduct began in the late 1960's. Subsidence had appeared to cease for a time after 1970, but

resumed again during the 1976-77 drought when heavy groundwater pumpage was needed. Land surface rebound after the 1976-77 drought suggests that subsidence during that period was elastic (Bertoldi et al., 1991). Subsidence has not been documented as extensively since the last major studies in the 1970's and 1980's, however, subsidence is still an issue of concern and as mentioned earlier, point estimates of subsidence as high as 2.44 m have been observed between 1972 and 2004 . The primary cause of significant land subsidence in the SJV is due to compaction of mainly fine grained sediments in the aquifer system due to overdraft of groundwater and subsequent decline in subsurface hydraulic heads.

2.7.1 Mechanics of Subsidence

The principle of effective stress for fully saturated soils presented by Terzaghi is formally defined by the following equation:

$$\sigma' = \sigma - u \qquad (2)$$

where σ' is the effective normal stress on a plane, representing the stress transmitted through the soil skeleton only (effective overburden pressure or grain-to-grain load); σ is the total normal stress on a plane within the soil mass, being the force per unit area transmitted in a normal direction across the plane (geostatic pressure); and u is the pore fluid pressure, being the pressure of the fluid filling the void space between the solid particles (Craig, 1997 and Bertoldi et al., 1991). When groundwater pumping causes the hydraulic head to decline below the preconsolidation stress level, the effective stress (effective load born by grains) increases and the fine-grained sediments compact, releasing water from the aquifer system. Speaking in terms of equation 2, groundwater pumping causes the pore fluid pressure to decrease, with the total normal stress not changing significantly, thereby causing the effective stress to increase.

Chapter 3 Model Development

3.1 Discretization

As stated previously, the model domain is roughly 17,232 km^2. The coarse finite element target size for the model is approximately 3000 m aerially and varies across the domain. The centreline of the major rivers in the domain is refined to approximately 60 m aerially to provide a detailed representation of the main surface water features of concern and the corresponding interaction with the subsurface. Stream element size is targeted at 120 m and is variable throughout the domain. The two-dimensional grid is made up of 36,138 nodes and 71,726 elements. The three-dimensional mesh is made up of 289,104 nodes and 502,082 elements. A close up of the three-dimensional mesh at the outlet of the model is illustrated in Figure 13. The smallest elemental area is roughly 140.9 m^2, while the largest is roughly 7,541,546 m^2 (754.15 km^2).

Vertically, the model is discretized to conform to the primary hydrostratigraphic units: surficial sediments in the unsaturated zone, upper unconsolidated aquifer zone, Corcoran Clay semi-confining unit, and lower unconsolidated aquifer zone. The upper and lower unconsolidated zones are part of one main aquifer, yet are distinguished based on their different material properties such as hydraulic conductivities and level of confinement. The model has a total of 11 layers; 5 layers to represent 5 m of surficial sediments, 3 layers to represent the upper unconsolidated aquifer zone, 1 layer to represent the Corcoran Clay, and 2 layers to represent the lower unconsolidated aquifer zone. There are five 1 m thick surficial layers in the model in order to simulate ET from the root zone. A pseudo thickness of 5 m was assigned to non-clay elements sharing the same layer number as the Corcoran Clay, in order to represent the discontinuity (pinching out) of the clay. These non-clay pseudo elements were assigned material properties identical to that of the respective upper aquifer zone materials above the Corcoran Clay. The finite element prisms in the model were assigned different hydraulic properties based on the major hydrostratigraphic units. The hydraulic properties of the hydrostratigraphic units are discussed in section 2.6.2.

3.2 Subsidence Grid Adjustment

The elevations of the land surface (model top) and the top surface of the Corcoran Clay were adjusted based on estimates of land subsidence. These two top surfaces were raised by an amount based on estimates of subsidence that occurred during two periods; a period prior to the beginning of 1972 and a period from 1972 until present.

3.2.1 Pre-1972

A digitized version of a land subsidence contour map titled "Land Subsidence, 1926-72, Los Banos-Kettleman City area" (Poland et al., 1975, Figure 17, p. H22) was used to provide point subsidence values for the period 1926 to end of 1971. These points represent contours of subsidence, and were interpolated to obtain subsidence estimates for each model node by the method of exponential ordinary kriging, specifying a variable search radius, 5 interpolation points within the search radius, and a 200 m output cell size. The resulting total subsidence values as of 1972 estimated using kriging are shown in Figure 14.

3.2.2 Post 1972

Point measurements of subsidence that occurred from 1972 to 2004 along Highways 152 and 198 were obtained from the California DWR. This data was combined with published point data of subsidence that occurred from 1972 to 1982 (Ireland, 1986, Table 1, p. 31) as well as added soft points, to provide point subsidence values for the period 1972 to present. The point estimates were collectively interpolated to obtain subsidence estimates for each model node by the method of inverse distance weighted to the power of 2, specifying a variable search radius, 11 interpolation points within the search radius, and a 200 m output cell size. Location coordinates for the post 1972 point estimates were obtained by looking up the well number at the DWR website or by looking up the benchmark designation and permanent identifier (PID) on the National Geodetic Survey (NGS) web site.

3.3 Boundary Conditions

HydroGeoSphere is capable of employing numerous boundary conditions to constrain a model, which must be specified in consistent units. The units of parameters specified in this investigation are consistently kilograms (km), metres (m), and days (d). In order to be

consistent, all data incorporated in this model, including boundary conditions, are specified in these units. Long term average rates such as river flow rates, precipitation, and ET are therefore converted to daily estimates. Both subsurface and surface flow boundary conditions are employed in this investigation.

3.3.1 Subsurface Flow Boundary Conditions

In the subsurface domain, the system is bounded by no-flow boundaries. The application of no flow boundary conditions is supported by the assumptions that bedrock bounds the subsurface domain both along the east and west margins of the valley (east and west model bounds) and below the aquifer materials (model bottom), that the bedrock materials are essentially impermeable, and that the north and south ends of the model coincide with groundwater flow divides. Therefore it is assumed no water can enter or exit the subsurface domain except via the land surface.

3.3.2 Surface Flow Boundary Conditions

The flow rates of the major rivers in the model domain were applied as specified volumetric flow rates, a special case of the second-type, Neumann, specified or constant flux boundary condition (Therrien et al., 2007). These specified volumetric flow rates were applied at the corresponding river centreline node where the given river enters the model domain. The values for specified volumetric flow rates are the same as the long term mean inflow rates for the six major rivers introduced in section 2.5.2 and are shown in Table 4.

A critical depth boundary condition was applied at the boundary nodes in the central trough area of the valley on the Northern and Southern boundaries of model to allow water to exit the system. In HydroGeoSphere, critical depth boundary conditions are third-type (Cauchy) boundaries.

Second-type (Neumann) no-flow surface water boundary conditions were applied at the remaining outer boundary nodes (not assigned specified volumetric flow rates or critical depth boundary conditions) which coincide with surface water divides and/or major surface water features.

Precipitation

The spatially variable long term mean precipitation data discussed in section 2.2 was applied as non-uniform rain fall (specified flux) to the element faces at ground surface. Non-uniform rain fall is a second-type, Neumann, specified or constant flux boundary condition (Therrien et al., 2007). Non-uniform implies that the depth of rain fall applied is not constant across the domain but rather varies spatially.

Evapotranspiration (ET)

Specified evaporation boundary conditions were applied to the model surface with flux values equal to the long term average annual potential ET estimates (converted to daily rates) for the various delineated zones within the model. Specified evaporation is a special form of the second-type, Neumann, specified or constant flux boundary condition (Therrien et al., 2007). Actual ET is calculated by the model based on the reference ET (specified evaporation) discussed in section 2.2 and the ET parameters associated with the various vegetation types discussed in section 2.5.3. Water is withdrawn from the root zone via transpiration, and is withdrawn from the root zone and land surface via evaporation. In order to simulate ET distributed vertically through the root zone, there are five 1 m thick surficial layers.

The flow boundary conditions described above contribute to establishing long term steady state flow conditions for the model which can be used as a predevelopment initial condition.

Chapter 4 Results and Discussion

The objective of this modelling investigation is to develop a regional-scale integrated surface-subsurface model at a steady state initial condition of the hydrologic system at predevelopment time. The model was not calibrated (no adjustment of model input parameters such as subsurface hydraulic properties) due the absence of actual data at the modeled point in time. The model is constrained by the boundary conditions discussed in section 3.3 that are considered reasonably representative of the long term average behaviour of the predevelopment system. As explained previously, long term averages of precipitation, potential ET, vegetation parameters, and river flows were applied as boundary conditions for the model.

In the process of obtaining a long term steady state initial condition for this model containing five 1 m surface layers (11 total model layers), an intermediate step involved establishing a long term steady state initial condition for the same model but with only one 5 m surface layer (7 total model layers). As one might expect, the 7 layer model arrives at a steady state condition quite quickly compared to the 11 layer model. The final steady state condition for the 7 layer model serves as the initial condition for the 11 layer model.

4.1 Water Balance

The water balance for the steady state model is summarized in Table 11. The total average annual water balance input is 37,321,731 m^3/d and is comprised of the total river inflow (Q_{S1} of equation 1) and precipitation ($P \cdot A$ of equation 1). The specified mean annual inflow rates for the six major rivers and the total river inflow are summarized in Table 4. The total river inflow of the water balance (Q_{S1}) estimated by HydroGeoSphere matches the sum of the values used as input (Table 4), 23,695,008 m^3/d, and represents about 63.5 % of the total average annual water balance input. The spatially variable long term average distribution of precipitation is shown in Figure 5. When the precipitation rates represented by Figure 5 are multiplied by the receiving areas of the watershed to which they are applied, the resulting flux in is approximately 13,626,723 m^3/d, which represents the precipitation input of the water balance ($P \cdot A$), about 36.5 % of the total average annual water balance input. If one divides

the total precipitation estimated in the water balance by the entire area of the model domain, one will estimate the spatially averaged rate of precipitation to be 0.79 mm/d. The total average annual water balance output for the model is 37,321,730 m^3/d, and is comprised of the total actual evapotranspiration ($ET_S + ET_G$ of equation 1) and the total river outflow (Q_{S2} of equation 1). In an ideal water balance, the total output should be equal to the total input, and the net exchange rate (difference between total input and total out) should be close to zero. For this investigation the net exchange rate is 0.78 m^3/d rounded up to 1 m^3/d. The estimate for the total actual evapotranspiration component of the average annual water balance for the model is 16,737,707 m^3/d. By dividing the total actual ET estimated in the water balance by the entire area of the model domain, one will estimate the spatially averaged rate of actual ET for the entire domain to be 0.97 mm/d. The total actual ET component is about 44.8 % of the total water balance input. The current total river outflow component of the water balance is 20,584,023 m^3/d. The total river outflow component for the 11 layer model is estimated to be about 55.2 % of the total water balance input. Both the rate of subsurface storage and rate of surface storage for the steady state model are equal to zero. The total storage, or net accumulation rate for the steady state model, is therefore also equal to zero. A net exchange rate of 1 m^3/d indicates a good water balance. This difference between input and output is very minor relatively speaking, and represents less than 3 x 10^{-6} % of the total water balance input, a very low magnitude of error.

4.2 Match of Model Results with Estimated Predevelopment Data

As mentioned previously, no attempt was made to calibrate the model or to adjust input parameters to match subsurface heads or match surface flow rates of the model interior or outlet. However, the model does provide a good match between simulated and actual estimated predevelopment water table elevations. Figure 15 illustrates this match by over laying the position of predevelopment water table elevation contours estimated by the US Geological Survey (USGS) based on historical data on top of the water table elevation contours produced by HydroGeoSphere (HGS). The USGS contours were digitized using published maps of predevelopment water table elevation. Both Figure 79 of Planert and Williams (1995), and Figure 11 of Bertoldi et al. (1991) are modifications of Figure 14B of Williamson et al.

(1989), and were used to digitize the USGS predevelopment water table elevation contours. The pattern of water elevation contours produced by HGS is quite similar to that documented by the USGS. The value of USGS water table elevation contours generally lies within the intervals simulated by HGS. From Figure 15, one will note the higher water table elevations (dark blue areas) along the margins of the valley (east and west model edges), in particular the north-east region of the model where the rate of precipitation is more intense. The higher water table elevations at the model margins, lower elevations in the central area is consistent with previous studies describing recharge as primarily occurring at high elevations in the Sierra Nevada and close to where the major rivers enter the valley, as well as the direction of groundwater mainly being towards and along the trough of the valley. The general trend of the water table appears to follow the path of the lower San Joaquin River in the central part of the valley, gently sloping toward the model outlet. This outcome is consistent with previous work that describes the water table in the unaltered setting as following the same general trend as the axis of the valley and being roughly parallel to ground surface (Williamson et al., 1989). At the south-west margin of the model in Figure 15, it is interesting to note the three semi-circular patterns of higher water table elevation contours. The shape of these three semi-circles is quite similar to the shape of the alluvial fans in this same location. By the features described above, one can state with confidence that the predevelopment water table was a subdued reflection of the general surface topography. A scatter plot of estimated versus simulated predevelopment water table elevations is provided in Figure 16. This scatter plot was created by extracting simulated values along each estimated contour line using a sampling interval of roughly 1,000 m. Figure 16 generally indicates a good fit between the estimated and simulated water table elevations. In general, the lower elevation contours ($\leq$ 85.3 m) have better agreement between estimated and simulated values, while the two highest contours have the least agreement. The amount of variation and spread or deviation of simulated values from estimated values appears to be lowest for the three lowest contours and highest for the 61.1 m and 73.2 m contours. The low agreement between estimated and simulated values for the two highest contours may have several causes, including a lack of wells and actual data in these higher elevation areas, lack of time appropriate measurements, approximations in the estimated contours, model assumptions (uniform hydraulic conductivity field, boundary conditions at the southern extent of the

model), and imperfect geo-referencing/locating of estimated contours while digitizing the USGS predevelopment water table elevation maps. One can see some bias in the agreement of the lowest two contours of the water table, the simulated values mostly being higher than the estimated values, possibly due assuming a uniform hydraulic conductivity field. Overall, the fit of simulated water table elevations with actual estimates is good considering that no calibration effort was made and that the actual data set (measurements and locations) for the USGS maps was not available for comparison.

4.3 Groundwater-Surface Water Interaction

The three-dimensional position of the water table is shown in Figure 17. One can see where the water table intersects the ground surface (the clear areas or 'holes' in the blue water table surface), indicating subsurface-surface water interaction. These clear areas occur along the entire paths of all the rivers, as well as along the banks of the SJR north of the Merced River right up to the model outlet. These areas of subsurface-surface water interaction are visible in a similar manner in Figure 15.

The simulated surface water depth at a steady state initial condition is shown in Figure 18. The surface water depth simulated by HGS for this model range from less than 1 mm to 6.2 m. One can see from the pools of surface water along the SJR between the Fresno and Merced Rivers in Figure 18 that the surface water from the San Joaquin River (SJR) does flood the land surface south of where it meets the Merced River, confirming the presence and cause of large freshwater marshes in the trough of the valley claimed by others (Gronberg et al., 1998; Katibah, 1984; Warner and Hendrix, 1985). The pools of surface water shown in Figure 18 are also fairly consistent with the location of historical wetlands as shown in the historical map of natural vegetation circa 1874 (California State University at Chico et al., 2003), Figure 10. The outline of the wetland areas in Figure 10 has been overlain in Figure 18 and Figure 19 for quick comparison. From Figure 18, one can observe that the model has roughly simulated parts of 2 out of 3 major wetland areas within the domain without attempting to refine the mesh or adjust model elevations in these areas. One could therefore state that the pools of surface water along the SJR north of the Merced River right up to the model outlet are consistent with the historical presence of wetlands. Note that the locations of simulated surface water features

in Figure 18 are consistently within the areas of where the water table intersects the ground surface (clear areas) indicated in Figure 15 and Figure 17. Finally, from Figure 18, one can observe that the presence and path of the major rivers in the domain are well defined, and are simulated by the model fairly well wherefore Figure 18 has good agreement with the actual locations of the major rivers as shown in a number of the figures in this investigation.

The simulated surface-subsurface water exchange flux at ground surface for the steady state initial condition is shown in Figure 19. The red, orange, and pink shaded spots represent areas of the domain where water is exiting the subsurface into the surface and/or atmosphere. The green, yellow, and light and dark blue shaded spots represent areas of the domain where water is entering the subsurface from the surface. The majority of the domain is green shaded, implying that a minimal level of water (greater than 0.1 mm/d and less than 1 mm/day) is entering the subsurface across the majority of the modeled area. It is likely that this minimal amount of water entering the subsurface (via precipitation) gets used up via evapotranspiration as it enters the root zone, and therefore the exchange flux is not an exact estimate of recharge. A large proportion of the river reaches (where visible) in the model appear to be losing reaches (water in the river channel is lost by infiltration to the subsurface) at rates roughly between 10 and over 100 mm/d, as indicated by the dark blue shaded areas. Some of the wide stretches of light blue areas (flux into the ground between 1 and 10 mm/d) are consistent with areas of surface water flooding and pooling indicated by Figure 18, as well as with areas of higher precipitation (north-east region of model) indicated by Figure 5. There are some significant portions of the river reaches that appear to be gaining reaches (water enters the river channel by exfiltrating from the subsurface) at rates roughly between 1 and 100 mm/d, indicated by the pink shaded areas. The most visible areas of groundwater exfiltration are the middle reaches of the Tuolumne River, followed by the middle reaches of the Merced River, then the lower parts of the other tributary rivers where they meet the SJR, and finally small scattered parts of the SJR itself within the valley trough and near the model outlet. Note that the most significant areas of simulated water exchange flux at ground surface in Figure 19 are generally consistent with the locations of simulated surface water features in Figure 18, and thereby also generally

consistent with the areas where the water table intersects the ground surface indicated in Figure 15 and Figure 17.

The simulated vertical Darcy fluxes at the bottom of the root zone (5.5 m bgs) for the steady state initial condition is shown in Figure 20. This figure represents the flux of water flowing into the root zone from the material below (red and pink shaded areas), as well as the flux of water flowing out of the root zone into the material below (yellow, green, and blue shaded areas). The areas where water appears to enter the root zone from below (red and pink shaded areas) appear to be quite large, at times surrounding entire areas of groundwater-surface water interaction in Figure 15, and surrounding areas of moderate downward flux in Figure 20 and Figure 19 (wetland areas of Figure 18), and at other times matching up well with areas of gaining river reaches shown in Figure 19. The areas of upward flux into the root zone vary at rates roughly between 0.01 to 50 mm/d. As conceded to above, areas of downward flux in Figure 20 generally agree location wise (at lower rates) with areas of downward flux in the central areas of Figure 19 along many reaches of the rivers and in the pooled surface water features (wetland areas) along the banks of the SJR, and are also generally consistent with the location of wetland areas in Figure 18. Due to the less prominent presence of the large upward fluxes at ground surface, one may infer that water entering the root zone from below is being taken out of the subsurface domain largely through ET, and to a lesser extent through exfiltration to surface water features. This confirms previous claims that most groundwater exiting the subsurface was discharged as ET in the trough of the valley, and to a lesser extent, to streams during predevelopment times (Gronberg et al., 1998). The presence of large upward fluxes at the bottom of the root zone is consistent with claims that artesian conditions and upward vertical gradients were present in the trough of the valley during predevelopment times (Hall, 1889; Mendenhall et al., 1916; Planert and Williams, 1995). Minor infiltration past the root zone into the lower material appears to occur throughout the majority of the model area at very low rates between 0.01 and 0.1 mm/d, which is much less than the spatially averaged rate of precipitation (0.79 mm/d). Minimal infiltration suggests that much of the water that enters the subsurface via precipitation is used up by ET. The dark blue shaded areas in Figure 20 (consistent location wise with that of Figure 19) indicate the most significant areas of

infiltration past the root zone, occurring very noticeably along the upper reaches of the major rivers after they enter the model domain. The location of recharge simulated by HGS (dark blue areas) is consistent with that documented by previous investigations (Gronberg et al., 1998, and Belitz and Heimes, 1990). Infiltration past the root zone due to losing river reaches occurs at rates roughly between 10 and 100 mm/d.

One can surmise that Figure 15 through Figure 20 are generally consistent and describe the complex hydrologic processes, features and conditions that are characteristic of the San Joaquin Valley in its natural setting. From these plots, one can gather that much of the wetland areas simulated by the model are actually areas of downward infiltration of flooded surface water, as opposed to areas of groundwater exfiltration which is commonly assumed.

Figure 21 shows the spatial distribution of actual ET across the model domain as simulated by HGS, with the majority of actual ET rates being between 0.5 and 1 mm/d. As described in section 4.1, the spatially averaged rate of actual ET is 0.97 mm/d; this is consistent with that shown in Figure 21, and much lower than the estimates of potential ET for this area which range from 3.42 to 4.35 mm/d as shown in Figure 6. The moisture deficit of the SJV on an annual basis is simulated by the model wherefore the spatially averaged actual ET (0.97 mm/d) is less than the spatially averaged rate of precipitation (0.79 mm/d). The higher rates of ET occur in areas of open water such as river channels and wetland areas. Significant rates of ET also occur in areas where the upward vertical flux of water into the root zone is high as shown in Figure 20. Significant rates of ET also occur in areas where precipitation is higher (north-east region of model shown in Figure 5). The complex role of actual ET as a major component in the water balance, and the significant impacts of ET on other hydrologic processes in the root zone (such as removing large amounts of water as it enters the root zone from above and below) has important implications for the overall model results. This emphasises the need for vertical mesh refinement within the root zone in order to simulate the complex processes occurring there.

The need for an integrated model is shown by the ability of HydroGeoSphere to successfully resolve the predevelopment water balance and to capture the dynamics of the complex

groundwater-surface water interactions occurring in this hydrologic system, particularly by simulating the gaining and losing reaches of the major rivers in agreement with the historic recharge-discharge relationship documented by others, by simulating the significant processes occurring within the root zone, and the match of simulated water table elevations with documented historical data.

4.4 Potential Sources of Discrepancy

There are a few potential sources of discrepancy between the simulation results and documented historical hydrologic conditions. The major discrepancies include that between the simulated and estimated water table elevations, and that between the simulated and mapped presence of historical wetlands. The possible causes of discrepancy in estimating the predevelopment water table was discussed previously in section 4.2. The quality of model assumptions, in particular the simplified and uniform hydraulic conductivity field applied to the subsurface units, as well as the southern model extent boundary conditions may explain the discrepancy between the simulation results and documented historical hydrologic conditions. Perhaps applying different boundary conditions at the southern model boundary (Kings River and the historical Tulare Lake) or changing the southern extent of the model (increasing or decreasing) would yield a better replication of historical wetlands and a better fit between simulated and estimated water table elevations. Other possible sources of discrepancy include the averaging of data for model input (river flows, precipitation rates, evapotranspiration rates, rooting depths, LAI), inaccuracies in forming river channel cross-sections from elevation data, not attempting to discretize the Fresno Slough (axial back water feature between SJR and southern model boundary), adjustments to model elevations to account for large magnitudes of land surface subsidence, the empirical method of representing evapotranspiration processes, and the appropriateness of evapotranspiration parameters from literature. Perhaps increasing the specified rooting depth to 5 m for zones assigned shallower depths (particularly wetland areas) would result in better replication of historical wetlands wherefore less water would be removed from the uppermost surficial layer.

4.5 Future Applications

Transient simulations were not performed in this investigation. However, this steady state initial condition has been shown to be a reasonable representation of the predevelopment hydrologic condition, capturing the essence of the complex groundwater-surface water characteristics in the natural setting of the San Joaquin Valley. This steady state model is the first step toward developing an integrated hydrologic model of the present day SJV that is capable of estimating and predicting present and future water budgets, hydrologic processes and stresses. The recommended next step is to use this steady state model as the reasonable initial condition for transient runs that bring the model up to the current hydrologic conditions of the San Joaquin Valley.

Chapter 5 Summary and Conclusions

The physically-based surface-subsurface HydroGeoSphere model was successfully applied to examine the regional-scale hydrologic budget of a large portion of the San Joaquin Valley. A steady state model was developed, characterized by historical long term average data assumed to be representative of the natural system. Results indicate that the predevelopment hydrologic condition in the San Joaquin Valley is a complex one. Complex hydrologic processes, including significant groundwater-surface water interaction along the major rivers and within wetland areas formed by flooded surface water, as well as ET and impacted root zone processes were identified in the model domain. Simulation of the complex recharge and discharge relationships in the model domain sheds insight into the hydrologic nature of some historic natural wetlands. Evapotranspiration is a very significant sink of both surface water and groundwater (44.8 % of the water balance input), and has a major impact on hydrologic processes in the root zone. The presence and path of the major rivers in the domain are well defined in the model output and agree well with their actual locations. The model simulates gaining and losing reaches of the major rivers, replicating the historic recharge-discharge relationship documented by others. The general location, formation, and hydrologic processes of some wetlands simulated by the model have a fair agreement with historical records. There is also a fair match between simulated and actual estimated predevelopment water table elevations. Successful simulation of the complex hydrologic processes and features that characterize the predevelopment hydrologic conditions and resolve the water balance of the natural system underscores the necessity of using an integrated model. This steady state model should serve as a reasonable initial condition for future transient runs that bring the model up to current hydrologic conditions capable of estimating present and future water budgets.

Appendix I

Governing processes and equations

Subsurface flow

To capture the complex and transient nature of the variably-saturated subsurface flow regime, Richards' equation is used to approximate flow of groundwater in both the saturated and unsaturated zones in the presence of a passive gas phase. Richards' equation is given as:

$$-\nabla \cdot (\mathrm{q}) + \sum \Gamma_{\mathrm{ex}} \pm \mathrm{Q}_{\mathrm{G1,G2}} = \mathrm{S_W S_S} \frac{\partial \psi}{\partial \mathrm{t}} + \frac{\partial (\phi \mathrm{S_w})}{\partial \mathrm{t}} \quad (3)$$

where $\nabla = (\partial/\partial x, \partial/\partial y, \partial/\partial z)$, Γ_{ex} is the volumetric fluid exchange rate between the subsurface and all other domains within the model [$L^3/L^3/T$], $Q_{G1,G2}$ is a source/sink term due to enforcement boundary conditions [$L^3/L^3/T$], S_W is the water saturation [–], S_S is the specific storage [L^{-1}], ψ is the pressure head of water [L], ϕ is the porosity [–], and q is the Darcy flux of water [L/T] given as:

$$\mathrm{q} = -\mathrm{K} \cdot \mathrm{k_{rw}} \nabla(\psi + z) \quad (4)$$

where K is the hydraulic conductivity tensor [L/T], $\mathrm{k_{rw}}$ is the relative permeability of the water phase [–], and z is the elevation. Note that the right hand side of Eq. (I-1) is the equivalent of ΔS_G in Eq. (2-1). All subsurface units are assumed to have capillary-pressure and relative permeability versus water saturation relationships based on Van Genuchten (1980) as:

$$\mathrm{S_W} = \mathrm{S_{W_r}} + \left(1 - \mathrm{S_{W_r}}\right)\left[1 + |\alpha\psi|^{\beta}\right]^{-\nu} \quad \text{for } \psi < 0$$

$$\mathrm{S_W} = 1 \quad \text{for } \psi > 0 \quad (5)$$

with $\mathrm{S_{W_r}}$ being the residual water saturation, and

$$\mathrm{k_{rw}} = \mathrm{S_e}^{1/2}\left[1 - \left(1 - \mathrm{S_e}^{1/\nu}\right)^{\nu}\right]^2 \quad (6)$$

and

$$S_e = \frac{S_W - S_{W_r}}{1 - S_{W_r}} \tag{7}$$

Note, however, that the HydroGeoSphere model allows for other forms of the above constitutive relationships, including the use of tabulated data.

Overland flow

Surface water flow is represented by the two-dimensional depth-averaged diffusion-wave approximation to the Saint Venant equation. The assumptions inherent in the approximation include neglecting inertial terms, depth-averaged flow velocities, a hydrostatic vertical head distribution, mild stream bed slopes, and a dominant bottom shear stress. The resulting equation is written as:

$$-\nabla \cdot (d_s q_s) - d_s \Gamma_s \pm Q_s^w = \frac{\partial(\phi_s h_s)}{\partial t} \tag{8}$$

where d_s is the depth of surface water flow [L], $h_s (= z_s + d_s)$ is the water surface elevation [L] and z_s is the stream bed elevation [L], Γ_s is the volumetric fluid exchange rate between the surface and all other domains within the model [$L^3/L^3/T$], ϕ_s is the surface water domain "porosity" [–] and varies from unity in a stream to zero over rills, uneven surfaces and other obstructions, Q_s^w is the surface water withdrawal shown in Eq. (1) and the right hand side of Eq. (I-8) is the equivalent of ∇S_S in Eq. (1), and q_s is the flux of water [L/T] given as:

$$q_s = K_s \cdot k_{rs} \nabla (d_s + z_s) \tag{9}$$

where k_{rs} is the relative permeability of the surface water domain [–], and K_s is the conductivity [L/T] which is derived using Manning's formula:

$$K_{S_{xx}} = \frac{d_s^{2/3}}{n_{xx}} \cdot \frac{1}{(\partial h_s / \partial s)^{1/2}}, \; K_{S_{yy}} = \frac{d_s^{2/3}}{n_{yy}} \cdot \frac{1}{(\partial h_s / \partial s)^{1/2}}, \; K_{S_{xy}} = K_{S_{yx}} = 0 \tag{10}$$

where s is the length along the direction of maximum slope [L], and n_{xx} and n_{yy} are Manning's coefficients [$T/L^{1/3}$].

A non-linear critical depth boundary condition is used along part of the perimeter of the surface water domain. The advantage of this boundary condition is that it neither constrains the flow rate nor the surface water depth along the perimeter where it is applied. Instead, discharge leaving the domain is allowed to vary naturally throughout a given simulation period depending on the calculated depth of water along the perimeter. This boundary condition can be written as:

$$Q_s^w = \sqrt{g\, d_s^3} \tag{11}$$

Depression storage and storage exclusion

The overland flow and channel flow equations are modified to account for depression storage and obstruction storage exclusion for the more realistic cases when surface water flow does not occur over a flat plane. The height of storage within obstructions could be things such as stones, vegetation, crops, buildings and structures. Depression storage accounts for the unevenness of the ground surface including rills, furrows, microtopographic relief, and other detention features. The storage effects of depression storage and obstruction storage exclusion are modeled by assuming that the geometry of depressions and exclusions combined has a maximum height and that the horizontal area covered by surface-water varies between zero at land surface (defined here as the bottom of the depressions) and increases towards unity (full area) as the water level rises up to a maximum height, h_s [L], defined by:

$$h_s = h_{ds} + h_{os} \tag{12}$$

where h_{ds} [L] is the height of depression storage or rill storage (the height at which overland flow starts to occur), and h_{os} [L] is the height of storage within obstructions. This theory is illustrated in Figure 3 of Panday and Huyakorn (2004). Only if the flow of water is high enough to completely cover the obstructions and completely fill depressions (if height of water reaches h_s), is the full area available for flow and storage of water

Interception and evapotranspiration

Interception is the first process to reduce the amount of precipitation reaching the surface, and involves the retention of precipitation on leaves, branches, and stems of vegetation or on buildings and structures in urban areas. The interception process is simulated using the bucket model whereby precipitation in excess of interception storage and evaporation from interception reaches the ground surface. The interception storage ranges from zero to S_{int}^{max} [L] according to:

$$S_{int}^{max} = C_{int} LAI \tag{13}$$

where LAI is the leaf area index [–] and C_{int} is the canopy storage parameter [L]. In the context of the San Joaquin Valley, LAI represents the cover of leaves over the ground surface and changes from season to season dependant on climate. Constant mean LAI's were applied to achieve the predevelopment initial condition. LAI is also spatially variable based on the different vegetation zones. Spatial and temporal changes in LAI are accommodated by the HydroGeoSphere model.

Evapotranspiration is rigorously modeled as a combination of plant transpiration (E_T) and of evaporation (E_{SG}), and affects both surface and subsurface flow domains. Transpiration from vegetation occurs within the root zone of the subsurface which may be above or below the water table. The rate of transpiration (E_T) is estimated using the following relationship that distributes the net capacity for transpiration among various factors (Kristensen and Jensen, 1975):

$$E_T = [f_1(LAI)][f_2(\theta)][RDF(L_r)]\left[E_p - E_{can}\right] \tag{14}$$

where, $f_1(LAI)$ is the vegetation term [–], $f_2(\theta)$ is the moisture content term [–], $RDF(L_r)$ is the time-varying root distribution function, E_p is the potential evapotranspiration [L/T], and E_{can} is the canopy evaporation [L/T] of water held in interception storage. The vegetation term is a function of the leaf area index and is expressed as:

$$f_1(LAI) = \max\{0, \min[1, (C_2 + C_1 LAI)]\} \tag{15}$$

The function f_1 effectively relates the plant transpiration rate in a linear manner to the leaf area index. The root zone density function $RDF(L_r)$ [–] acts to cumulatively distribute the water extracted from the root zone (for the purpose of plant transpiration E_T) over the entire depth of the root zone L_r. In general, more water is extracted near the ground surface where the density of roots is greatest, while the least amount of water extracted at the bottom where the root density is the least. The moisture content term $f_2(\theta)$ [–] is defined as:

$$f_2(\theta) = \begin{cases} 0 & \text{for } 0 \le \theta \le \theta_{wp} \\ 1 - \left[\frac{\theta_{fc} - \theta}{\theta_{fc} - \theta_{wp}}\right]^{C_3/E_p} & \text{for } \theta_{wp} \le \theta \le \theta_{fc} \\ 1 & \text{for } \theta_{fc} \le \theta \le \theta_o \\ 1 - \left[\frac{\theta_{an} - \theta}{\theta_{an} - \theta_o}\right]^{C_3/E_p} & \text{for } \theta_o \le \theta \le \theta_{an} \\ 0 & \text{for } \theta_o \le \theta \end{cases} \quad (16)$$

where C_1, C_2 and C_3/E_p are dimensionless fitting parameters; θ_{fc}, θ_{wp}, θ_o and θ_{an} are the soil moisture contents at field capacity, wilting-point, oxic limit and anoxic limit, respectively. The function f_2 relates plant transpiration E_T to the moisture content of the subsurface surrounding the root zone. Below the wilting-point moisture content, transpiration is zero. Transpiration then increases to a maximum at the field capacity moisture content. This maximum is maintained up to the oxic moisture content, beyond which the transpiration rate decreases to zero at the anoxic moisture content. When the moisture content exceeds the anoxic limit, the roots become inactive due to a lack of aeration. It is clear that the function f_2 and RDF couple E_T to the subsurface moisture content θ, given as ϕS_w in Eq. (I-1), in a non-linear manner.

The potential evapotranspiration (E_p) may be derived from pan measurements or computed from vegetation and climatic factors (solar radiation, wind speed, relative humidity and air temperature) using the Penman–Monteith (PM) equation for vegetated surfaces (Monteith, 1981). The potential evapotranspiration is specified at the start of a simulation, for further use in determining the actual evapotranspiration. In this case, potential evapotranspiration estimates are calculated by CIMIS (California Department of Water Resources, 2009) which employs a modified version of the PM equation (Pruitt and Doorenbos, 1977) and a wind

function developed at the University of California at Davis (California Department of Water Resources, 2009).

Additional evaporation of water E_{SG} [L/T] from the surface and subsurface domains occurs if the potential evapotranspiration has not been met by the above process of plant transpiration and canopy evaporation. In this case, we assume that additional evaporation occurs along with transpiration due to extraterrestrial radiation energy penetrating the vegetation cover and evaporation of water from the soil surface and subsurface soil layers. This process is described by:

$$E_{SG} = \alpha^{*}\left[E_p - E_{can}\right][1 - f_1(LAI)]EDF(B_{soil}) \tag{17}$$

where α^{*} is a wetness factor given as:

$$\alpha^{*} = \begin{cases} (\theta - \theta_{e2})/(\theta_{e1} - \theta_{e2}) & \text{for } \theta_{e2} \le \theta \le \theta_{e1} \\ 1 & \text{for } \theta > \theta_{e1} \\ 0 & \text{for } \theta < \theta_{e2} \end{cases} \tag{18}$$

where θ_{e1} is the moisture content at the end of the energy limiting stage (above which full evaporation can occur), and θ_{e2} is the limiting moisture content below which evaporation is zero. Eq. (I-15) relates the moisture availability from the subsurface domain. For the surface domain, a* ranges from unity when the depth of surface water flow d_s is above depression storage, and linear decreases to zero as d_s falls below the height of depression storage as the surface water elevation reaches the ground surface elevation. This reflects the decreased contribution of flowing and pooled water at the surface to evaporation. The term $EDF(B_{soil})$ cumulatively distributes E_{SG} vertically between the surface and subsurface domains, to a maximum prescribed depth below the ground surface B_{soil} [L]. Once again, multiple layers of nodes are placed within the depth B_{soil} to resolve the non-linear interaction between E_{SG} and θ.

Written Copyright Permission for Figure 2 of thesis

U.S. Geological Survey. Information Policies and Instructions. Accessible: <http://www.usgs.gov/laws/info_policies.html>

Copyrights and Credits

USGS-authored or produced data and information are considered to be in the U.S. public domain. While the content of most USGS Web pages is in the U.S. public domain, not all information, illustrations, or photographs on our site are. Some non USGS photographs, images, and/or graphics that appear on USGS Web sites are used by the USGS with permission from the copyright holder. These materials are generally marked as being copyrighted. To use these copyrighted materials, you must obtain permission from the copyright holder under the copyright law.

When using information from USGS information products, publications, or Web sites, we ask that proper credit be given. Credit can be provided by including a citation such as the following:

Credit: U.S. Geological Survey

Department of the Interior/USGS

U.S. Geological Survey/photo by Jane Doe (if the photographer/artist is known)

Additional information on Acknowledging or Crediting USGS as Information Source is available.

Policy - For relevant USGS policy on copyrights and trademarks, refer to the Survey Manual chapter entitled, "Use of Copyrighted Material in USGS Information Products."

Contact - If you have questions concerning the use of USGS information, contact the Office of Communications.

U.S. Geological Survey. USGS Visual Identity System. Accessible:

<http://www.usgs.gov/visual-id/credit_usgs.html>

Acknowledging or Crediting USGS as Information Source

Revised May 10, 2006

Most U.S. Geological Survey (USGS) information resides in the public domain and may be used without restriction. There is no legal requirement for users to acknowledge or credit USGS as the source for public domain information, but they may wish to do so as a courtesy. If you wish to acknowledge or credit USGS as an information source of data or products, use a line of text as shown in the guidance below.

If you are an outside organization that has a cooperative partnership or contractual agreement with the USGS that will result in the creation of various information products and you plan to use the trademarked USGS identifier, refer to http://www.usgs.gov/visual-id/outside_use.html for guidance.

When Using USGS Information at No Cost:

- (Product or data name) courtesy of the U.S. Geological Survey
- (Photograph) courtesy of the U.S. Geological Survey

  Example: dlvg32 software courtesy of the U.S. Geological Survey

Optional Statement

The following statement may be added after an acknowledgment or credit:

The USGS home page is http://www.usgs.gov.

References

Abdul, A.S., 1985. Experimental and Numerical studies of the effect of the capillary fringe on streamflow generation, Ph.D. Thesis, University of Waterloo, Waterloo, Ontario, Canada, 210 p.

Allen, R.G., Pereira, L.S., Raes, D., Smith, M., 1998. Crop Evapotranspiration: Guidelines for computing crop water requirements. FAO Irrigation and Drainage Paper No 56, FAO, Food and Agriculture Organization of the United Nations, Rome, Italy, 300 p.

Andersen, H.E., Hansen, S., Jensen, H. E., 2005. Evapotranspiration from a riparian fen wetland. Nordic Hydrology, v. 36, no. 2, p. 121–135.

August, M., 1997. California Geology 1:750,000. Geospatial Data Presentation Form: vector digital data [GIS polygon shapefile]. U.S. Geological Survey, Reno, NV.

Belitz, K., Heimes, F.J., 1990. Character and evolution of the ground-water flow system in the central part of the western San Joaquin Valley: U.S. Geological Survey Water-Supply Paper 2348.

Belitz, K., Phillips, S.P., 1995. Alternative to agricultural drains in California's San Joaquin Valley—Results of a regional-scale hydrogeologic approach. Water Resources Research, v. 31, no. 8, p. 1845–1862.

Bertoldi, G.L., Johnston, R.H., Evanson, K.D, 1991. Groundwater in the Central Valley, California - A summary report: U.S. Geological Survey Professional Paper 1401-A.

Brekke, L.D., Miller, N.L., Bashford, K.E., Quinn, N.W.T., Dracup, J.A., 2004. Climate change impacts uncertainty for water resources in the San Joaquin River Basin, California. American Water Resources Association, v. 40, no. 1, p. 149-164.

Brush, C.F., Belitz, K., Phillips, S.P., 2004. Estimation of a Water Budget for 1972–2000 for the Grasslands Area, Central Part of the Western San Joaquin Valley, California: U.S. Geological Survey Scientific Investigations Report 2004–5180.

Bull, W.B., 1964a. Geomorphology of segmented alluvial fans in western Fresno County, California: U.S. Geological Survey Professional Paper 352-E, 129 p.

Bull, W.B., 1964b. Alluvial fans and near-surface subsidence in western Fresno County, California: U.S. Geological Survey Professional Paper 437-A, 71 p.

Bull, W.B., Poland, J.F., 1975. Land subsidence due to ground-water withdrawal in the Los Banos-Kettleman City area, California, Part 3. Interrelations of water level change, change in

aquifer-system thickness, and subsidence: U.S. Geological Survey Professional Paper 437-G, 62 p.

Burow, K.R., Shelton, J.L., Hevesi, J.A., Weissmann, G.S., 2004. Hydrogeologic characterization of the Modesto area, San Joaquin Valley California: U.S. Geological Scientific Investigations Report 2004–5232, 54 p.

Burow, K.R., Panshin, S.Y., Dubrovsky, N.M., Van Brocklin, D., Fogg, G.E., 1999. Evaluation of Processes Affecting 1,2-Dibromo-3-Chloropropane (DBCP) Concentrations in Ground Water in the Eastern San Joaquin Valley, California: Analysis of Chemical Data and Ground-Water Flow and Transport Simulations. U.S. Geological Survey Water-Resources Investigations Report 99-4059.

California Department of Water Resources (DWR), 2009. CIMIS – Evapotranspiration – equations. Accessed 8 April 2009.
<http://wwwcimis.water.ca.gov/cimis/infoEtoEquation.jsp>

California Department of Water Resources (DWR), 2009. Bulletin 118 - Groundwater Basin Definition. Accessed 20 April 2009.
<http://www.groundwater.water.ca.gov/bulletin118/basin_maps/definition.cfm>

California Department of Water Resources (DWR), 2003. California's Groundwater, Bulletin 118 - Update 2003. Department of Water Resources, The Resource Agency, and The State of California. Accessed 8 April 2009.
<http://www.dpla2.water.ca.gov/publications/groundwater/bulletin118/Bulletin118_Entire.pdf>

California Department of Water Resources (DWR), 2000. gwbsn250p - Groundwater Basins from CA DWR. Geospatial Data Presentation Form: vector digital data [GIS polygon shapefile].

California Department of Water Resources (DWR), University of California at Davis, Jones, D.W., Snyder, R.L., Eching, S., MacPherson, H.G., 1999. CIMIS Reference Evapotranspiration. Available: <http://www.cimis.water.ca.gov/cimis/images/etomap.jpg>

California Division of Water Resources, 1930. Report to the legislature of 1931 on State water plan: Calif. Dept. Public Works, Div. Water Resources, Bull. 25, 204 p.

California State University at Chico, U.S. Fish and Wildlife, U.S. Bureau of Reclamation, 2003. veg1874cv - Vegetation 1874 Central Valley. Geospatial Data Presentation Form: vector digital data [GIS polygon shapefile]. Chico, CA.

Canadell, J., Jackson, R.B., Ehleringer, J.R., Mooney, H.A., Sala, O.E., Schulze, E.-D., 1996. Maximum rooting depth of vegetation types at the global scale. Oecologia, 108, p. 583–595.

CERES (California Environmental Resources Evaluation System), 2007. The San Joaquin Valley Bioregion - An Overview. California Resources Agency. Accessed 14 March 2009. <http://ceres.ca.gov/geo_area/bioregions/San_Joaquin_Valley/about.html>

Chow, V.T., 1959. Open Channel Hydraulics. McGraw-Hill. New York, NY.

Conley, L.M., Dick, R.I., Lion, L.W., 1991. An Assessment of the Root Zone Method of Wastewater Treatment. Research Journal of the Water Pollution Control Federation, v. 63, no. 3 p. 239-247.

Craig, R.F., 2002. Soil Mechanics. Sixth Edition. Spon Press, New York, NY.

CWIS (California Wetland Information System), 1998. California's Valuable Wetlands. California Resources Agency. Accessed 5 May 2009. <http://ceres.ca.gov/wetlands/introduction/values.html>

Dale, R.H., French, J.J., Wilson Jr., H.D., 1964. The story of ground water in the San Joaquin Valley, California: U.S. Geological Survey Circular 459, 11 p.

Darvishzadeh, R., Skidmore, A., Schlerfa, M., Atzberger, C., Corsi, F., Cho, M., 2008. LAI and chlorophyll estimation for a heterogeneous grassland using hyperspectral measurements. ISPRS Journal of Photogrammetry & Remote Sensing 63 (2008) 409-426.

Davis, G.H., Poland, J.F., 1957. Ground-water conditions in the Mendota-Huron area, Fresno and Kings Counties, California, in Contributions to the hydrology of the United States, 1955: U.S. Geological Survey Water-Supply Paper 1360-G, p. 408-588.

Flay, R.B., 2002. Managing Groundwater Quality and Quantity in the San Joaquin Valley, California: Integrated Strategies for Protecting Groundwater in Arid Regions. Master Thesis. University of California at Berkeley, Berkeley, California, USA.

Gersberg, R.M., Elkins, B.V., Lyon, S.R., Goldman, C.R., 1986. Role of aquatic plants in wastewater treatment by artificial wetlands. Water Res., v. 20, no. 3, p. 363-368.

Gronberg, J.M., Dubrovsky, N.M., Kratzer, C.K., Domagalski, J.L., Brown, L.R., Burow, K.R., 1998. Environmental setting of the San Joaquin-Tulare Basins, California: U.S. Geological Survey Water-Resources Investigations Report 97-4205, 45 p.

Hall, W.H., 1886. Physical data and statistics of California: State Engineering Department of California, 396 p.

Hall, W.H., 1889. Irrigation in California: The National Geographic Magazine, v. 1, no. 4, 14 p.

Hamilton, F., 1916. Geological map of the State of California: California Division of Mines and Geology, 1 sheet, scale, 1:750,000.

Harradine, F.F., 1950. Soils of western Fresno County: Berkeley, University of California Press, 86 p.

Harrington, R., Steinwand, A., Hubbard, P., Martin, D., 2004. Evapotranspiration from Groundwater Dependent Plant Communities: Comparison of Micrometeorological and Vegetation-Based Measurements. A Cooperative Study Final Report Prepared by The County of Inyo Water Department and Los Angeles Department of Water and Power.

Hodgson, A.B., 2001. Characterising wetland plant communities: an analysis of hyperspectral and biophysical relationships in three taxa of wetland macrophytes. Ph.D. Thesis. The Graduate College, University of Nebraska, Lincoln, Nebraska, USA.

Hunt, E.R., 2003. Leaf area index and cover of shortgrass steppe using AVIRIS imagery, Proceedings of the Eleventh JPL Airborne Earth Science Workshop (R.O. Green, editor), 05-08 March 2002, Pasadena, California (Jet Propulsion Laboratory, National Aeronautics and Space Administration, Pasadena, California).

Hussey, B., Odum, W.E., 1992. Evapotranspiration in Tidal Marshes. Estuaries, v. 15, no. 1, p. 59-67.

HydroGeoLogic, 2000. MODHMS: a comprehensive MODFLOW-based hydrologic modeling system. Version 1.1. Code Documentation and User's Guide. HydroGeoLogic Inc., Herndon, VA, USA.

Ireland, R.L., 1986. Land subsid-ence in the San Joaquin Valley, California, as of 1983: U.S. Geological Survey Water-Resources Investigations Report 85-4196, 50 p.

Ireland, R.L., Poland, J.E, Riley, F.S., 1984. Land subsidence in the San Joaquin Valley, California, as of 1980: U.S. Geological Survey Professional Paper 437-1, 93 p., 1 pl. in pocket.

Islam, M.N., 2004. Automated calibration of a physically based hydrologic model to simulate water balance variables for water and crop management. Ph.D. Thesis. University of California at Davis, Davis, California, USA.

Jackson, R.B., Sala, O.E., Paruelo, J.M., Mooney, H.A., 1998. Ecosystem water fluxes for two grasslands in elevated CO2: a modeling analysis. Oecologia, 113, p. 537-546.

Johnson, A.I., 1984. Laboratory tests for properties of sediments in subsiding areas, pt. 1, chap. 4 of Poland, J.F., ed., Guidebook to studies of land subsidence due to ground-water withdrawal: Paris, UNESCO, Studies and Reports in Hydrology 40, p. 55–88.

Johnson, A.I., Moston, R.P., Morris D.A., 1968. Physical and hydrologic properties of water-bearing deposits in subsiding areas in central California: U.S. Geological Survey Professional Paper 497-A, 71 p.

Jones, J.P., 2005. Simulating hydrologic systems using a physically based, surface–subsurface model: Issues concerning flow, transport and parameterization. Ph.D. Thesis. Department of Earth Sciences, University of Waterloo, Waterloo, Ontario, Canada, 145 pp.

Jones, J.P., Sudicky, E.A. and McLaren, R.G., 2008. Application of a fully-integrated surface-subsurface flow model at the watershed-scale: A case study, Water Resour. Res., v. 44.

Jones, D.W., Snyder, R.L., Eching, S., 1999. etozones. Geospatial Data Presentation Form: vector digital data [GIS polygon shapefile]. Sacramento, CA.

Katibah, E.E, 1984. A brief history of the riparian forests in the central valley of California, in Warner, R.E., and Hendrix, K.M. eds., California Riparian Systems: Ecology, Conservation, and Productive Management: Berkeley, California, University of California Press, p. 23-29.

Kristensen, K.J., Jensen, S.E., 1975. A model for estimating actual evapotranspiration from potential evapotranspiration. Nordic Hydrology, 6, 170–188.

Lee, S.-Y., Carle, S.F., Fogg, G.E., 2007. Geologic heterogeneity and a comparison of two geostatistical models: Sequential Gaussian and transition probability-based geostatistical simulation. Adv. Water Resour., v. 30, p. 1914–1932.

Li, Q., 2006. A physically-based hydrologic model of the Duffins Creek watershed, Ontario, Canada. Master Thesis. Department of Earth Sciences, University of Waterloo, Waterloo, Ontario, Canada, 58 pp.

Li, Q., Unger, A.J.A., Sudicky, E.A., Kassenaar, D., Wexler, E.J., Shikaze, S., 2008. Simulating the multi-seasonal response of a large-scale watershed with a 3D physically-based hydrologic model. Journal of Hydrology (2008) 357, p. 317– 336.

Lofgren, B.E., 1976. Hydrogeologic effects of subsidence, San Joaquin Valley, California: International Symposium on Land Subsidence, 2nd, Anaheim, Calif., December 13-17, program and abstracts, no. 12, unnumbered pages.

Manning, J.C., 1967. Report on ground-water hydrology in the southern San Joaquin Valley. American Water Works Association Journal, v. 59, no. 12, p. 1513-1526.

McGlashin, H.D., Dean, H.J., 1912. Water resources of California Part II, Stream measurements in San Joaquin River Basin: U.S. Geological Survey Water-Supply Paper 299, 439 p.

McLaren, R., 2008. GRID BUILDER – A pre-processor for 2-D, triangular element, finite-element programs. Groundwater Simulations Group, University of Waterloo, Waterloo, Ontario.

Mendenhall, W.C., 1908. Preliminary report on the ground waters of the San Joaquin Valley, California: U.S. Geological Survey Water-Supply Paper 222, 53 p.

Mendenhall, W.C., Dole, R.B., Stabler, H., 1916. Ground water in the San Joaquin Valley, California: U.S. Geological Survey Water-Supply Paper 398, 310 p.

Montaldo, N., Rondena, R., Albertson, J.D., Mancini, M., 2005. Parsimonious modeling of vegetation dynamics for ecohydrologic studies of water-limited ecosystems. Water Resour. Res., 41, W10416.

Monteith, J.L., 1981. Evaporation and surface temperature. Q J R Meteorol Soc 1981; 107:1-27.

Nagler, P., Jetton, A., Fleming, J., Didan, K., Glenn, E., Erker, J., Morino, K., Milliken, J., Gloss, S., 2007. Evapotranspiration in a cottonwood (Populus fremontii) restoration plantation estimated by sap flow and remote sensing methods. Agricultural and Forest Meteorology, 144, p. 95–110.

Nelson, C., Lasagna, B., Holtgrieve, D., Quin, M., 2003. The Central Valley Historic Mapping Project. California State University at Chico, Geographic Information Center and Department of Geography and Planning. Chico, CA.

Page, R.W., 1977. Guide for data collection to calibrate a predictive digital ground-water model of the unconfined aquifer in and near the city of Modesto, California: U.S. Geological Survey Water-Resources Investigations Report 76-41, 46 p.

Page, R.W., 1986. Geology of the fresh ground-water basin of the Central Valley, California with texture maps and sections: U.S. Geological Survey Professional Paper 1401-C, 54 p.

Page, R.W., 1998. A compressible diatomaceous clay, Sacramento Valley, California. "Land Subsidence Case Studies and Current Research: Proceedings of the Dr. Joseph F. Poland Symposium on Land Subsidence".

Page, R.W., Bertoldi, G.L., 1983. A Pleistocene diatomaceous clay and pumiceous ash, Yolo County, California: California Geology, v.36, no.1, p.14-20.

Panday, S., Huyakorn, P.S., 2004. A fully coupled physically-based spatially-distributed model for evaluation surface/subsurface flow. Adv. Water Resour., v. 27, p. 361–382.

Peacock, C.E., Hess, T.M., 2004. Estimating evapotranspiration from a reed bed using the Bowen ratio energy balance method. Hydrological Processes. 18, p. 247–260.

Phillips, S.P., Belitz, K., 1991. Calibration of a Texture-Based Model of a Ground-Water Flow System, Western San Joaquin Valley, California. Groundwater, v. 29, no. 5, p. 702–715.

Phillips, S.P., Green, C.T., Burow, K.R., Shelton, J.L., Rewis, D.L., 2007. Simulation of multiscale ground-water flow in part of the northeastern San Joaquin Valley, California: U.S. Geological Survey Scientific Investigations Report 2007-5009, 43 p.

Planert, M., Williams, J.S., 1995. Central Valley Aquifer System. Ground Water Atlas of the United States. California, Nevada. HA 730-B. Accessed 14 March 2009. <http://capp.water.usgs.gov/gwa/ch_b/B-text3.html>

Poland, J.F., Lofgren, B.E., Ireland, R.L., Pugh, R.G., 1975. Land subsidence in the San Joaquin Valley, California as of 1972: U.S. Geological Survey Professional Paper 437-H, 78 p.

PRISM Group, Oregon State University, 2008. Precipitation (Normals) - Total Precipitation (30-yr average), Annual 1971-2000. Accessed 31 March 2009. <http://www.prismclimate.org> created 23 June 2008.

Pruitt, J., Doorenbos, O.W., 1977. Proceeding of the International Round Table Conference on "Evapotranspiration", Budapest, Hungary.

Quinn, N.W.T., Brekke, L.D., Miller, N.L., Heinzer, T., Hidalgo, H., Dracup, J.A., 2004. Model integration for assessing future hydroclimate impacts on water resources, agricultural production and environmental quality in the San Joaquin Basin, California. Environmental Modelling & Software, 19, p. 305–316.

Quinn, N.W.T., Miller, N.L., Dracup, J.A., Brekke, L.D., Grober, L.F., 2001. An integrated modeling system for environmental impact analysis of climate variability and extreme weather events in the San Joaquin Basin, California. Advances in Enviro. Res., 5, p. 309-317.

Rantz, S.E., compiler, 1969, Mean annual precipitation in the California region: U.S. Geological Survey Basic Data Compilation, scale 1:1,000,000, 11 sheets, 5 p.

Riley, E.S., McClelland, E.J., 1972. Application of the modified theory of leaky aquifers to a compressible multiple-aquifer system: U.S. Geological Survey open-file report, 96 p.

Rocha, A.V., Goulden, M.L., 2008. Large interannual CO2 and energy exchange variability in a freshwater marsh under consistent environmental conditions. J. Geophys. Res., 113, G04019.

San Joaquin Valley Drainage Program, 1990. Fish and wildlife resources and agricultural drainage in the San Joaquin Valley, California: U.S. Department of the Interior, Final report of the San Joaquin Valley Drainage Program, v. 1, 440 p.

Schroeder, P.R., Aziz, N.M., Lloyd, C.M., Zappi, P.A., 1994. The Hydrologic Evaluation of Landfill Performance (HELP) Model: User's Guide for Version 3, EPA/600/R-94/168a, September 1994, U.S. Environmental Protection Agency Office of Research and Development, Washington, DC.

Scurlock, J.M.O., Asner, G.P., Gower, S.T., 2001. Global Leaf Area Index Data from Field Measurements, 1932-2000. Data set. Available on-line [http://www.daac.ornl.gov] from the Oak Ridge National Laboratory Distributed Active Archive Center, Oak Ridge, Tennessee, U.S.A.

Seaber, P.R., Kapinos, F.P., Knapp, G.L., 1987. Hydrologic Unit Maps., US Geological Survey Water Supply Paper 2294.

Sneed, M., 2001. Hydraulic and Mechanical Properties Affecting Ground-Water Flow and Aquifer-System Compaction, San Joaquin Valley, California: U.S. Geological Survey Open-File Report 01-35.

Steeves, P., Nebert, D., 1994. huc250k - 1:250,000-scale Hydrologic Units of the United State. Geospatial Data Presentation Form: vector digital data [GIS polygon shapefile]. U.S. Geological Survey, Reston, VA. Available: < http://water.usgs.gov/lookup/getspatial?huc250k>

Steinwand, A.L., Harrington, R.F., Or, D., 2006. Water balance for Great Basin phreatophytes derived from eddy covariance, soil water, and water table measurements. J. Hydrology, 329, p. 595-605.

Sudicky, E.A., Jones, J.P., Park, Y.-J., Brookfield, A.E., Colautti, D., 2008. Simulating complex flow and transport dynamics in an integrated surface-subsurface modelling framework, Geosciences Journal, 12(2), 16 p.

Swain, E.D., Wolfert, M.A., Bales, J.D., Goodwin, C.R., 2004. Two-Dimensional Hydrodynamic Simulation of Surface-Water Flow and Transport to Florida Bay through the Southern Inland and Coastal Systems (SICS): U.S. Geological Survey Water-Resources Investigations Report 03-4287, 62 p.

Taylor, J.L., 2000. Populus fremontii. In: Fire Effects Information System, [Online]. U.S. Department of Agriculture, Forest Service, Rocky Mountain Research Station, Fire Sciences Laboratory (Producer). Available: http://www.fs.fed.us/database/feis/ [2009, March 2].

Therrien, R., McLaren, R.G., Sudicky, E.A., Panday, S.M., 2007. HydroGeoSphere: a three-dimensional numerical model describing fully-integrated subsurface and surface flow and solute transport, Groundwater Simulations Group, University of Waterloo, Waterloo, Ontario, Canada, 360 p.

U.S. Bureau of Reclamation, 2004. hydro24ca - Selected hydrologic features 1:24,000-scale for California. Geospatial Data Presentation Form: vector digital data [GIS polygon shapefile]. Sacramento, CA.

U.S. Geological Survey (USGS), 1999. National Elevation Dataset. Accessed from: The National Map Seamless Server. Presentation Form: raster digital data [GIS raster files]. Sioux Falls, SD.

VanderKwaak, J.E., 1999. Numerical simulation of flow and chemical transport in integrated surface–subsurface hydrologic systems. Ph.D. Thesis. University of Waterloo, Waterloo, Ontario, Canada, 217 p.

Wang, D., Poss, J.A., Donovan, T. J., Shannon, M.C., Leschw, S.M., 2002. Biophysical properties and biomass production of elephant grass under saline conditions. Journal of Arid Environments, 52, p. 447-456.

Warner, R.E., Hendrix, K.M., 1985. Riparian resources of the Central Valley and California desert: Sacramento, California, California Department of Fish and Game, variously paged.

Weissmann, G.S., Carle, S.F., Fogg, G.E., 1999. Three-dimensional hydrofacies modeling based on soil surveys and transition probability geostatistics. Water Resources Research, v. 35, no. 6, p. 1761–1770.

White, F.M., 2003. Fluid Mechanics. Fifth Edition. McGraw-Hill. New York, NY.

Williamson, A.K., Prudic, D.E., Swain, L.A., 1989. Ground-water flow in the Central Valley, California: U.S. Geological Survey Professional Paper 1401-D, 127 p.

WRCC (Western Regional Climate Center), 2008. California Climate Data Archive. NCDC 1971-2000 Monthly Normals. Accessed 17 April 2009. <http://www.calclim.dri.edu/stationlist.html>

Table 1: Monthly and annual mean weather station temperature from 1971 to 2000.

Time Period	Stockton WSO Mean Temperature [°C]	Fresno WSO AP Mean Temperature [°C]	Five Points 5 SSW Mean Temperature [°C]
January	7.8	7.8	8.5
February	10.6	10.8	11.2
March	12.7	13.1	13.4
April	15.6	16.2	16.2
May	19.3	20.4	20.6
June	22.9	24.5	23.9
July	25.2	27.4	26.3
August	24.7	26.6	25.6
September	22.7	23.7	23.4
October	18.1	18.3	18.7
November	11.7	11.5	12.0
December	7.4	7.3	7.9
Annual	16.6	17.3	17.3

Note:
WRCC (2008), based on NCDC 1971-2000 Monthly Normals From NCDC Station Historical Listing for NWS Cooperative Network
http://www.calclim.dri.edu/stationlist.html

WRCC - Western Regional Climate Center
NWS - National Weather Service
NCDC - National Climatic Data Center

Table 2: Monthly and annual mean weather station precipitation from 1971 to 2000.

Time Period	Stockton WSO Mean Precipitation [mm]	Fresno WSO AP Mean Precipitation [mm]	Five Points 5 SSW Mean Precipitation [mm]
January	68.8	54.9	39.9
February	62.5	53.8	35.8
March	57.9	55.9	36.3
April	24.4	19.3	11.2
May	12.7	9.9	6.6
June	2.3	5.8	3.3
July	1.3	0.3	0.3
August	1.3	0.3	0.8
September	8.4	6.6	7.1
October	20.8	16.5	10.9
November	45.0	27.9	16.0
December	46.2	34.0	19.8
Annual	351.5	285.2	188.0
Daily	0.96	0.78	0.51

Note:

WRCC (2008), based on NCDC 1971-2000 Monthly Normals From NCDC Station Historical Listing for NWS Cooperative Network

http://www.calclim.dri.edu/stationlist.html

WRCC - Western Regional Climate Center
NWS - National Weather Service
NCDC - National Climatic Data Center

Table 3: Comparison of PRISM and historical precipitation data.

Hall (1886)					PRISM Group (2008)[2]
Station Name	**Years Used**	**County**	**Page No.**	**Precipitation [mm/d]**	**Precipitation [mm/d]**
Fresno (Average)	1877-1884	Fresno	185	0.60	0.81
Borden (CPRR Co.)	1875-1884	Fresno[1]	184	0.60	0.82
Kingsburgh (CPRR Co.)	1878-1884	Fresno	185	0.61	0.75
Merced (CPRR Co.)	1871-1884	Merced	188	0.73	0.87
Central Point	1879-1884	Merced	188	0.65	0.69
Stockton (CPRR Co.)	1870-1884	San Joaquin	194	0.96	0.97
Farmington (CPRR Co.)	1876-1884	San Joaquin	194	1.05	0.92
La Grange	1869-1884	Stanislaus	197	1.09	1.00
Grayson	1870-1884	Stanislaus	197	0.82	0.82
Modesto (CPRR Co.)	1870-1884	Stanislaus	197	0.65	0.93

Note: 1 - county name used by Hall (1886), presently called Madera
2 - Extracted from annual average (1971 - 2000)
CPRR Co - Central Pacific Rail Road Company

Table 4: Mean annual river inflow rates over the period from 1878 to 1884.

River	Mean Inflow [m^3/d]	Mean Inflow m^3/s
San Joaquin	7,531,777	87.2
Fresno	407,727	4.7
Chowchilla	373,423	4.3
Merced	3,988,725	46.2
Tuolumne	6,592,159	76.3
Stanislaus	4,801,197	55.6
Total Inflow	23,695,008	274.2

Note: data summarized from Hall (1886)

Table 5: Model area covered by each vegetation type.

Land Cover / Vegetation	Area [km^2]	Percentage of Model Area
Grassland	12,123	70.4
Other Floodplain Habitat	3,584	20.8
Wetland	749	4.3
Riparian	429	2.5
Alkali Desert Scrub	261	1.5
Aquatic	49	0.3
Valley / Foothill Hardwood	36	0.2
Chaparral	1	0.0
Total Model Domain	17,232	100.0

Based on spatial data from California State University at Chico et al. (2003)

Table 6: Dominant plant species for modelled predevelopment vegetation types.

Land Cover	Dominant Species	Common Name
Grasslands	N.A.	Grass
Other Floodplain Habitat	mixture of wetlands, grasslands, and riparian forests	Grass, Trees
Wetlands	Typha spp.	Cattails
	Scirpus spp.	Bullrushes or Tules
	Juncus spp.	Rushes
	Carex spp.	Sedges
Riparian	Platanus racemosa	California Sycamore
	Quercus lobata	Valley Oak
	Populus fremontii	Fremont Cottonwood
	Alnus rhombifolia	White Alder
	Fraxinus latifolia	Oregon Ash
	Salix spp.	numerous species of Willow
	Acer negunde subsp. Californicum	California Box Elder
	Baccharis pilularis ssp consanguinea	Coyotebrush
	Rubus spp.	Blackberries
	Rosa californica	Sand Wild Rose
	various annual/perennial herbaceous sp	-
	Vitus califonica	California Grape
	Toxicodendron diversilobum	Poison Oak
	Aristolochia californica	Dutchman's Pipe
Alkali Desert Scrub	Allenrolfea occidentalis	Iodine Bush
	Suaeda fruticosa	Shrubby Seablite
	frankenia grandifolia	Alkali Heath
	Distichilis spicata	Seashore Saltgrass
	Haplopappus acradenius ssp. Bracteosus	Alkali goldenbush
	Wislizenia californica	California Stink-weed
	Lasthenia chrysantha	Alkali Goldfield
	Puccinellia simplex	California Alkali Grass
	Atriplex spinifera	Spiney Saltbush
	Atriplex phyllostegia	Leafcover Saltbush
	Delphinium recurvatum	Recurved Larkspur
	Hemizonia pungens	Common Spikeweed

Note: sp - species, ssp - subspecies. Source: Nelson et al. (2003). CVHMP.
N.A. - not available

Table 7: ET parameters.

Land Cover	max. LAI	mean LAI	L_r [m]	RDF(L_r)	B_{soil} [m]	EDF(B_{soil})	θ_{e1}	θ_{e2}	θ_{wp}	θ_{fc}	θ_o	θ_{an}	C_{int} [m]	C_1	C_2	C_3/E_p	Source
Grasslands	N.A.	N.A.	0.6	N.A.	N.A.	N.A.	N.A.	N.A.	N.A.	N.A.	N.A.	N.A.	N.A.	N.A.	N.A.	N.A.	Allen et al. (1998)
	N.A.	N.A.	2.6	N.A.	N.A.	N.A.	N.A.	N.A.	N.A.	N.A.	N.A.	N.A.	N.A.	N.A.	N.A.	N.A.	Canadell et al. (1996)
	5	1.71	N.A.	N.A.	N.A.	N.A.	N.A.	N.A.	N.A.	N.A.	N.A.	N.A.	N.A.	N.A.	N.A.	N.A.	Scurlock (2001)
	N.A.	1, 2, 3.5, 5	N.A.	N.A.	N.A.	N.A.	N.A.	N.A.	N.A.	N.A.	N.A.	N.A.	N.A.	N.A.	N.A.	N.A.	Schroeder et al. (1994)
	> 2	N.A.	N.A.	N.A.	N.A.	N.A.	N.A.	N.A.	N.A.	N.A.	N.A.	N.A.	N.A.	N.A.	N.A.	N.A.	Andersen et al. (2005)
	N.A.	2.4	N.A.	N.A.	N.A.	N.A.	N.A.	N.A.	N.A.	N.A.	N.A.	N.A.	N.A.	N.A.	N.A.	N.A.	Jackson et al. (1998)
	5.2 to 3	N.A.	N.A.	N.A.	N.A.	N.A.	N.A.	N.A.	N.A.	N.A.	N.A.	N.A.	N.A.	N.A.	N.A.	N.A.	Wang et al. (2002)
	1.8	N.A.	N.A.	N.A.	N.A.	N.A.	N.A.	N.A.	N.A.	N.A.	N.A.	N.A.	N.A.	N.A.	N.A.	N.A.	Hunt (2003)
	N.A.	N.A.	0.5	N.A.	N.A.	N.A.	N.A.	N.A.	N.A.	N.A.	N.A.	N.A.	N.A.	N.A.	N.A.	N.A.	Montaldo et al. (2005)
	7.34	2.76	N.A.	N.A.	N.A.	N.A.	N.A.	N.A.	N.A.	N.A.	N.A.	N.A.	N.A.	N.A.	N.A.	N.A.	Darvishzadeh et al. (2008)
	-	2	2.6	linear	2.6	linear	N.A.	N.A.	N.A.	N.A.	N.A.	N.A.	N.A.	N.A.	N.A.	N.A.	Selected for this study
Wetlands	8.4	6.34	N.A.	N.A.	N.A.	N.A.	N.A.	N.A.	N.A.	N.A.	N.A.	N.A.	N.A.	N.A.	N.A.	N.A.	Scurlock (2001)
	N.A.	1.394	0.3	N.A.	N.A.	N.A.	N.A.	N.A.	N.A.	N.A.	N.A.	N.A.	N.A.	N.A.	N.A.	N.A.	Hussey and Odum (1992)
	3.5 to 6	N.A.	N.A.	N.A.	N.A.	N.A.	N.A.	N.A.	N.A.	N.A.	N.A.	N.A.	N.A.	N.A.	N.A.	N.A.	Rocha (2008)
	N.A.	N.A.	0.5	N.A.	N.A.	N.A.	N.A.	N.A.	N.A.	N.A.	N.A.	N.A.	N.A.	N.A.	N.A.	N.A.	Andersen et al. (2005)
	N.A.	N.A.	0.3, 0.6, 0.76	N.A.	N.A.	N.A.	N.A.	N.A.	N.A.	N.A.	N.A.	N.A.	N.A.	N.A.	N.A.	N.A.	Conley et al. (1991) after
	3.39 to 5.71	N.A.	N.A.	N.A.	N.A.	N.A.	N.A.	N.A.	N.A.	N.A.	N.A.	N.A.	N.A.	N.A.	N.A.	N.A.	Peacock and Hess (2004)
	N.A.	2.64	N.A.	N.A.	N.A.	N.A.	N.A.	N.A.	N.A.	N.A.	N.A.	N.A.	N.A.	N.A.	N.A.	N.A.	Hodgson (2001)*
	N.A.	2.64	0.76	linear	0.76	linear	N.A.	N.A.	N.A.	N.A.	N.A.	N.A.	N.A.	N.A.	N.A.	N.A.	Selected for model
Riparian	5, 10.5	3.1 to 3.8	N.A.	N.A.	N.A.	N.A.	N.A.	N.A.	N.A.	N.A.	N.A.	N.A.	N.A.	N.A.	N.A.	N.A.	Nagler et al. (2007)
	N.A.	N.A.	3 to 5	N.A.	N.A.	N.A.	N.A.	N.A.	N.A.	N.A.	N.A.	N.A.	N.A.	N.A.	N.A.	N.A.	Taylor (2000)
	N.A.	3.5	5	cubic	5	cubic	N.A.	N.A.	N.A.	N.A.	N.A.	N.A.	N.A.	N.A.	N.A.	N.A.	Selected for this study
Alkali Desert Scrub	1.35	N.A.	N.A.	N.A.	N.A.	N.A.	N.A.	N.A.	N.A.	N.A.	N.A.	N.A.	N.A.	N.A.	N.A.	N.A.	Steinwand et al. (2006)
	N.A.	0.397	2	N.A.	N.A.	N.A.	N.A.	N.A.	N.A.	N.A.	N.A.	N.A.	N.A.	N.A.	N.A.	N.A.	Harrington et al. (2004)
	N.A.	1.35	2	linear	2	linear	N.A.	N.A.	N.A.	N.A.	N.A.	N.A.	N.A.	N.A.	N.A.	N.A.	Selected for this study
Other Floodplain	N.A.	2.71	5	cubic	5	cubic	N.A.	N.A.	N.A.	N.A.	N.A.	N.A.	N.A.	N.A.	N.A.	N.A.	Selected for this study
Entire Domain	N.A.	N.A.	N.A.	N.A.	N.A.	N.A.	$\phi \cdot 0.32$	$\phi \cdot 0.2$	$\phi \cdot 0.2$	$\phi \cdot 0.32$	$\phi \cdot 0.76$	$\phi \cdot 0.9$	N.A.	0.3	0.2	N.A.	Panday and Huyakorn (2004)
	N.A.	N.A.	N.A.	N.A.	N.A.	N.A.	N.A.	N.A.	N.A.	N.A.	N.A.	N.A.	0.05	0.31	0.2	N.A.	Islam (2004)
	N.A.	N.A.	N.A.	N.A.	N.A.	N.A.	$\phi \cdot 0.32$	$\phi \cdot 0.2$	$\phi \cdot 0.2$	$\phi \cdot 0.32$	$\phi \cdot 0.76$	$\phi \cdot 0.9$	0.05	0.31	0.2	N.A.	Li et al. (2008)
	N.A.	N.A.	N.A.	N.A.	N.A.	N.A.	$\phi \cdot 0.5$	$\phi \cdot 0.1$	$\phi \cdot 0.05$	$\phi \cdot 0.2$	$\phi \cdot 0.6$	$\phi \cdot 0.8$	0.04	0.5	0	1	Therrien et al. (2007)
	N.A.	N.A.	N.A.	N.A.	N.A.	N.A.	N.A.	N.A.	0.13	0.28	N.A.	N.A.	N.A.	N.A.	N.A.	N.A.	Schroeder et al. (1994)
	N.A.	N.A.	N.A.	N.A.	N.A.	N.A.	$\phi \cdot 0.32$	$\phi \cdot 0.2$	$\phi \cdot 0.2$	$\phi \cdot 0.32$	$\phi \cdot 1$	$\phi \cdot 1$	0	0.3	0.2	1	Selected

Note: moisture content, $\theta = \phi \cdot S_W$; N.A. - not available; * average for Typha and Schoenoplectus over full range from Hodgson (2001) Table 3.1

Table 8: Overland flow parameters.

Overland Zone	Land Cover	n_{xx} , n_{yy} [$d/m^{1/3}$]	h_{ds} [m]	h_{os} [m]	Source
1	Grasslands	4.05×10^{-7}	N.A.	N.A.	Chow (1959)
		4.05×10^{-7}	0.01	0	Selected for this study
2	Other Floodplain Habitat	1.07×10^{-6}	N.A.	N.A.	Mean (zones 1 & 2)
		1.07×10^{-6}	0.01	0	Selected for this study
3	Wetlands	5.32×10^{-6}	N.A.	N.A.	Swain et al. (2004)
		5.79×10^{-7}	N.A.	N.A.	Jones (2005)
		5.79×10^{-7}	0.01	0	Selected for this study
4	Riparian	1.74×10^{-6}	N.A.	N.A.	Chow (1959)
		N.A.	N.A.	2	mean (grass, shrub, tree)
		1.74×10^{-6}	0.01	0	Selected for this study
5	Alkali Desert Scrub	5.79×10^{-7}	N.A.	N.A.	Chow (1959)
		5.79×10^{-7}	0.01	0	Selected for this study
6	River Channel	4.05×10^{-7}	N.A.	N.A.	White (2003)
		4.05×10^{-7}	2.0×10^{-3}	0	Selected for this study

Note: N.A. - not available

Table 9: Groundwater sub-basin numbers and names.

Sub-basin Number	Sub-basin Name
5-22.01	Eastern San Joaquin
5-22.02	Modesto
5-22.03	Turlock
5-22.04	Merced
5-22.05	Chowchilla
5-22.06	Madera
5-22.07	Delta-Mendota
5-22.08	Kings
5-22.09	Westside

Note: Groundwater basin data from California Department of Water Resources (DWR).

Table 10: Subsurface hydraulic properties.

Material / Unit	K_{xx}, K_{yy} [m/d]	K_{zz} [m/d]	ϕ	S_s (m^{-1})	S_{Wr}	α [m^{-1}]	β	Source
Upper aquifer zone	33.90	0.09	N.A.	N.A.	N.A.	N.A.	N.A.	Phillips et al. (2007)
	N.A.	N.A.	0.35	3.05×10^{-6}	N.A.	N.A.	N.A.	Ireland et al. (1984)
	N.A.	N.A.	N.A.	N.A.	0.18	1.90	6.00	Abdul (1985)
	33.90	0.09	0.35	3.05×10^{-6}	0.18	1.90	6.00	Selected for this study
Corcorran clay	N.A.	N.A.	0.52	N.A.	N.A.	N.A.	N.A.	Page (1998) after Johnson et al. (1968)
	N.A.	N.A.	0.55	N.A.	N.A.	N.A.	N.A.	Page and Bertoldi (1983)
	1.30×10^{-3}	1.30×10^{-3}	N.A.	N.A.	N.A.	N.A.	N.A.	Phillips et al. (2007)
	N.A.	3.35×10^{-5}	N.A.	N.A.	N.A.	N.A.	N.A.	Page (1998) after Page and Bertoldi (1983)
	N.A.	1.0×10^{-6} to 3.0×10^{-6}	N.A.	N.A.	N.A.	N.A.	N.A.	Page (1977)
	N.A.	1.6×10^{-4}	N.A.	N.A.	N.A.	N.A.	N.A.	Belitz and Phillips (1995)
	N.A.	1.90×10^{-6}	N.A.	6.5×10^{-4}	N.A.	N.A.	N.A.	Sneed (2001) after Johnson et al. (1968)
	1.90×10^{-6}	1.90×10^{-6}	0.52	6.5×10^{-4}	N.A.	N.A.	N.A.	Selected for this study
Lower aquifer zone	26.43	0.08	N.A.	N.A.	N.A.	N.A.	N.A.	Phillips et al. (2007)
	N.A.	N.A.	0.35	3.05×10^{-6}	N.A.	N.A.	N.A.	Ireland et al. (1984)
	N.A.	N.A.	N.A.	1.08×10^{-5}	N.A.	N.A.	N.A.	Sneed (2001) after Bull and Poland (1975)
	26.43	0.08	0.35	3.05×10^{-6}	N.A.	N.A.	N.A.	Selected for this study

Note: N.A. - not available

Table 11: Water balance for model at steady state initial condition.

Water Budget Component	Flux [m^3/d]	% of Total In
Q_{S1}	23,695,008	63.5
Q_{S2}	20,584,023	55.2
$P \cdot A$	13,626,723	36.5
$(ET_S + ET_G) \cdot A$	16,737,707	44.8
$(\Delta S_S + \Delta S_G)\Delta t$	0	0.0
Total In ($Q_{S1} + P \cdot A$)	37,321,731	100.0
Total Out ($Q_{S2} + ET_S + ET_G$)	37,321,730	100.0
In – Out (Net Exchange rate)	1	0.0

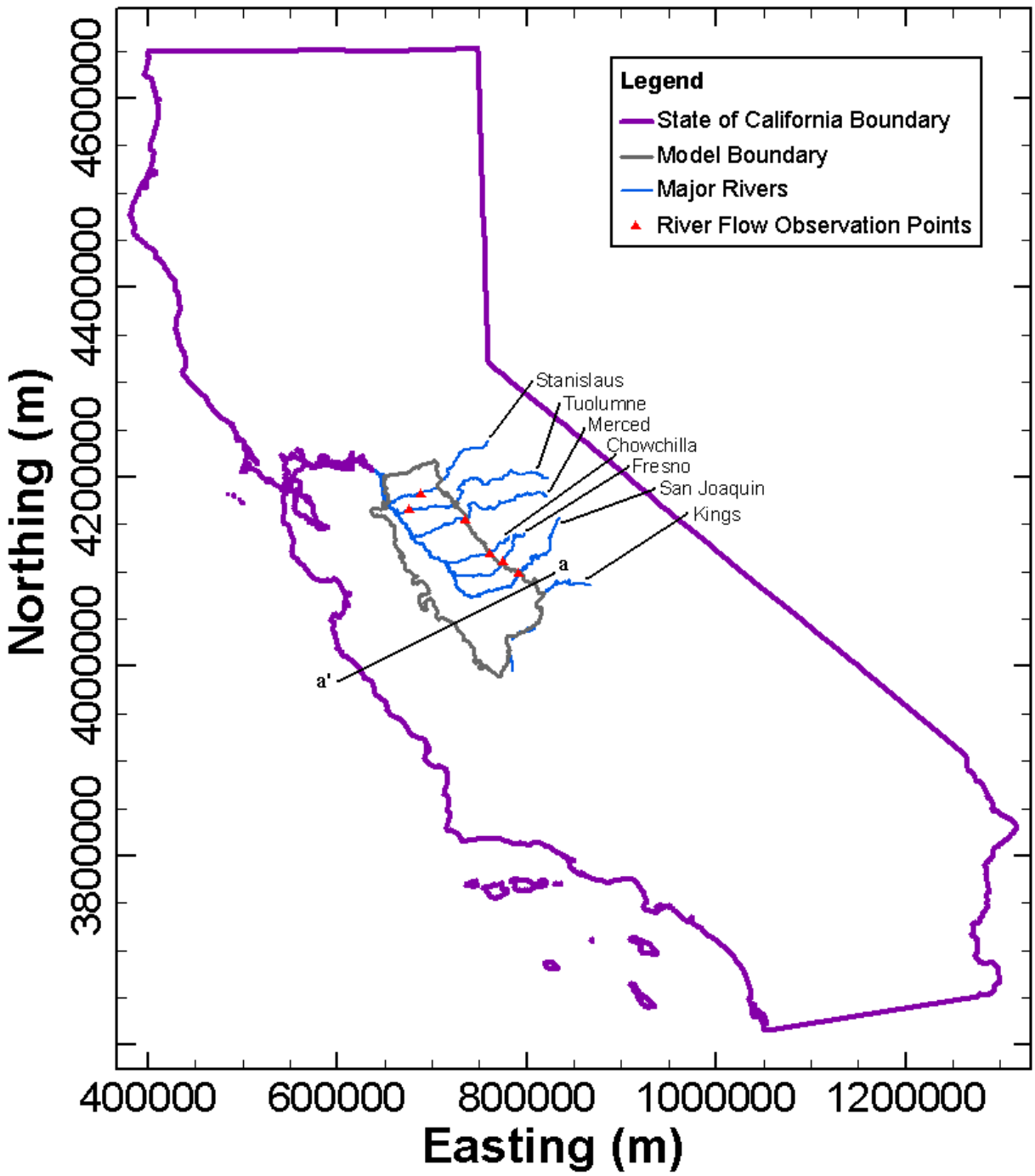

Figure 1: Study area location and model boundary.

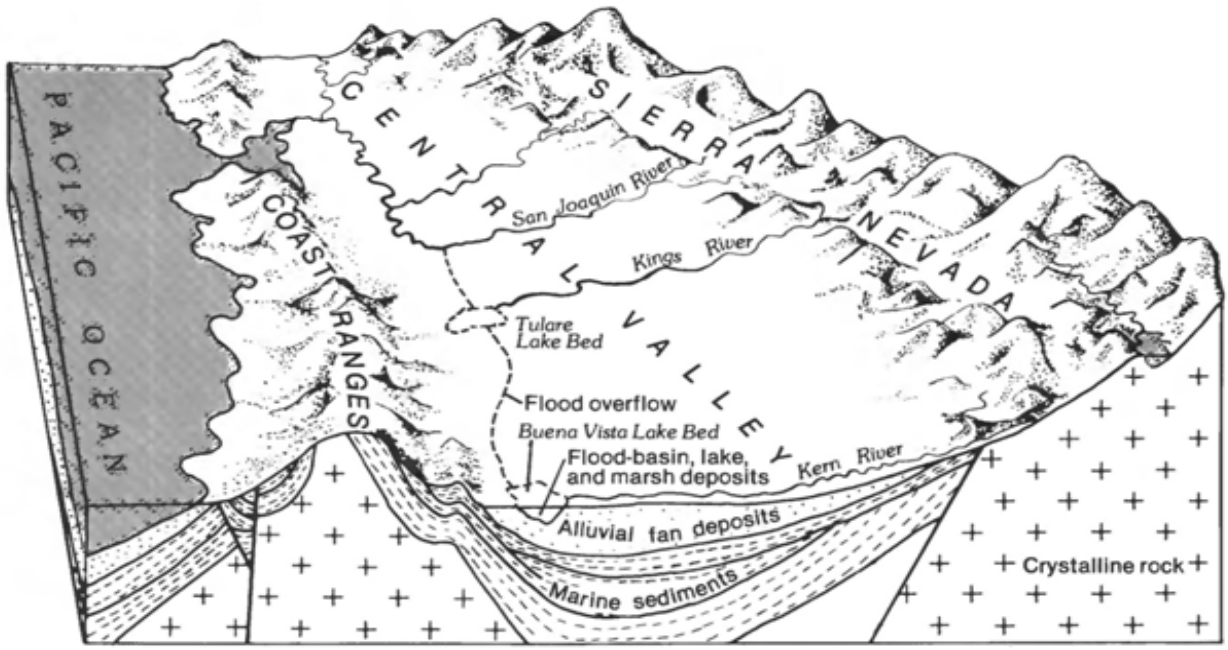

Credit: U.S. Geological Survey
Department of the Interior/USGS
U.S. Geological Survey/illustration by Page (1986, fig.3) after Dale et al. (1964, fig.7)
Illustration courtesy of the U.S. Geological Survey
http://www.usgs.gov

Figure 2: Conceptual diagram of San Joaquin Valley and generalized geologic cross-section.

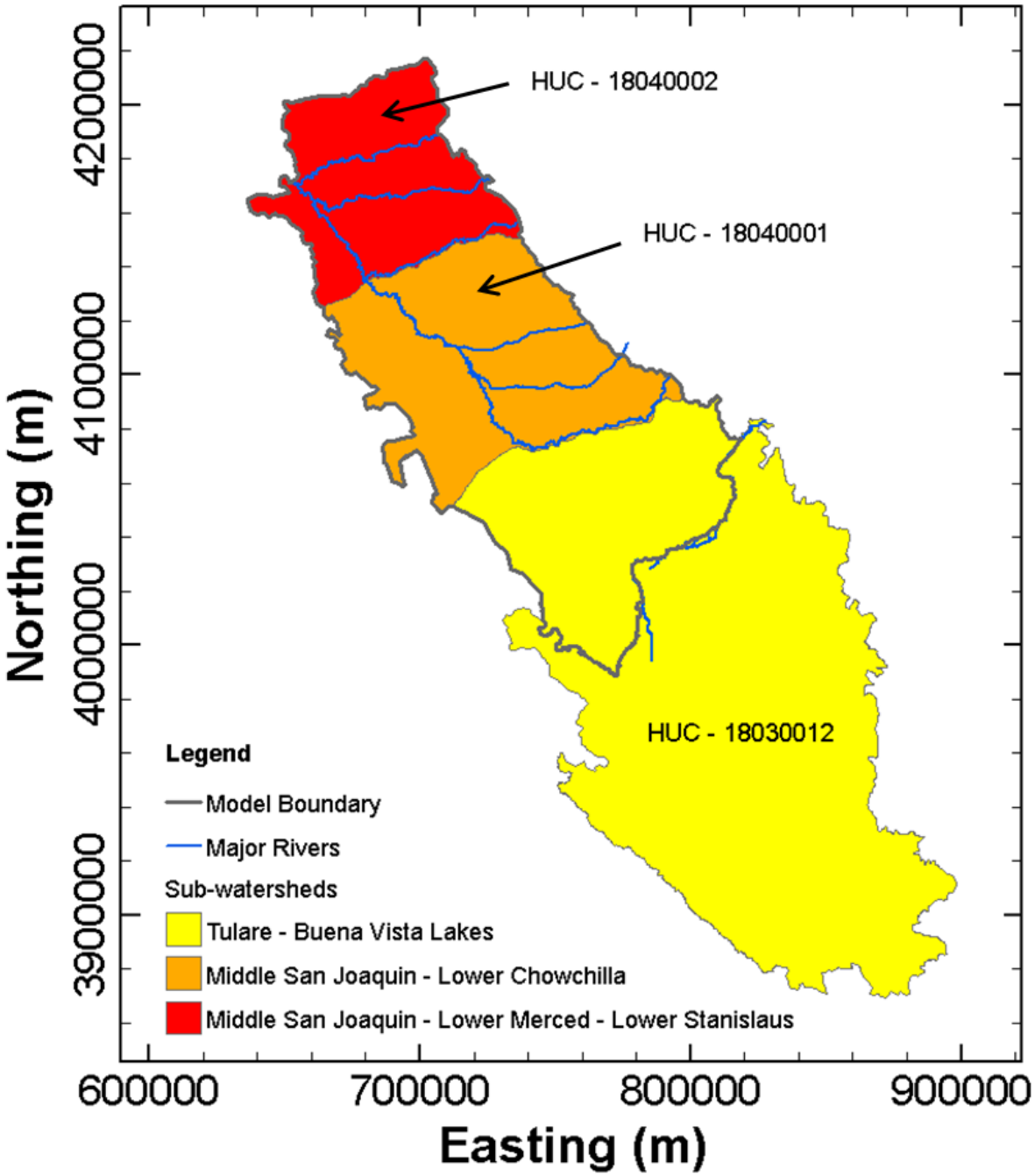

Figure 3: Model and sub-watershed boundaries [using spatial data from Steeves and Nebert (1994)].

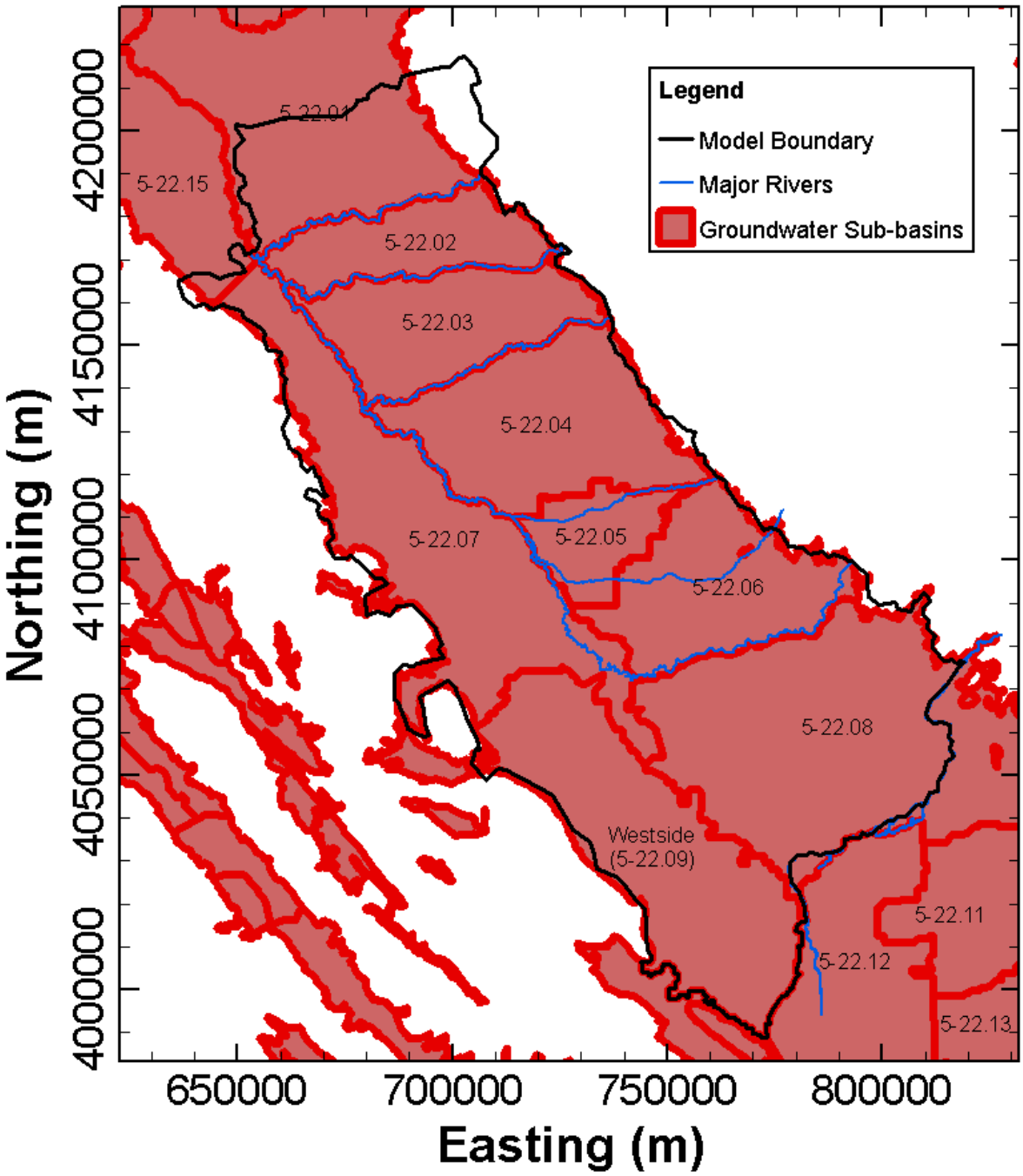

Figure 4: Model and groundwater sub-basin boundaries [using spatial data from California Department of Water Resources (2000)].

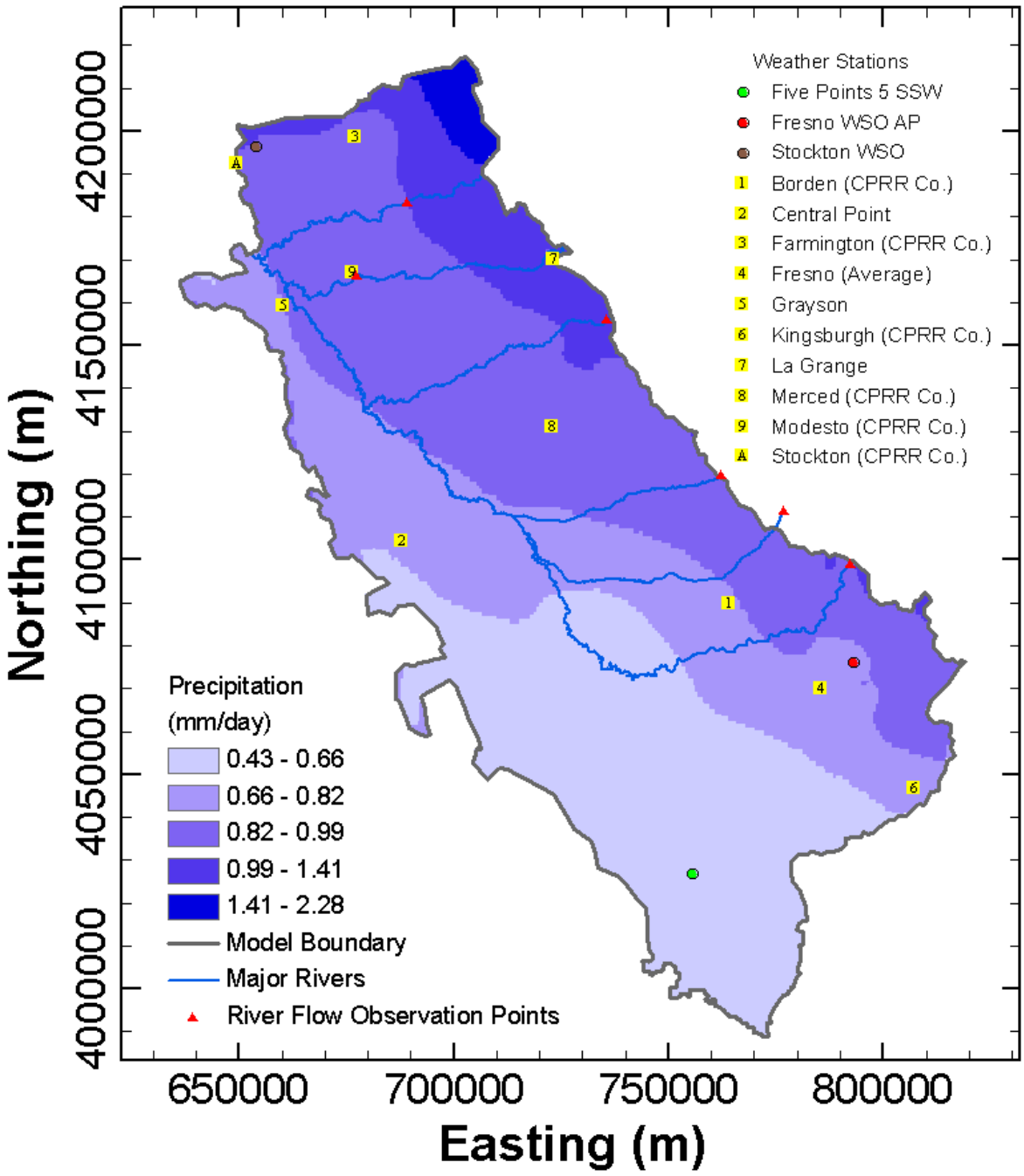

Figure 5: Average annual precipitation and weather station locations [using spatial data from PRISM Group (2008)].

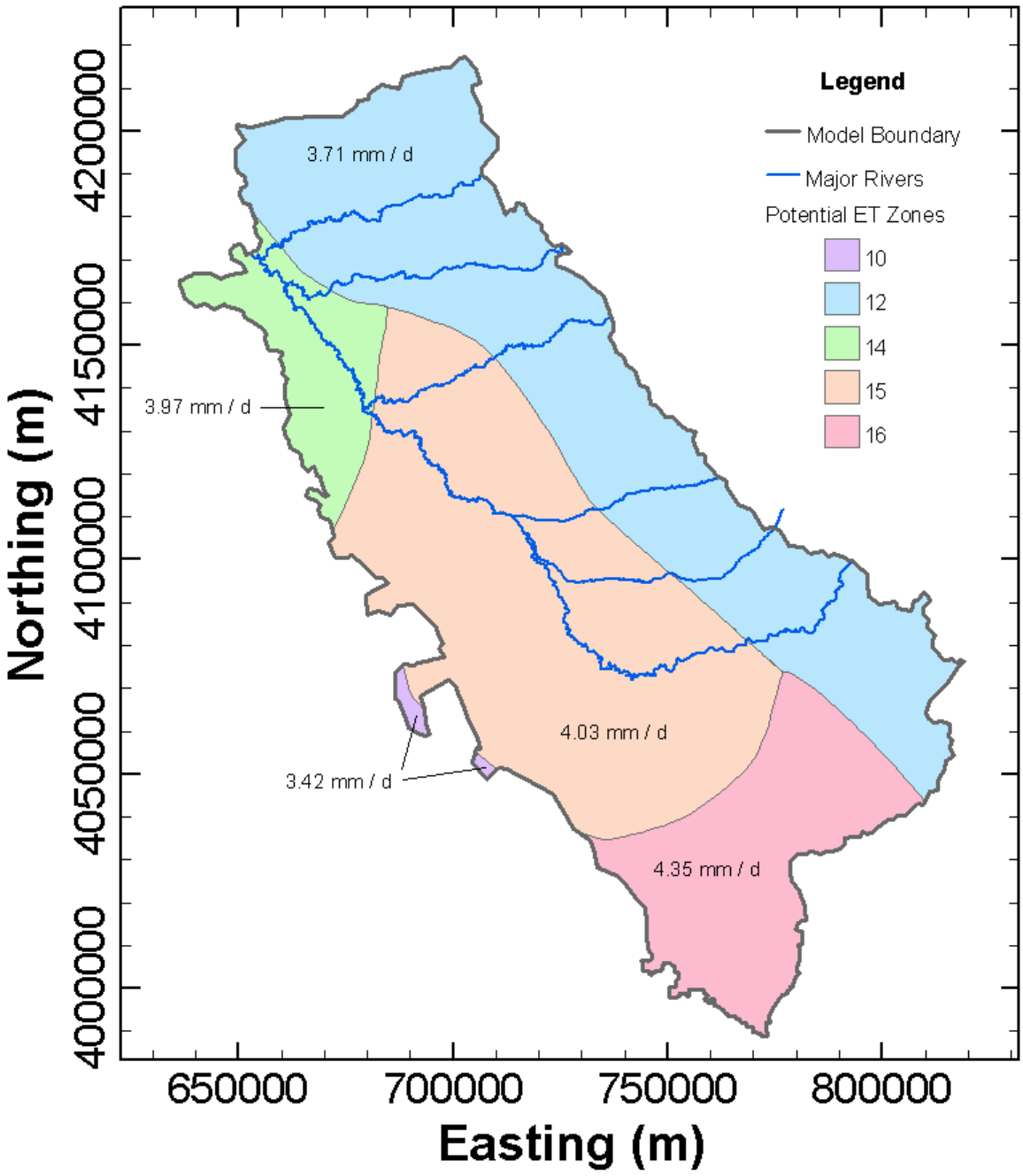

Figure 6: Potential ET zones and rates occurring in the model domain [using spatial data from Jones et al. (1999)].

Where zone 10 is North Central Plateau & Central Coast Range, zone 12 is East Side Sacramento-San Joaquin Valley, zone 14 is Mid-Central Valley, Southern Sierra Nevada, Tehachapi & High Desert Mountains, zone 15 is Northern & Southern San Joaquin Valley, and zone 16 is Westside San Joaquin Valley & Mountains East & West Of Imperial Valley.

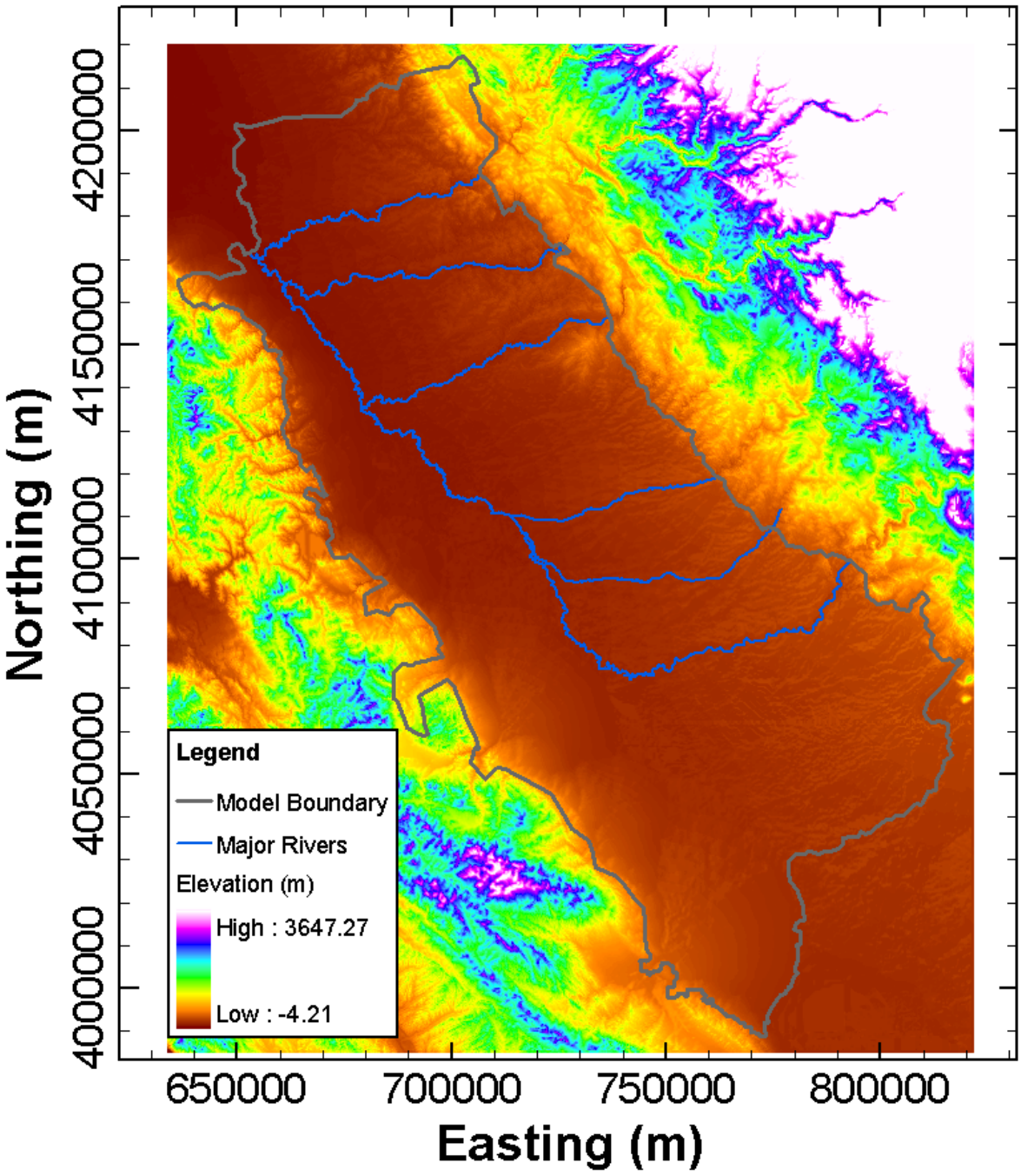

Figure 7: Present day topographic elevations for the modelled area [using spatial data from U.S. Geological Survey (1999)].

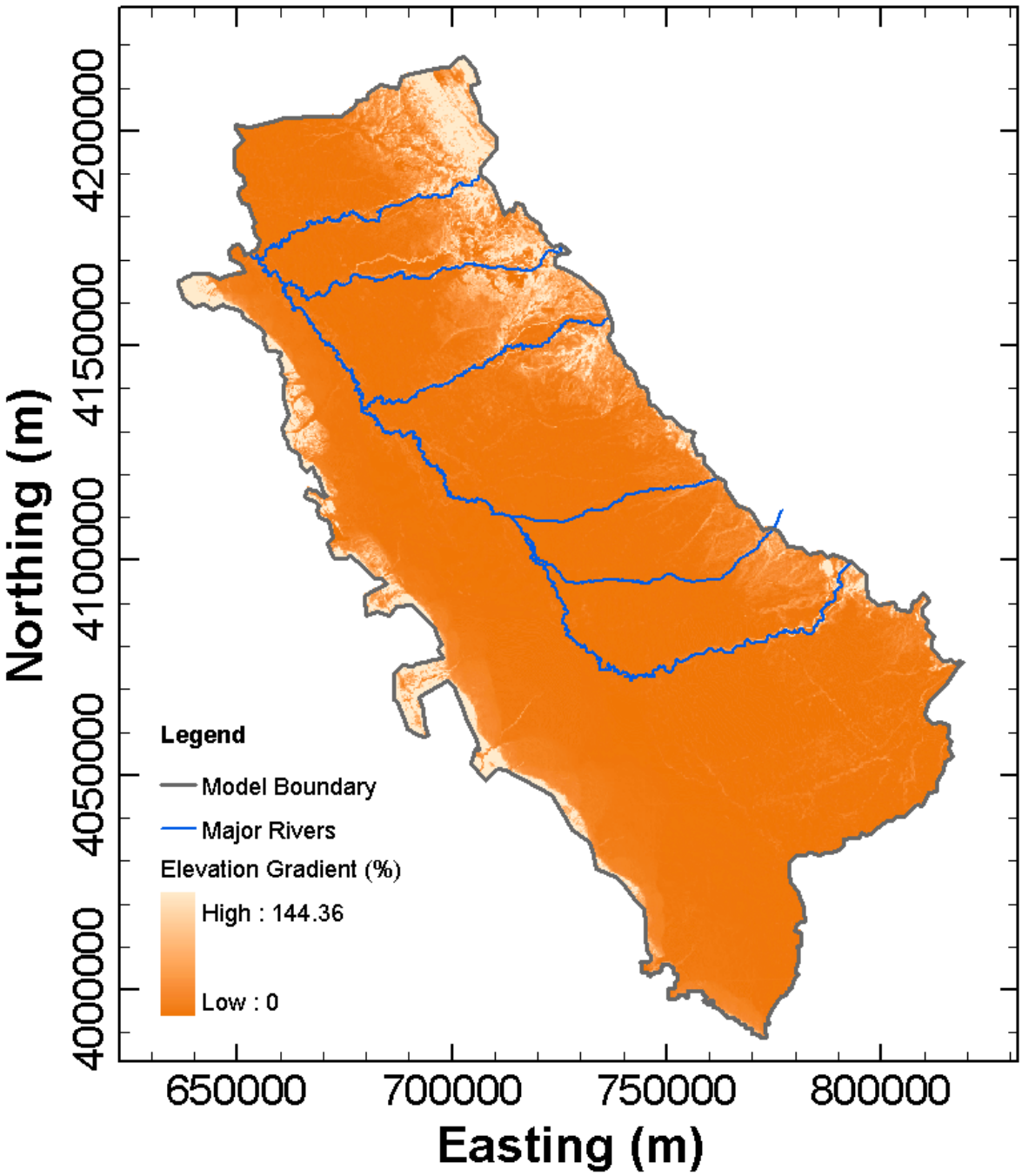

Figure 8: Present day elevation gradients (surface slope) across the model domain [calculated using spatial data from U.S. Geological Survey (1999)].

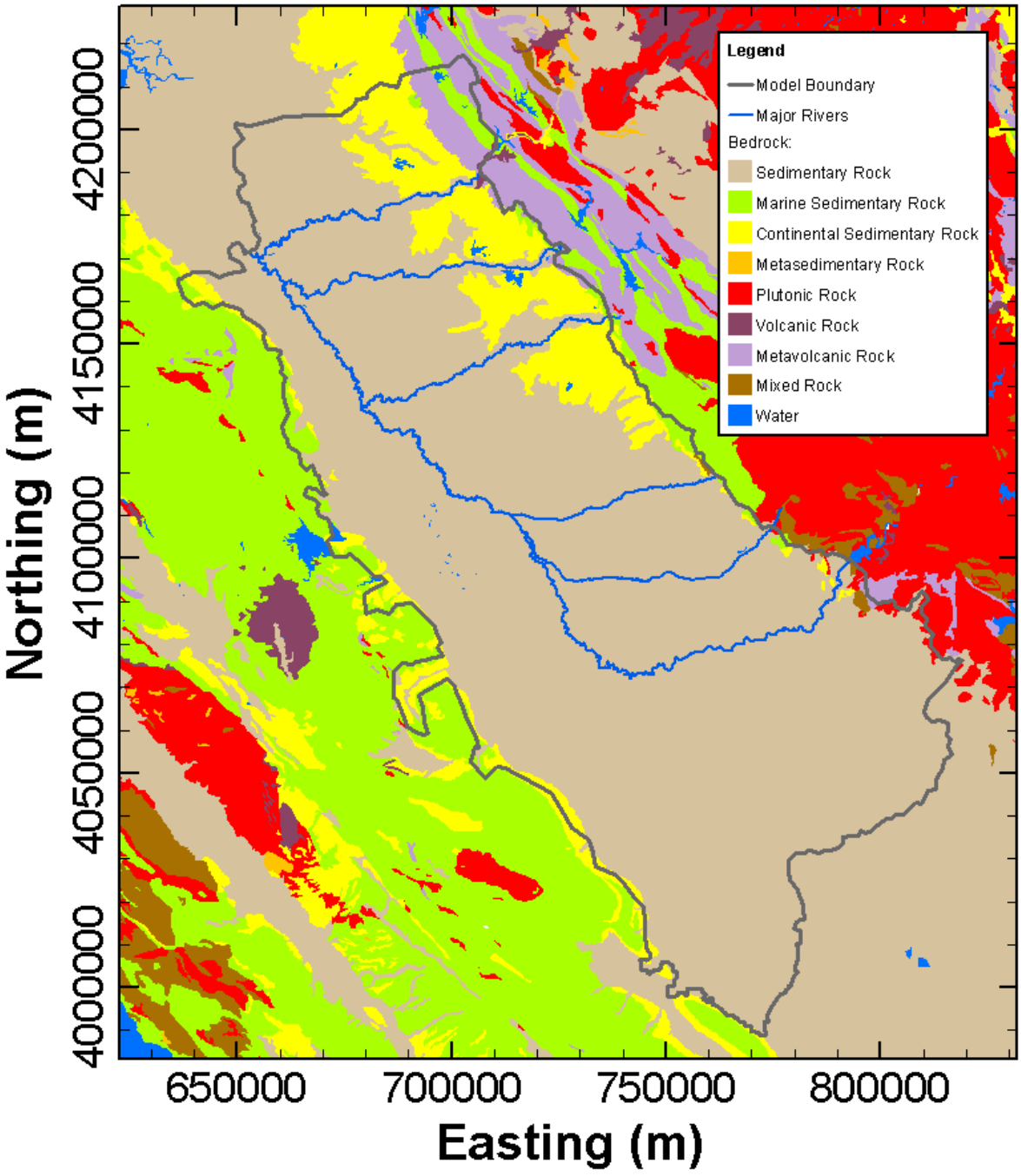

Figure 9: Bedrock geology [using spatial data from August (1997)].

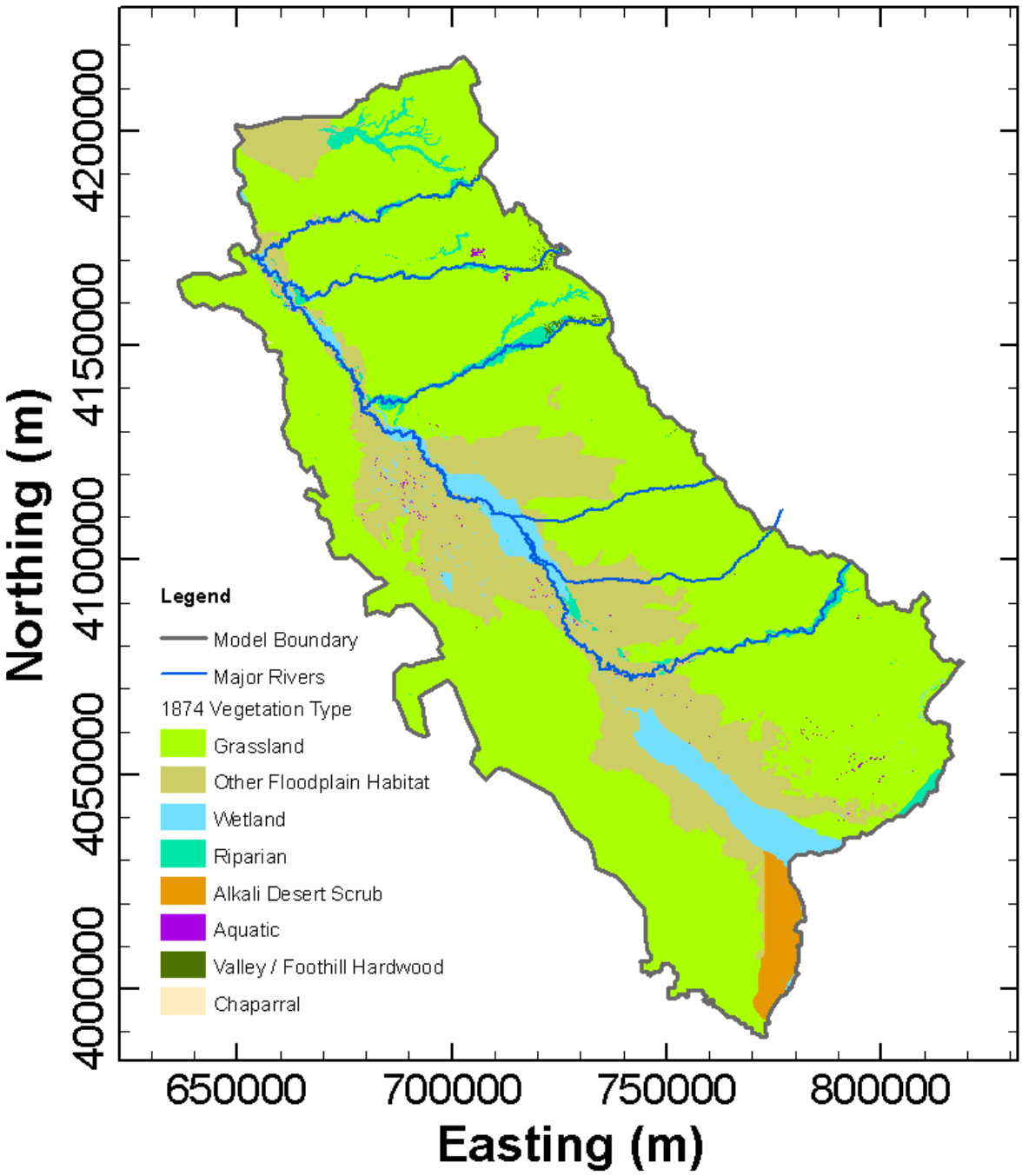

Figure 10: Distribution of natural vegetation across model domain circa 1874 [using spatial data from California State University at Chico et al. (2003)].

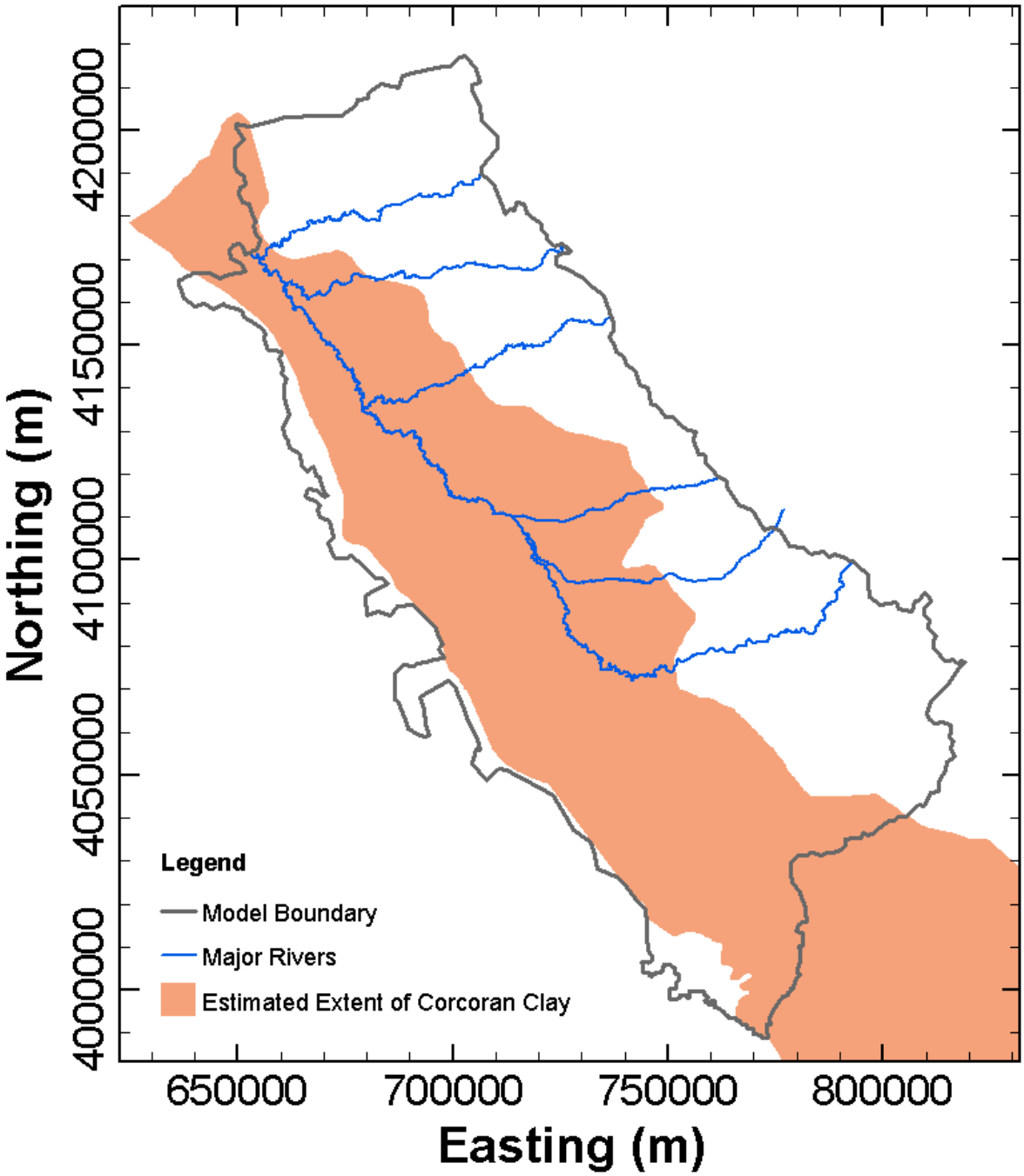

Figure 11: Estimated areal extent of the Corcoran Clay.

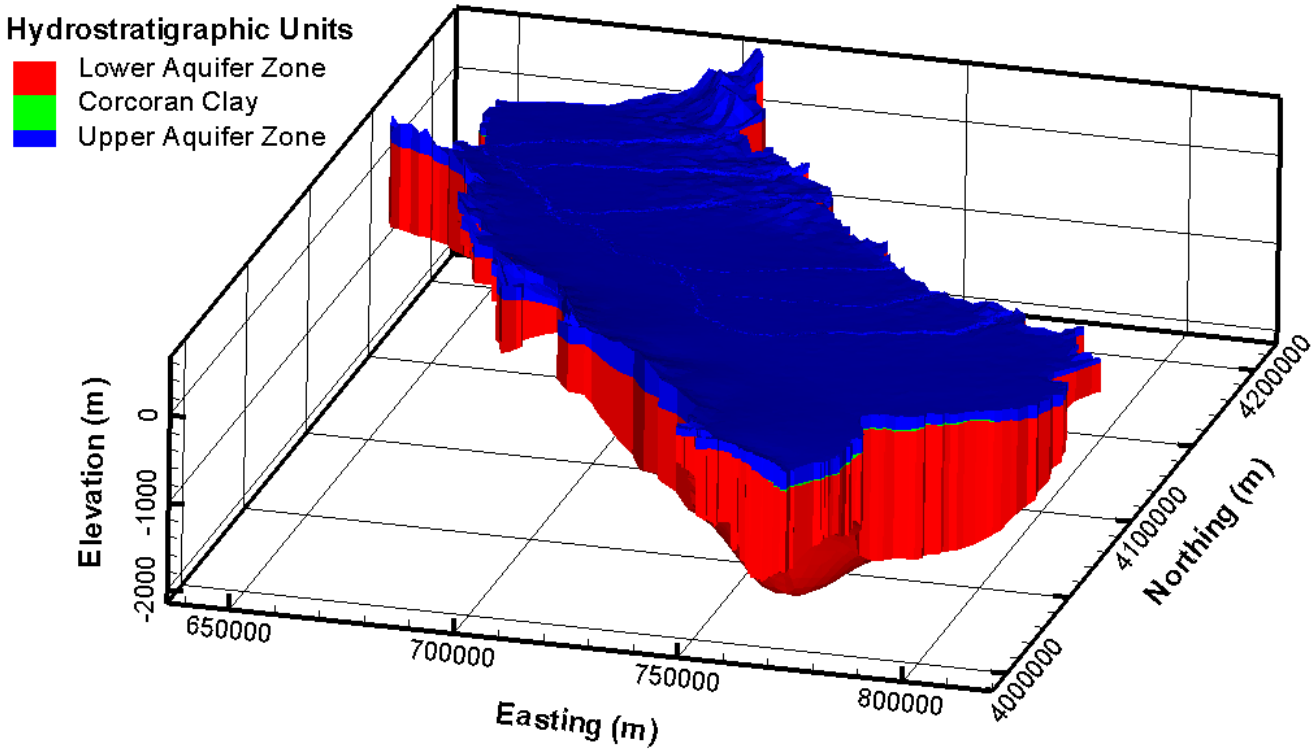

Figure 12: Three-dimensional model and hydrostratagraphic units.

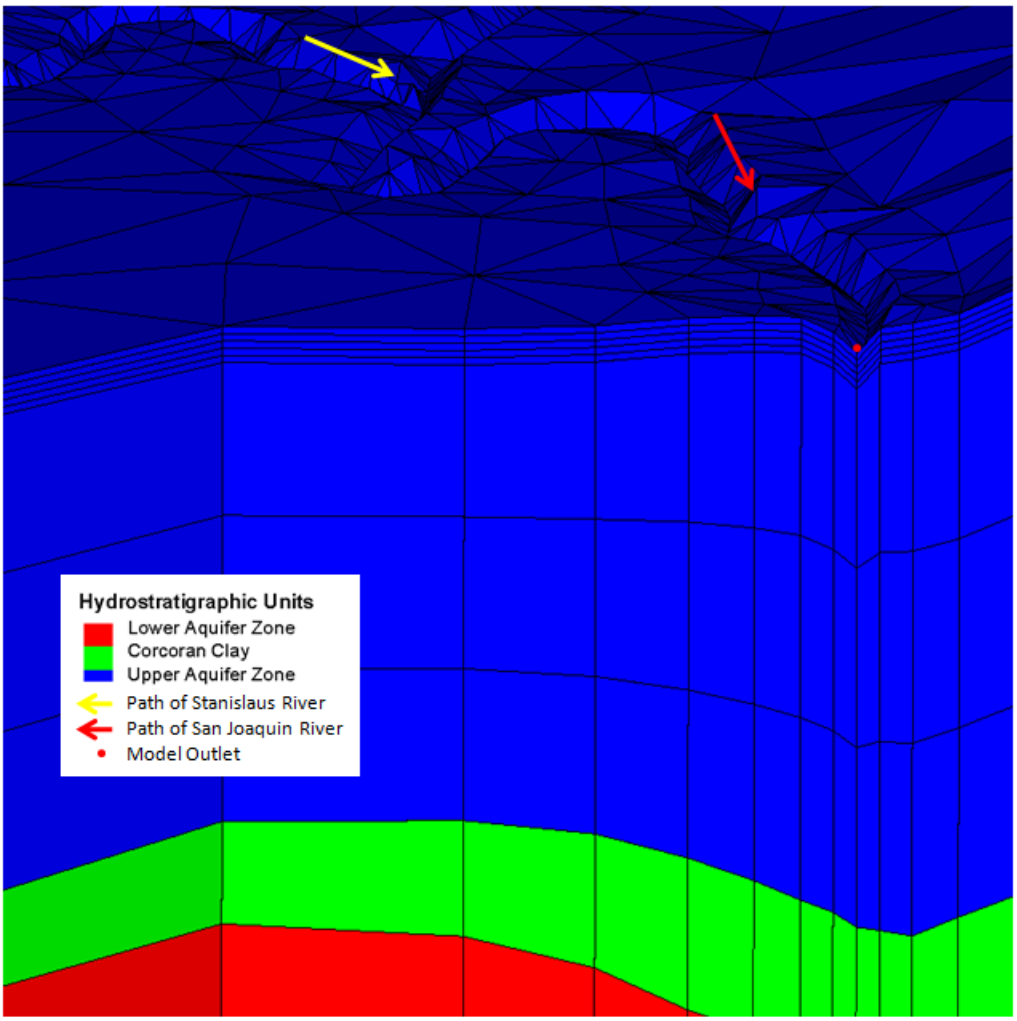

Figure 13: Close up of hydrostratigraphy and mesh at model outlet.

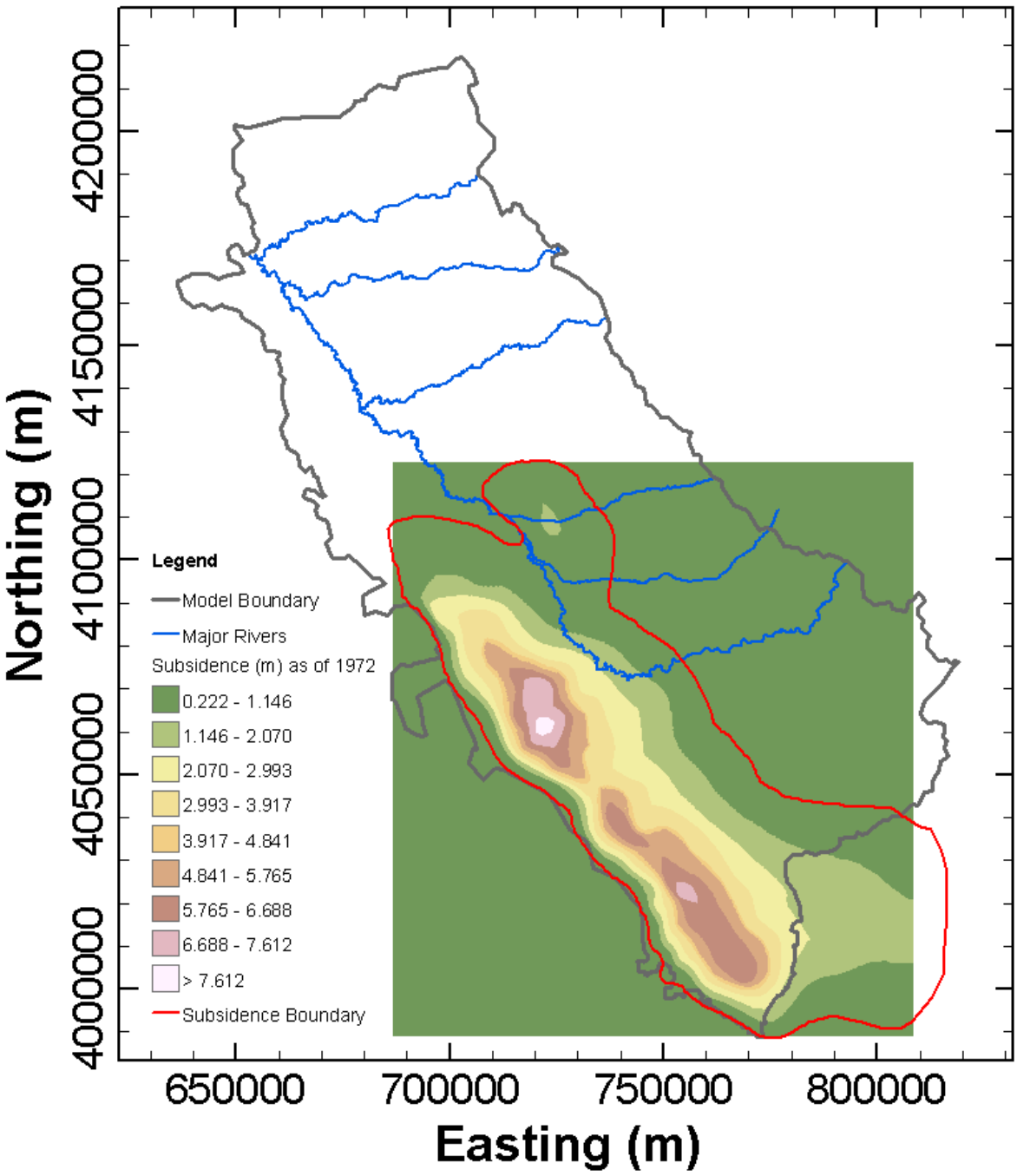

Figure 14: Subsidence values estimated using kriging and subsidence boundary as of 1972 [digitized from Poland et al. (1975), Figure 17].

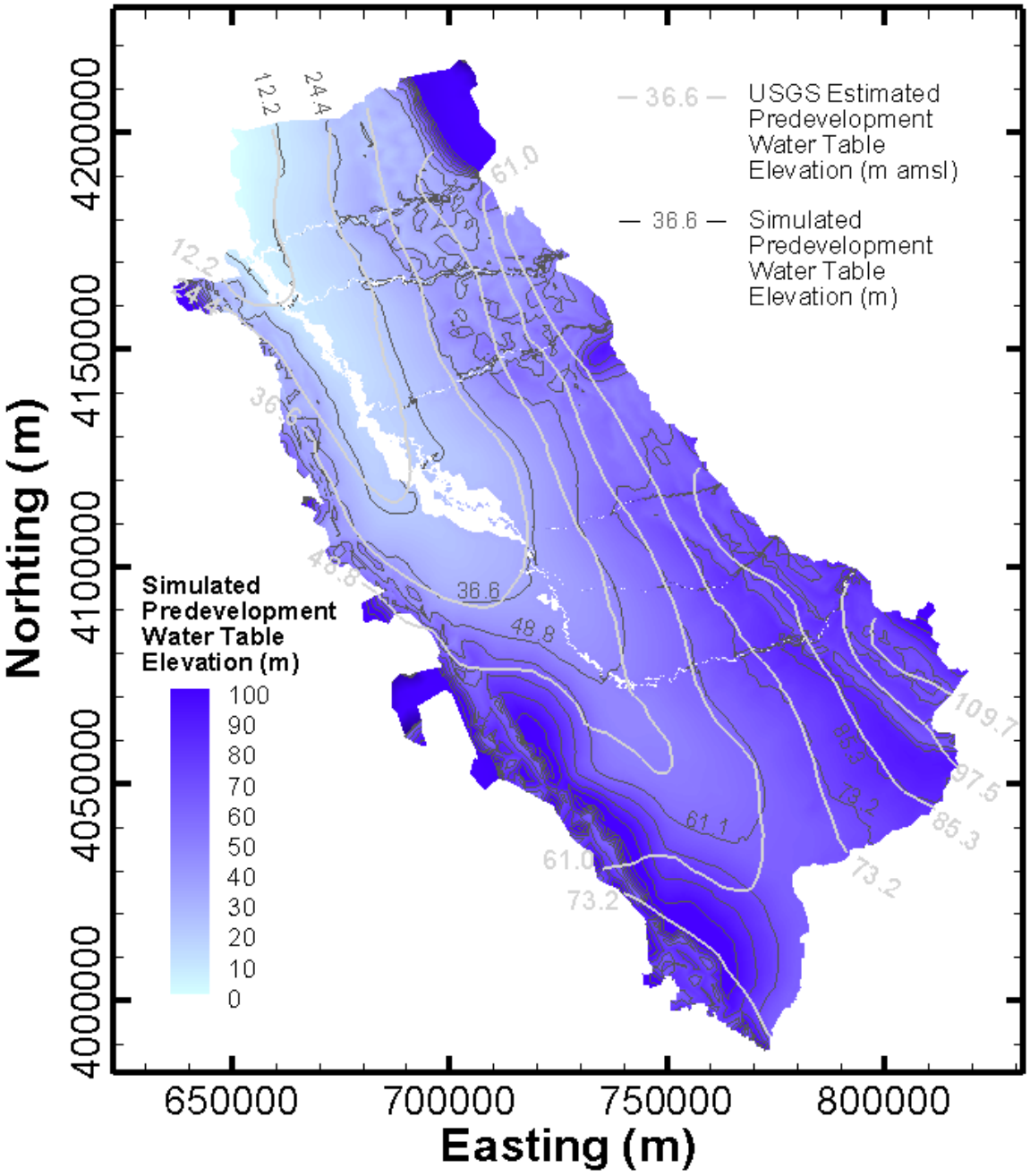

Figure 15: Simulated and estimated predevelopment water table elevations.

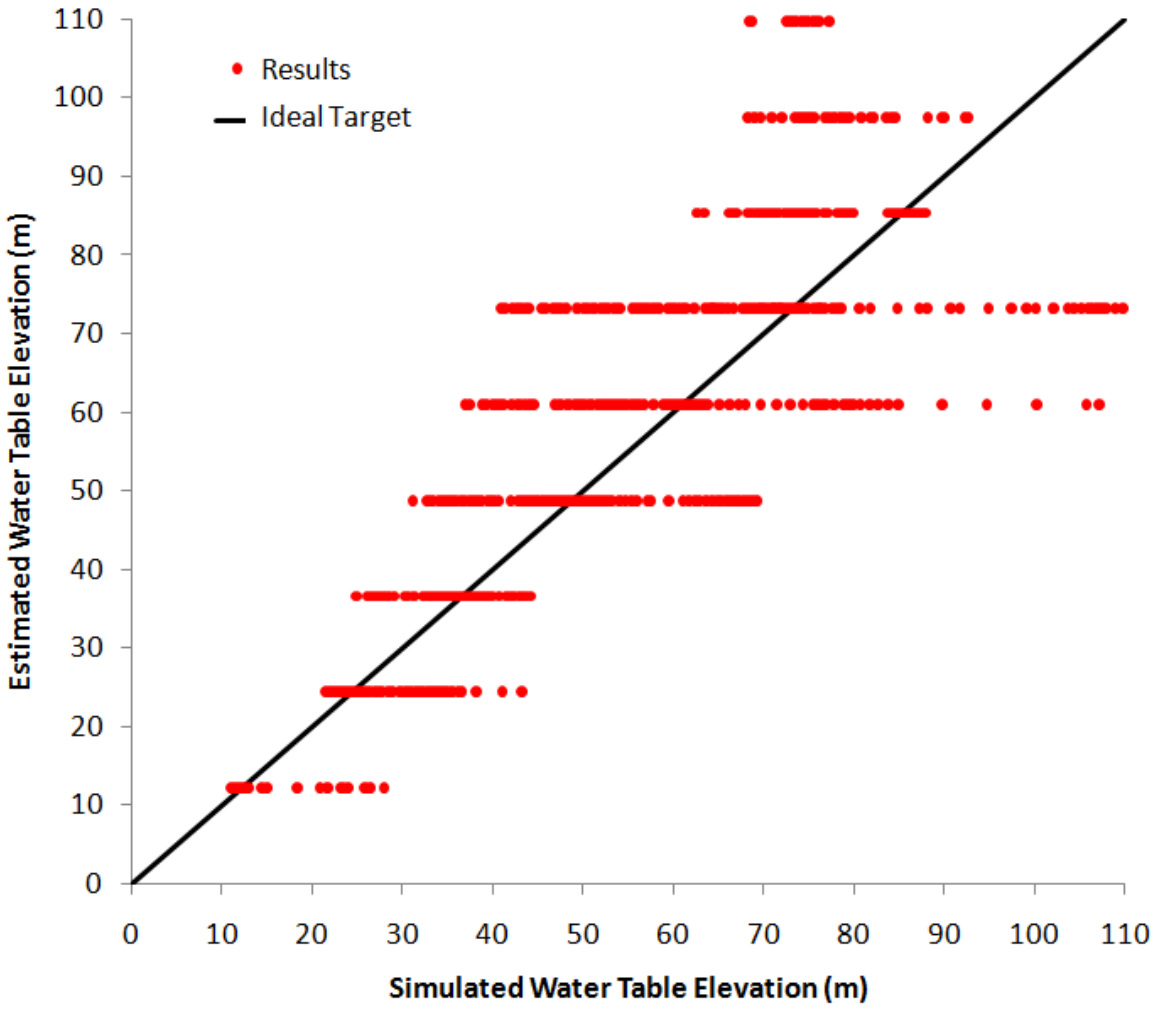

Figure 16: Estimated versus simulated predevelopment water table elevations.

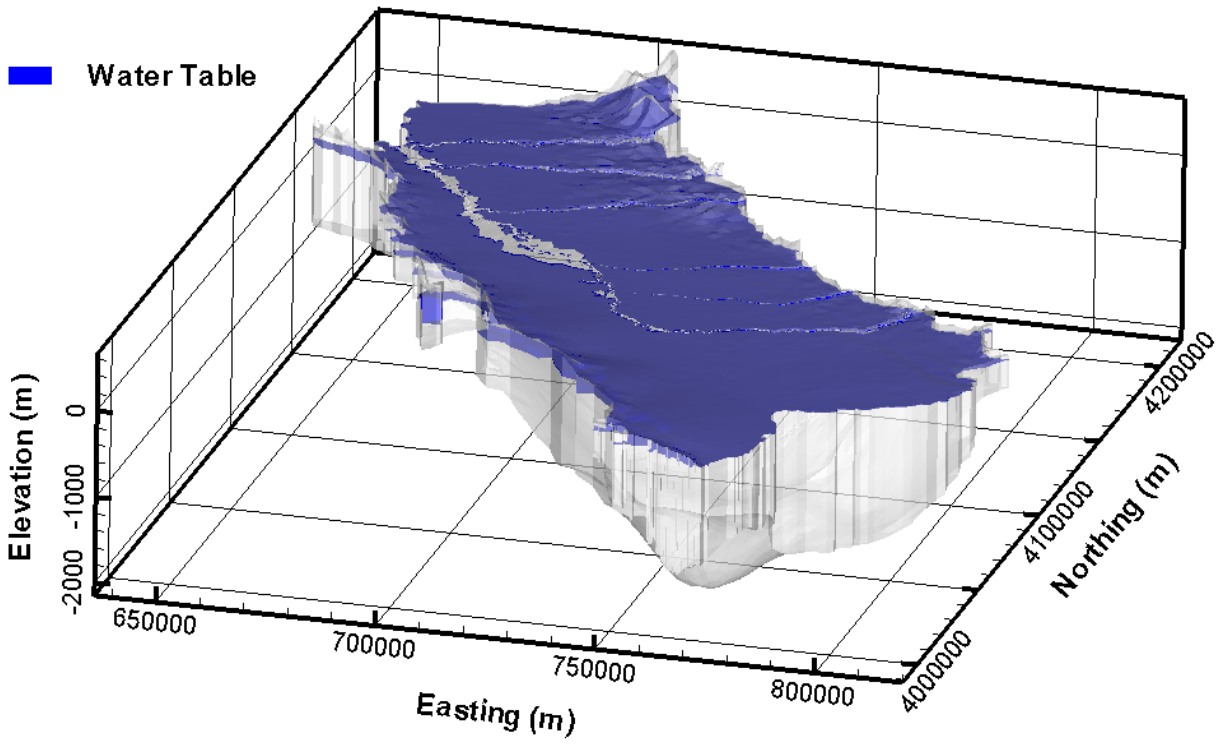

Figure 17: Three-dimensional position of water table at steady state initial condition.

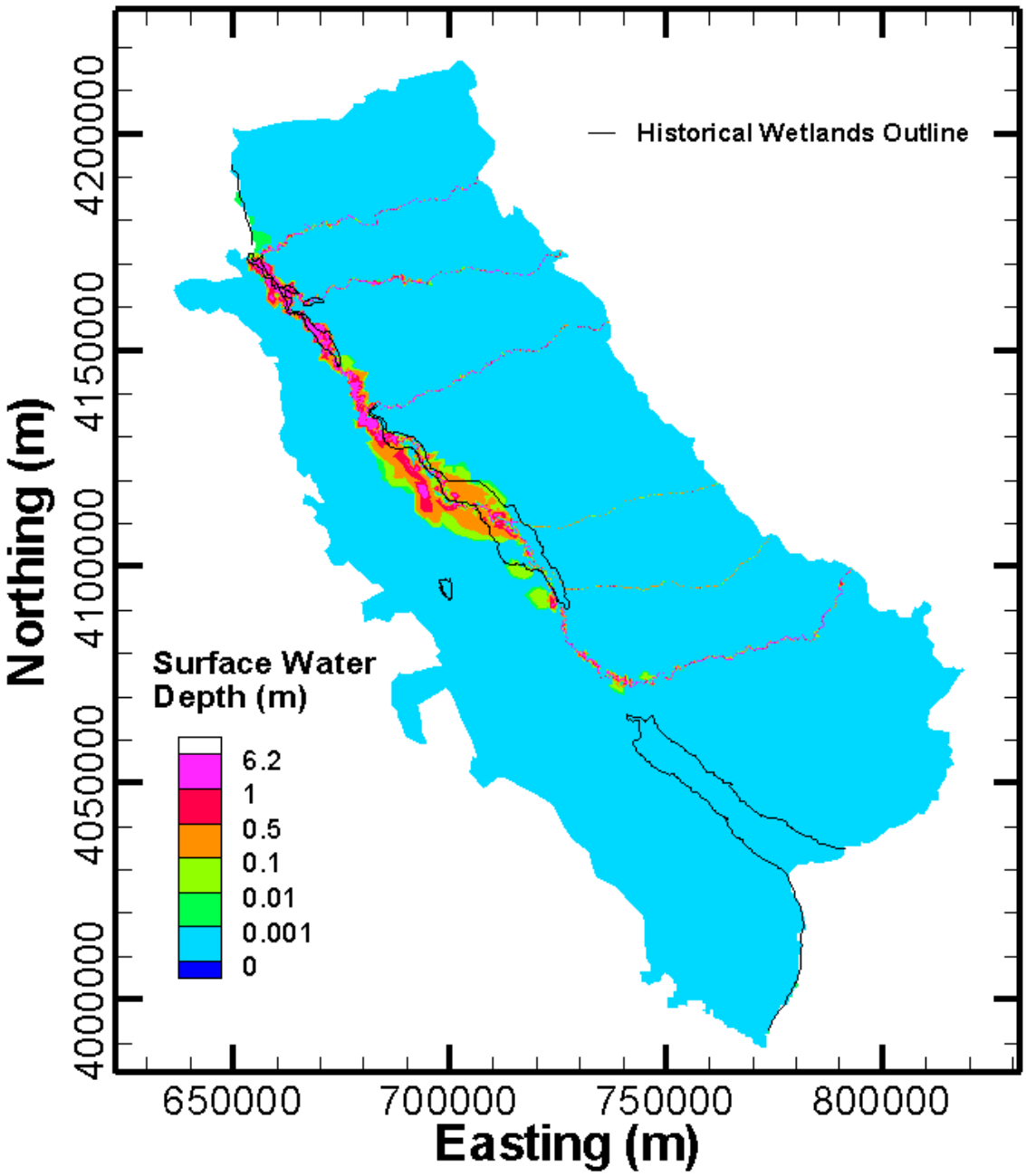

Figure 18: Simulated surface water depth for the steady-state hydrologic model.

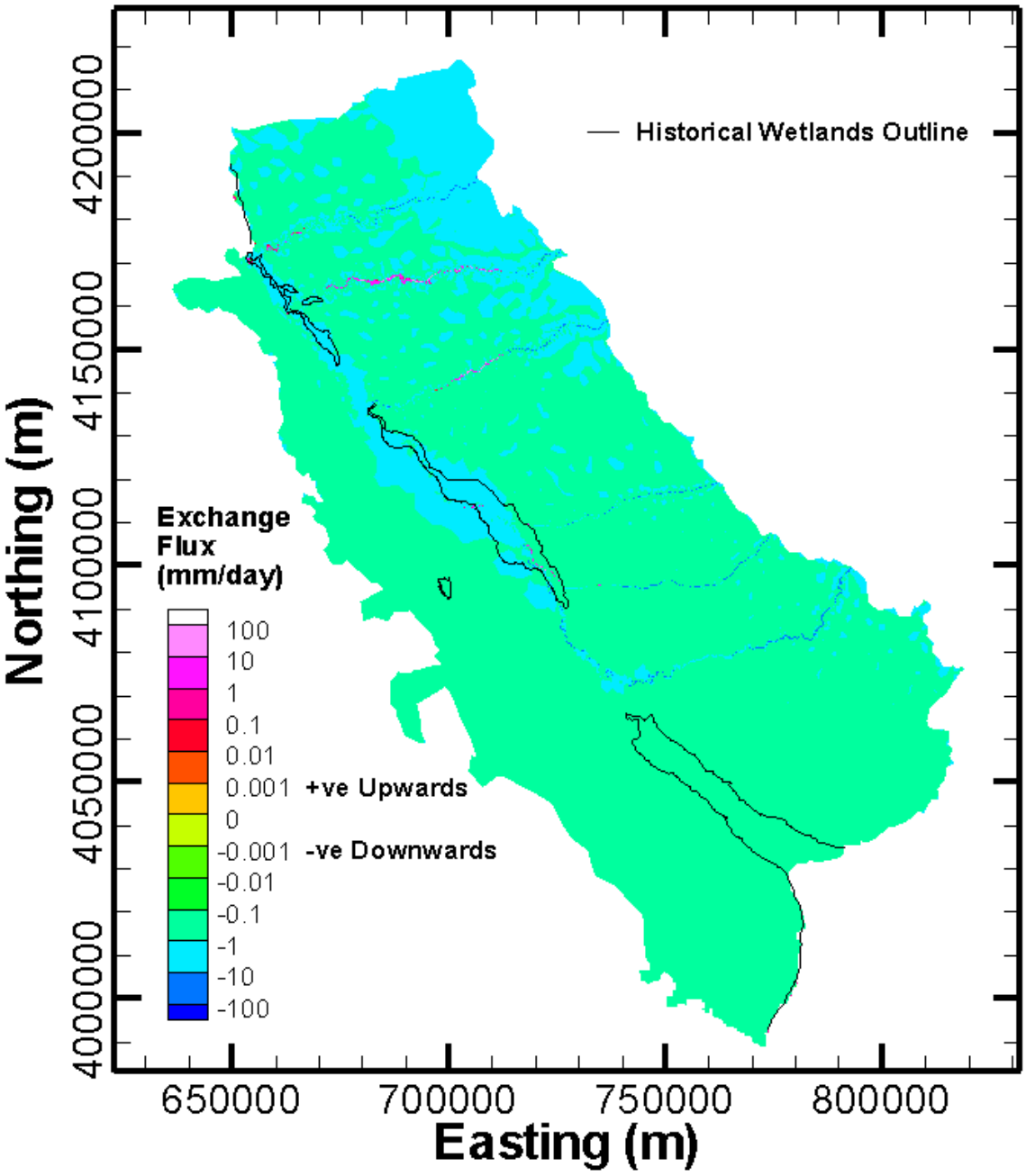

Figure 19: Simulated ground surface exchange flux for the steady-state hydrologic model.

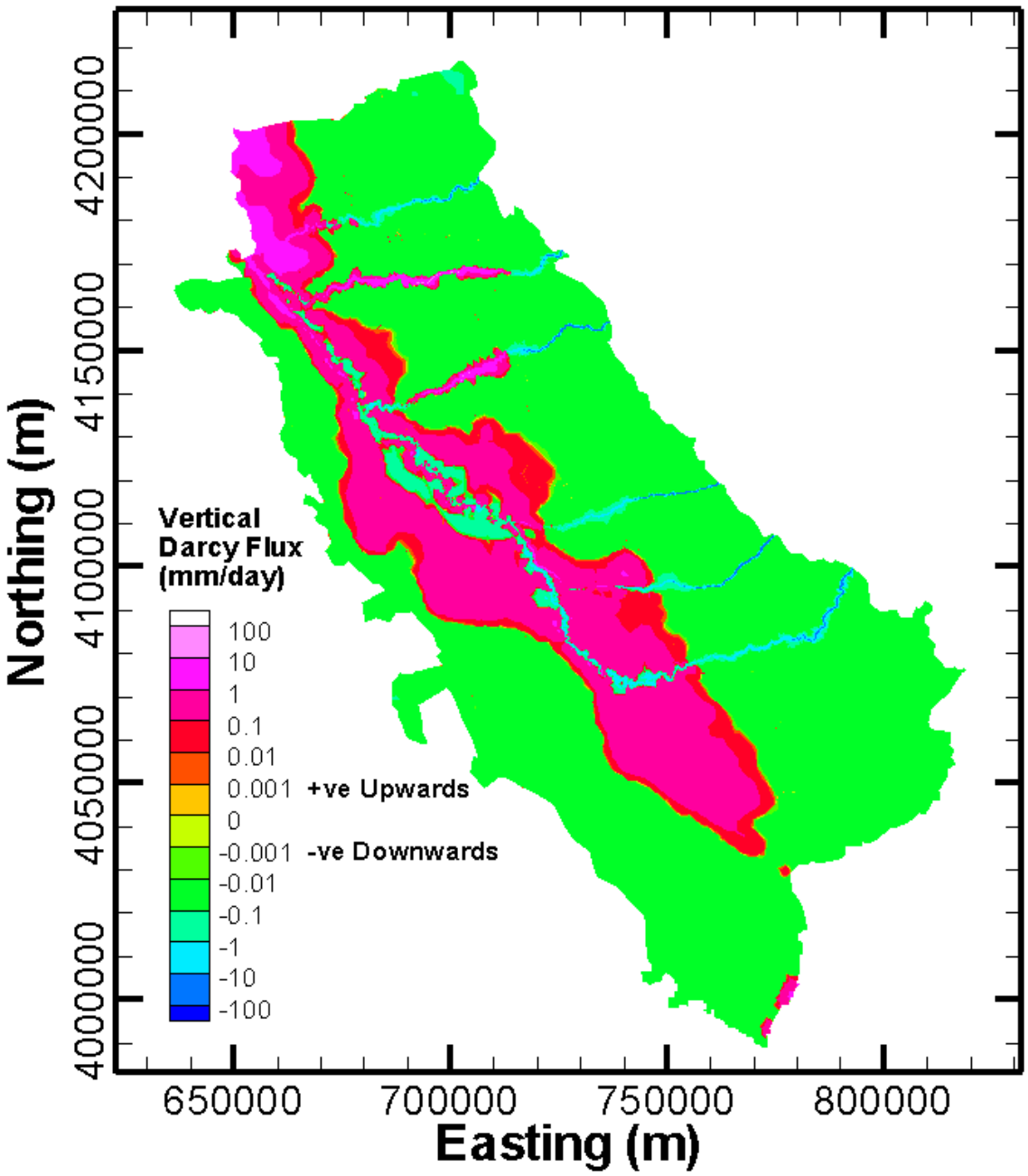

Figure 20: Simulated vertical Darcy flux at the bottom of root zone (5.5 m bgs).

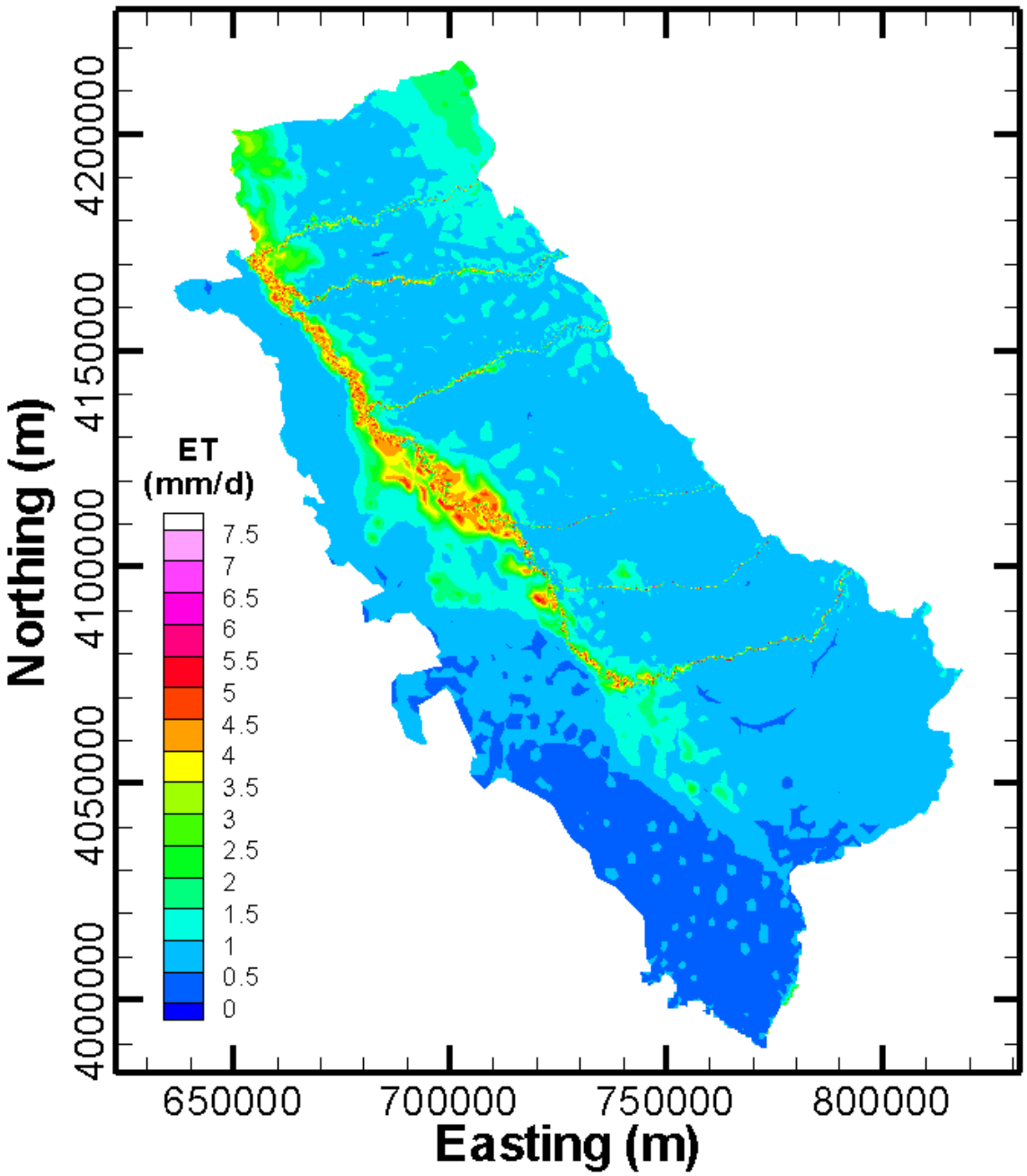

Figure 21: Simulated total evapotranspiration for the steady-state hydrologic model.